Triple-Detection Size-Exclusion Chromatography of Membrane Proteins

vom Fachbereich Biologie der
Technischen Universität Kaiserslautern

zur Erlangung des akademischen Grades
Doktor der Naturwissenschaften
(Doctor rerum naturalium; Dr. rer. nat.)

genehmigte Dissertation

von Frau Dipl.-Biophys. Katharina Gimpl

Vorsitzende:	Prof. Dr. rer. nat. Nicole Frankenberg-Dinkel
1. Gutachter:	Prof. Dr. rer. nat. Sandro Keller
2. Gutachter:	Prof. Dr. rer. nat. Rolf Diller

Wissenschaftliche Aussprache: 08. April 2016

D 386

Abstract

Membrane proteins are generally soluble only in the presence of detergent micelles or other membrane-mimetic systems, which renders the determination of the protein's molar mass or oligomeric state difficult. Moreover, the amount of bound detergent varies drastically among different proteins and detergents. However, the type of detergent and its concentration have a great influence on the protein's structure, stability, and functionality and the success of structural and functional investigations and crystallographic trials. Size-exclusion chromatography, which is commonly used to determine the molar mass of water-soluble proteins, is not suitable for detergent-solubilised proteins because the protein–detergent complex has a different conformation and, thus, commonly exhibits a different migration behaviour than globular standard proteins. Thus, calibration curves obtained with standard proteins are not useful for membrane-protein analysis. However, the combination of size-exclusion chromatography with ultraviolet absorbance, static light scattering, and refractive index detection provides a tool to determine the molar mass of protein–detergent complexes in an absolute manner and allows for distinguishing the contributions of detergent and protein to the complex.

The goal of this thesis was to refine the standard triple-detection size-exclusion chromatography measurement and data analysis procedure for challenging membrane-protein samples, non-standard detergents, and difficult solvents such as concentrated denaturant solutions that were thought to elude routine approaches. To this end, the influence of urea on the performance of the method beyond direct influences on detergents and proteins was investigated with the help of the water-soluble bovine serum albumin. On the basis of the obtained results, measurement and data analysis procedures were refined for different detergents and protein–detergent complexes comprising the membrane proteins OmpLA and Mistic from *Escherichia coli* and *Bacillus subtilis*, respectively.

The investigations on mass and shape of different detergent micelles and the compositions of protein–detergent complexes in aqueous buffer and concentrated urea solutions showed that triple-detection size-exclusion chromatography provides valuable information about micelle masses and shapes under various conditions. Moreover, it is perfectly suited for the straightforward analysis of detergent-suspended proteins in terms of composition and oligomeric state not only under native but, more importantly, also under denaturing conditions.

Zusammenfassung

Im Allgemeinen sind Membranproteine nur in Detergensmizellen oder anderen membranmimetischen Systemen löslich, was die Bestimmung von molaren Massen oder Oligomerisierungsgraden erschwert. Darüber hinaus variiert die Menge an Detergens, die an ein Protein gebunden ist, stark zwischen verschiedenen Detergentien und Proteinen. Proteinstruktur, -stabilität, und -funktion und ebenso der Erfolg von Struktur- und Faltungsstudien sowie der Kristallisation von Membranproteinen sind jedoch stark von der Art des Detergens und seiner Konzentration abhhängig. Größenausschlusschromatographie (GPC), welche standardmäßig für die Bestimmung von molaren Massen wasserlöslicher Proteine Anwendung findet, ist für in Detergens gelöste Proteine nicht geeignet. Proteindetergenskomplexe weisen eine andere Konformation auf als globuläre Standardproteine und unterscheiden sich deshalb für gewöhnlich auch in ihrem Migrationsverhalten von diesen. Deshalb können mit Standardproteinen erstellte Kalibrierkurven im Allgemeinen nicht für die Analyse von Membranproteinen verwendet werden. Kombiniert man jedoch GPC mit der Detektion von UV-Extinktion, statischer Lichtstreuung und Brechungsindex, erhält man eine Methode, welche die Bestimmung molarer Massen von Proteindetergenskomplexen ermöglicht und es erlaubt, die Einzelbeiträge von Protein und Detergens zu bestimmen.
Das Ziel dieser Arbeit war es, das Standardmessverfahren und die Datenanalyse dieser Methode für die Anwendung mit schwierigen Membranproteinproben, außergewöhnlichen Detergentien und anspruchsvollen Lösungsmitteln, wie beispielsweise hochkonzentrierte Denaturierungsmittellösungen, zu verfeinern. Dazu wurde der Einfluss von Harnstoff, der von der speziellen Probe unabhängig ist, auf das Verhalten der Methode an dem wasserlöslichen Rinderserumalbumin untersucht. Auf Grundlage der dadurch gewonnenen Erkenntnisse wurden Mess- und Analyseverfahren für verschiedene Detergentien sowie Proteindetergenskomplexe mit den Proteinen OmpLA und Mistic aus *Escherichia coli* beziehungsweise *Bacillus subtilis* verfeinert.
Die Untersuchungen bezüglich der Masse und Form verschiedener Detergentsmizellen sowie der Zusammensetzung der Proteindetergenskomplexe in verschiedenen Lösungsmitteln zeigt, dass GPC mit dreifacher Detektion nützliche Informationen über Masse und Form von Detergensmizellen unter verschiedenen Bedingungen liefert. Darüber hinaus ist die Methode hervorragend geeignet, um detergensgelöste Proteine bezüglich ihres Oligomerisierungsgrades und der Menge des gebundenen Detergens zu charakterisieren, und zwar sowohl unter nativen, als auch unter denaturierenden Bedingungen.

Contents

Abbreviations and symbols

$A_{280\,\mathrm{nm}}$	absorbance coefficient at 280 nm
A_2	second virial coefficient
abbr.	abbreviation
AF4	asymmetric-flow field-flow fractionation
agg. no.	aggregation number
AIX	anion exchange
AUC	analytical ultracentrifugation
BSA	bovine serum albumin
BWM	bio wet mass
$C_{12}EO_8$	octa(ethylene oxide) dodecyl ether
CD	circular dichroism
CF3	centrifugal field-flow fractionation
comp	protein–detergent complex (*subscript*)
CV	column volume
DDM	*n*-dodecyl-β-D-maltoside
DEAE	diethylaminoethanol
det	detergent (*subscript*)
DIBMA	poly(di-isobutylene-*alt*-maleic-acid)
DLPC	1,2-didodecanoyl-*sn*-glycero-3-phosphocholine
DLS	dynamic light scattering
DM	*n*-decyl-β-D-maltoside
DPC	*n*-dodecyl-phosphocholine
DTT	1,4-dithio-DL-threitol
EDTA	ethylenediamine tetraacetic acid
EK	enterokinase
EtOH	ethanol
ext	external
f	final (*subscript*)
F_6OM	tridecafluoro-*n*-octyl-β-D-maltoside
FFF	field-flow fractionation
FL	fluorescence
GdmCl	guanidinium hydrochloride
HC	hydrocarbon

i	initial (*subscript*)
int	internal
IPTG	isopropyl-β-D-thiogalactopyranoside
LB	lysogeny broth
LDAO	*n*-dodecyl-*N*,*N*-dimethylamine-*N*-oxide
LS	light scattering
MALS	multi-angle light scattering
MD	molecular dynamics
Mistic	membrane-integrating sequence for translation of integral membrane-protein constructs
NM	*n*-nonyl-β-D-maltoside
NMR	nuclear magnetic resonance
NOE	nuclear Overhauser effect
$OD_{600\,nm}$	optical density at 600 nm
OG	*n*-octyl-β-D-glucoside
OM	outer membrane
OmpLA	outer-membrane phospholipase A
ORF	open-reading frames
PDC	protein–detergent complex
POPC	1-palmitoyl-2-oleoyl-*sn*-glycero-3-phosphocholine
prot	protein (*subscript*)
RI	refractive index
RT	room temperature
S/N	signal-to-noise ratio
SANS	small-angle neutron scattering
SAXS	small-angle X-ray scattering
SDS	sodium dodecyl sulphate
SDS-PAGE	sodium dodecyl sulphate polyacrylamide gel electrophoresis
SEC	size-exclusion chromatography
SLS	static light scattering
SMA	styrene maleic acid
SMALP	SMA–lipid particle
SN	supernatant
sol	solvent
TEM	transmission electron microscopy
TLC	thin-layer chromatography
Tris	tris(hydroxymethyl)aminomethane
UM	*n*-undecyl-β-D-maltoside
UV	ultraviolet
c	concentration

$c_{\mathrm{det,final}}$	target detergent concentration
$c_{\mathrm{det,sample}}$	detergent concentration in samples
$c_{\mathrm{det,sol}}$	detergent concentration in solvent
d	Euclidean dimension
δ	detergent–protein mass ratio
ΔR_Θ	excess Rayleigh ratio
ΔR_{90°	excess Rayleigh ratio at a scattering angle of 90°
$\Delta\mathrm{RI}$	excess refractive index
$\Delta\mathrm{UV}_{280\,\mathrm{nm}}$	background-corrected UV absorbance signal at 280 nm
$\mathrm{d}n/\mathrm{d}c$	refractive index increment
$\mathrm{d}\Omega$	solid angle
$\varepsilon_{280\,\mathrm{nm}}$	extinction coefficient at 280 nm
η	number of molecule elements
f	calibration constant
$\hbar$	reduced Planck constant
I_0	incident light intensity
I	intensity
K	optical constant
L	measurement cell length
λ	solvent wavelength
λ_0	vacuum wavelength
l_{max}	maximum length
M	molar mass
m	mass
M_n	number-average molar mass
M_w	mass-average molar mass
M_z	z-average molar mass
N	number of molecules
n_0	solvent refractive index
n	molecular refractive index
N_A	Avogadro's number
n_c	apparent number of carbon atoms in tail
P_Θ	particle scattering function
pldA	phospholipid degrading enzyme A
Q	internal degrees of freedom
R_H	hydrodynamic radius
ρ	distribution function
R_RMS	root mean square radius
R^2_RMS	mean square radius
$R^2_{\mathrm{RMS},n}$	number-average mean square radius

$R^2_{\mathrm{RMS},w}$	mass-average mean square radius
$R^2_{\mathrm{RMS},z}$	z-average mean square radius
T	temperature
Θ	scattering angle
UV_λ	absorbance at a certain wavelength λ
V	volume
v	velocity
v_F	volume of a fluorocarbon chain
v_H	volume of a hydrocarbon chain
w	weight fraction
$\vec{k}$	wave vector
w/v	weight-per-volume ratio
w/w	weight-per-weight ratio
x_i	mole fraction

1 Introduction

The interaction of light and matter is one of the most basic principles in nature and the cause for almost all perceptions in daily life. Thus, it seems likely that the observation of light–matter interactions is of tremendous significance in many research disciplines. Light scattering (LS) is one of the main techniques relying on the analysis of such interactions to gain information about very different kinds of particles. It is applied as routine approach in various research areas and on very different samples, such as atoms and small molecules, polymers, or proteins, or more precisely, membrane proteins as in this work. The understanding of the biophysical nature of membrane proteins is one of the main topics in modern biophysics, because these proteins are of outstanding biological and pharmacological relevance [1]. However, progress in the biophysical, biochemical, and structural investigation of membrane proteins is hampered by the fact that these hydrophobic proteins are generally soluble in aqueous solution only in the presence of detergent micelles or other membrane-mimetic systems [2]. Hence, membrane proteins in solution can never be studied as pure substances, but are always associated with stabilising compounds. However, the true composition of these complexes is often unknown, and the aggregation state of these colloidal mixtures depends on the type and concentration of the detergent, lipid, or polymer used [3–7]. Moreover, the choice of detergent, or any other membrane mimetic, and its concentration has a great influence on the protein's structure, stability, and functionality [8, 9]. Membrane proteins tend to aggregate and precipitate if the detergent concentration is too low; conversely, excess detergent may lead to denaturation or dissociation of protein complexes [10, 11]. Therefore, detailed knowledge of detergent concentration and the composition of protein–detergent complexes (PDCs) is essential for many functional and structural studies [3, 12]. The same is true for biophysical investigations of membrane-protein folding based on the use of chemical denaturants [13, 14]. In such experiments, the unfolded protein in the presence of high denaturant concentrations serves as a common reference state enabling the comparison of protein conformational stability among different detergents, but this approach is applicable only if the unfolded state is not associated with detergent [15]. However, there are few techniques that allow fast and reliable determination of molar mass, oligomeric state, and degree of detergent association of membrane proteins and, thus, are suited as routine application. Most techniques used to achieve these information are either difficult to handle for inexperienced users, or they rely on the use of calibration standards that are of limited applicability for membrane proteins. Triple-detection size-exclusion chromatography (triple-detection

SEC) is both straightforward and easy to handle and, most importantly, an absolute technique, that is, it does not rely on the use of external standards [16–20]. All these factors render triple-detection SEC a promising method for the application on challenging membrane-protein samples beyond routine approaches.

1.1 Membrane proteins

The main driving force for protein folding is the hydrophobic effect [21, 22]. As a consequence, water-soluble proteins bury their hydrophobic residues in the protein core and expose the hydrophilic residues to the aqueous environment. In membrane proteins, polar and apolar residues have to be distributed differently because of the fundamentally different environment in which they reside. In early times of membrane-protein research, it was believed that membrane proteins deal with their environment by adopting an "inside-out" conformation, compared with water-soluble proteins, with a hydrophilic core and a hydrophobic surface [23]. This view was revised when the first high-resolution structures [24, 25] revealed that the interior of membrane proteins is as hydrophobic as that of water-soluble proteins. By contrast, the amino acid residues that are exposed to the hydrocarbon (HC) core of the lipid bilayer are on average even more hydrophobic than the residues buried in the proteins' inside. Polar and charged residues can be found mainly in regions of the protein surface that are in contact with lipid head groups or the polar environment [25, 26]. This distribution of amino acid residues clearly distinguishes membrane proteins from their water-soluble counterparts.
Membrane proteins appear in two main structural motifs: β-barrels and α-helices. Given the apolar environment of the membrane, it is extremely costly in terms of free energy to transfer unsatisfied hydrogen bond donors and acceptors from water into the lipid bilayer. Furthermore, unsatisfied hydrogen bonds cannot be saturated within the HC core of a lipid membrane. Hence, any transmembrane structure must involve all membrane-buried polar groups of the backbone in hydrogen bonds. The aforementioned structures are the only ones that can satisfy this requirement [27, 28]. From the entirety of β-sheet containing structures, the β-barrel conformation is the only structure that can meet the structural demands of membrane-embedded proteins [29]. The barrels are composed of membrane spanning meandering antiparallel bundles of β-sheets [30] and are found in the outer membrane (OM) of gram-negative bacteria, mitochondria, and chloroplasts [31, 32]. They are also known as porins and fulfil such divers functions as passive nutrient import, active transport of ions and proteins, and phospholipase and protease activities [30, 33]. However, the vast majority of membrane proteins consists of transmembrane bundles of α-helices [27]. 20–30% of all open-reading frames (ORF) encode for α-helical membrane

proteins [34], accounting for >50% of all drug targets in the human body [35], and their malfunction is responsible for a wide range of diseases [36, 37]. Contrary to β-sheets, single α-helices are stable within the membrane since hydrogen bonds can be satisfied intrahelically [38].

1.2 Model protein: OmpLA

Outer-membrane phospholipase A, hereafter referred as OmpLA, is an enzyme located in the OM of various pathogens and nonpathogens [39]. The *pldA* (phospholipid degrading enzyme A) gene from *E. coli* encoding for OmpLA is translated into a 289 amino acid long protein with the first 20 amino acids representing the signal sequence and, thus, results in a mature protein of 269 amino acids [40]. Scandella et al. first isolated and purified OmpLA in 1971 [41]. High-resolution X-ray diffraction structures of monomeric and dimeric OmpLA from 1999 [42] revealed the protein's β-barrel structure (**Figure 1 A** and **B**). The monomer comprises 12 antiparallel strands that form a barrel with a convex and a flat side (**Figure 1A**). Hydrophobic residues are presented to the HC core of the lipid bilayer. By contrast, the inside of the barrel pore is polar and comprises a complex hydrogen-bond network that accounts for the protein's rigid structure. Aromatic residues encase the hydrophobic region of OmpLA at the polar–apolar boundaries of both leaflets of the lipid bilayer [42]. It is necessary to strictly regulate the protein's phospholipase activity since uncontrolled activity has lethal consequences for bacteria [43]. As OmpLA is constitutively expressed, its activity is regulated at the protein level [44, 45] and is achieved by reversible dimerisation [39, 46]. Under physiological conditions, OmpLA resides as inactive monomers in the OM [39]. Upon membrane perturbation, caused by diverse events such as heat shock [44], phage-induced lysis [47], or decreased stability of the cell envelope [48], phospholipids are inserted into the OM. This increases the fluidity of the membrane and, thus, accelerates the lateral diffusion of OmpLA [49]. Thereby, dimerisation is facilitated. This is realised with only minor changes in secondary structure and results in the formation of a homodimer with its conforming parts being associated by their flat sides (**Figure 1C**) [42]. The dimerisation entails the formation of an active site with two substrate-binding pockets and a catalytic triad of Ser144, His142, and Asn156 at the interfacial boundary of the outer leaflet of the OM [42]. Upon dimerisation and in the presence of calcium [50, 51], OmpLA hydrolyses acyl ester bonds in phospholipids and lysophospholipids involving degradation of the lipids in its vicinity [50]. It has been shown that in *E. coli* OmpLA participates in the secretion of bacteriocins [49] and that it acts as a virulence factor in many pathogens [52, 53]. However, as it is constitutively expressed in various organisms, a general function of OmpLA as housekeeping enzyme is most likely [54].

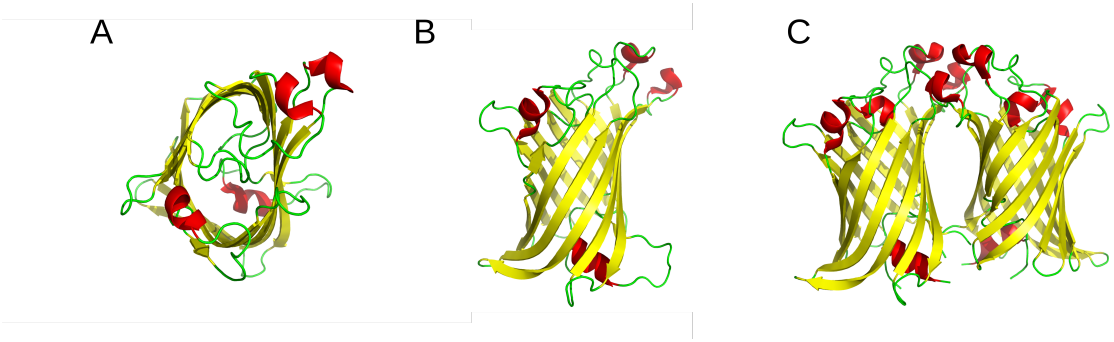

Figure 1: Crystal structure of OmpLA. The OmpLA structure is presented in ribbon representation as monomer in (A) top-view and (B) side-view (PDB 1QD5) and as (C) dimer (PDB 1QD6M) as determined by X-ray cristallography [42]. The protein structure of the monomer comprises twelve antiparallel β-strands, forming a barrel with a convex and a flat side. The structure shows large transmembrane regions (yellow), short α-helices (red), and extracellular and periplasmic loops (green). The periplasmic side is located at the bottom. Figure was created with PyMol [55].

1.3 Model protein: Mistic

Mistic is an 110 amino acid long α-helical membrane protein from *B. subtilis*. Its name is an acronym for "membrane-integrating sequence for translation of integral membrane-protein constructs" [56, 57]. Mistic forms a membrane-embedded helical bundle of four α-helices (**Figure 2**) as determined by nuclear magnetic resonance (NMR) spectroscopy on the detergent-solubilised protein in 2005 [56]. Three of the four α-helices are slightly shorter (∼14 instead of ∼20 amino acid residues) than expected for an membrane-traversing helix. The authors assigned this to an unravelling of the helices' ends because of the detergent environment. Numerous polar and charged residues are exposed on the protein surface. Additionally, with a predicted pI of 4.5 and a net charge of −12 at pH 7.0, Mistic should be more hydrophilic than typical globular water-soluble proteins. However, Mistic tightly associates with membranes in vivo [56, 58] and in vitro [56, 58, 59] despite its hydrophilic character and, thus, by definition [60], is counted as integral membrane protein. Moreover, NMR measurements of Mistic in *n*-dodecyl-*N*,*N*-dimethylamine-*N*-oxide (LDAO) micelles reveal a concentric ring of nuclear Overhauser effect (NOEs) interactions of the protein with the alkyl chains of the detergent as expected for classical membrane-embedded proteins. Additionally, folded Mistic aggregates rapidly when it is deprived of detergent micelles [14, 56]. All these features mark it as membrane protein. Mistic also lacks a intramembrane targeting sequence and spontaneously self-integrates into the lipid bilayer bypassing the translocon machinery [56]. Moreover, it is able to target other recombinantly expressed intramembrane proteins to the membrane when expressed as a fusion protein. This has been shown, for example, for voltage-gated K^+-channels, G-protein coupled receptors, and histidine kinase receptors [56, 57, 61]. Interestingly, it facilitates only the synthesis of integral membrane proteins, whereas fusion of Misitic to peripheral membrane proteins rather leads to a decrease in protein yield compared with the non-tagged

Figure 2: NMR structure of Mistic in LDAO detergent micelles. The Mistic structure is presented in ribbon representation (PDB 1YGM) [56]. The protein structure comprises four α-helices, with the second one exhibiting a central kink bending over the top of the protein. Figure was created with PyMol [55].

protein [62]. However, the guidance of other membrane proteins into the lipid bilayer does not seem to be Mistic's physiological function. Investigations of Lundberg and co-workers indicate that Mistic is an important factor in the biofilm formation of *B. subtilis* [63]. The spore-forming bacterium can switch between a planktonic and a sessile state depending on the environmental conditions. This switch is induced by the expression of genes that are required for either flagellum or biofilm formation. The expression of these genes is under the control of exclusive regulatory pathways. The work of Lundberg et al. shows that Mistic and the putative K^+-efflux channel YugO are important for successful biofilm formation. And, it reveals the location of the Mistic encoding gene just upstream and partially overlapping with the gene coding for the YugO. This identifies Mistic and YugO as potential regulators in one of the biofilm-formation-controlling pathways in *B. subtilis* [57, 63].
Mistic also gained relevance in chemical protein-folding studies since it is one of the few α-helical membrane proteins that recovers its native fold after complete unfolding [14, 64, 65]. With the aid of circular dichroism (CD) and intrinsic Trp fluorescence (FL) spectroscopy, it has been shown that Mistic unfolds completely and reversibly from various detergent micelles after addition and removal of high concentrations of urea or guanidinium hydrochloride (GdmCl) [66]. Subsequent quantitative investigations of the protein's conformational stability upon chemical denaturation revealed the strong influence of polar interactions in protein stabilisation [14].

1.4 Membrane-mimetic system: detergent micelles

For most biophysical and functional studies, structural investigations, and crystallisation trials, membrane proteins have to be extracted from their native membrane because most in vitro techniques cannot cope with the complex environment of a native membrane.

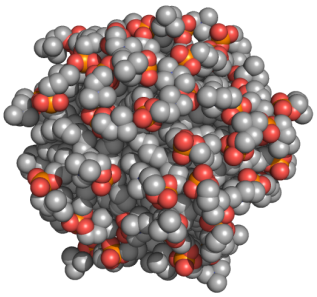

Figure 3: Snapshot of a molecular dynamics simulation of a detergent micelle. An n-dodecyl-phosphocholine (DPC) micelle comprising 65 monomers is depicted after a simulation of 1100 ps [75]. Colour code is black for carbon, red for oxygen, blue for nitrogen, and orange for phosphorus atoms. The PDB-file was kindly provided for download by Peter Tieleman (University of Calgary). Figure was created with PyMol [55].

Therefore, membrane mimetics are needed to support stability and functionality of membrane proteins under experimental conditions. Detergents are used for both the isolation of membrane proteins from the lipid membrane and the stabilisation of the native protein structure, either for direct use or for reconstitution into artificial lipid bilayers [11, 67, 68]. However, the success of several of these approaches, like crystallisation or reconstitution, drastically depends on the chosen detergent [6]. Thus, a detailed understanding of the complex behaviour of detergents in solution and the factors influencing this behaviour is required. The term detergents refers to a group of amphiphilic surface-active molecules that self-assemble into supramolecular structures and interact with and, at sufficiently high concentrations, disrupt lipid bilayers [3, 69]. Detergent molecules typically consist of a non-polar tail that is joined to a polar head group. The hydrophobic tail is mostly an n-alkyl chain comprising 8–18 methylene groups. Depending on the head group moiety, detergents are classified as ionic (e.g., sulphates), zwitterionic (e.g., betaines), or non-ionic (e.g., glucosides, maltosides, or polyoxyethylenes) [69]. The self-assembly of the monomers is generally concentration-dependent. At low concentrations detergents typically exist as monomers in aqueous solution. Since the monomers posses a low water-solubility, they self-assemble into detergent micelles at higher concentrations by shielding the hydrophobic chains in the micelle core and exposing the hydrophilic head groups towards the water. By doing this, the entropically unfavoured exposure of hydrophobic moieties to the polar environment is minimised [70], as demanded by the hydrophobic effect [21]. The highly curved structure of micelles results from the cone-like shape of the monomers, which is caused by the fact that the detergent head groups occupy more space than the single alkyl chain tails [71], as a consequence, detergent micelles are often described as essentially spherical. However, a less organised [72], ellipsoidal [73], or in special cases even rod-like [74] structure seems to match reality more closely.

1.4.1 Critical micellar concentration and aggregation number of detergent micelles

Detergent monomers do not assemble into micelles below a certain, detergent-dependent concentration due to electrostatic (ionic detergents) or steric repulsion (non-ionic detergents) that opposes the attraction of the alkyl chains. The minimum concentration at which micellisation starts is called the critical micellar concentration (CMC). By addition of detergent beyond the CMC, the number of micelles increases, whereas the monomer concentration in solution stays constant. Monomers and micelles exist in a dynamic equilibrium [70, 76]. The exact CMC drastically depends on the physical properties of the detergent itself. Among detergents with a common head group, the CMC decreases roughly 10-fold for every two methylenes added to the aliphatic chain due to the increased hydrophobic character of the detergent [11, 69]. By contrast, an increased hydrophilicity opposes micelle formation and leads to an increased CMC of ionic or zwitterionic detergents compared with their non-ionic analogous [69]. While long-chain alkyl detergents have a low CMC but suffer from poor solubility in water, short-chain alkyl detergents are more water-soluble but posses a high CMC. However, this is counteracted by a bigger head group moiety. While only glucosides with alkyl chain lengths of eight or nine C-atoms are soluble, alkyl maltosides can be used in aqueous solutions up to a chain length of 14 C-atoms [11]. Beside the chemical nature of the detergent, various parameters like pH, temperature, and solvent composition can influence the CMC [70, 77]. Especially, ionic detergents are influenced by changes in pH and ionic strength of the solvent, whereas non-ionic detergents are relatively unaffected by both parameters [21]. However, the influence of co-solvents, such as salts, sugars, or chemical denaturants, on the CMC must not be neglected for both classes of detergents, ionic and non-ionic. The presence of urea, for instance, has been shown to increase the CMC of the non-ionic detergents Triton X-100 [78], *n*-decyl-β-D-maltoside (DM) [79], *n*-dodecyl-β-D-maltoside (DDM) [79], *n*-octyl-β-D-glucoside (OG) [79, 80], and octa(ethylene oxide) dodecyl ether ($C_{12}EO_8$) [80]. Moreover, a systematic analysis of the influence of urea on non-ionic detergents within the homologous series of alkyl maltosides, cyclohexyl alkyl maltosides, and alkyl glucosides revealed that the CMC increases exponentially with increasing urea concentration, whereas the micelle size shows a linear decrease [81]. Only above the CMC are detergents able to stabilise and solubilise membrane proteins, resulting in PDCs, which then co-exist with protein-free (mixed) micelles and detergent monomers [82]. The exact composition of these PDCs depends again on the type of detergent and its concentration [3–5].

Additional to the CMC, the so-called mean aggregation number is used to characterise detergent micelles. It represents the average number of monomers that form a micelle [83]. Typically, a micelle comprises five to several hundred detergent monomers, which assemble into structures in the range of a few nanometres [11]. Detergent micelles are often assumed to be homogeneous in size, but their molar masses are distributed around a

mean value with the mean micellar size and shape depending on the detergent's features and the experimental conditions used, similar to what is observed to occur with the CMC but less predictable [69]. There are several methods allowing the determination of aggregation numbers [84]. However, the exact values very often depend on the specific method and if mass- or number-average values are obtained. This clearly indicates that at least some micellar systems may be polydispers [70]. Like the CMC, the aggregation number is also influenced by co-solvents such as urea [81].

1.5 Methods for studying molar masses

Experimental determination of molar mass and oligomeric state is an essential step in the biochemical and biophysical characterisation of proteins and protein complexes and there are various methods to gain such information. Sodium dodecyl sulphate polyacrylamide gel electrophoresis (SDS-PAGE) is one technique that is routinely used in the purification of both water-soluble and membrane proteins to confirm their identity and their molar mass [85, 86]. To this end, the distance migrated by the protein of interest is compared with the migration of standard proteins of known size. However, membrane proteins often reveal a migration behaviour different from that of soluble proteins, thus impeding mass determination by standard SDS-PAGE [87]. An other widely used method is SEC. It can yield valuable information on sample homogeneity and oligomeric state of water-soluble proteins but is of limited use for detergent-solubilised proteins. Mass estimation by SEC is based on a comparison of the elution behaviour of the protein of interest with the elution of standard proteins, which are typically globular and water-soluble. Since detergent binding substantially alters a protein's hydrodynamic behaviour [88] and, thus, its apparent size, analysing membrane proteins with SEC will provide, at best, a very crude size estimate. Nevertheless, with careful sample preparation, information on the coexistence of different oligomeric species can be deduced from SEC elution profiles even without knowledge of exact masses [5]. Hence, SEC is widely used for the qualitative analysis of PDCs, for example, to check homogeneity, stability, and purity of PDCs for use in structural studies such as crystallography. As a complementary technique to SDS-PAGE and SEC, dynamic light scattering (DLS) provides information on the hydrodynamic radius of a PDC and helps in identifying aggregates [89, 90]. By observing time-dependent fluctuations in the scattered light intensity, the translational diffusion coefficient of particles that arises from the particle's random Brownian motion is determined. Consequently, the hydrodynamic radius can be deduced from the Stokes–Einstein equation [90–92]. Although DLS represents an absolute method for the determination of the hydrodynamic radius, it lacks, like SEC, the ability to distinguish between the contributions of detergent and protein to the overall hydrodynamic behaviour of the PDC. A well-established method to overcome this problem is analytical ultracentrifugation (AUC) [82, 93, 94], which combines separation of different species with thermodynamic analysis and, thus, is particularly suitable for mul-

ticomponent systems [95] such as detergent micelles and PDCs [96]. Drawbacks of AUC, however, comprise long experimental timescales of several hours up to a day, which restricts its applicability to relatively stable proteins [97], and difficulties encountered with detergents comprising similar density as the solvent, that is, floating detergents such as LDAO, which elude analysis by this method [98]. Moreover, AUC is an expensive method, and sample preparation, adequate measurement, and data analysis can only be performed by an experienced user [98].

1.6 Principles of triple-detection size-exclusion chromatography

As noted above, SEC is an established method for protein mass determination [99]. However, it is not suited for quantitative analysis of the mass of membrane proteins. Thereby, the main problem is the determination of a reliable calibration that relates elution volumes to masses [100]. By contrast, static LS (SLS) is an absolute method for molar mass determination. However, it cannot differentiate between scattering particles of different size but yields only average values. Thus, by combining SEC and SLS it is possible to overcome the calibration problem, at least, for homopolymers [100], and it allows for investigation of macromolecular mixtures.

1.6.1 Methods for size-based particle separation

SEC allows for separation of particles on the basis of their size or, more precisely, their hydrodynamic radius, and is one of the most popular separation techniques. For a detailed review of the technique, see reference [101]. Shortly, particle separation in SEC relies on the diverging diffusion behaviour of particles of different hydrodynamic volume while travelling through a porous matrix. SEC columns are packed with a resin of particles of defined size and porosity. For large solutes, less of the pores are accessible. Hence, they pass faster through the column as compared with smaller particles, because they are more excluded from the resin matrix. Once the particle size has reached a certain limit, all particles of this size or bigger are completely excluded from penetrating any pores. This size is referred to as the exclusion limit. The smaller the particles the more column volume is accessible, as a consequence smaller particles elute later.
The success of triple-detection techniques does not necessarily depend on the use of SEC, but any method separating particles based on their size is suitable. However, SEC is probably the most widespread separation technique in (membrane) protein research. For completeness, field-flow fractionation (FFF) as a second separation technique has to be mentioned. The development of this technique has given cause to the appearance of asymmetric-flow field-flow fractionation (AF4) [102] and centrifugal field-flow fractionation (CF3) [103] as alternatives to SEC [104]. Unlike SEC, where separation relies on

differential diffusion through a porous matrix, FFF uses a flow field to separate different species. A so-called cross flow produces a stream of mobile phase that is applied perpendicularly to a channel flow that transports particles along a channel. By variation of the strength of the cross flow and the ratio of cross and channel flows, elution time of different particles and separation range and resolution of the channel can be adjusted [102, 105]. In general, FFF provides a broader separation range, which is translated in a better particle-size resolution than SEC and is more easily adaptable to specific sample requirements. In particular, this technique prevents the sample from interacting with column material, minimises sample loss, and is particularly suited for samples containing particles of very different sizes [104, 106]. However, sample dilution is even more pronounced than in SEC, and to achieve good separation results, some effort must usually be invested into optimising experimental conditions.

1.6.2 Triple-detection

For triple-detection measurements, SEC is coupled to a detector system consisting of ultraviolet (UV) absorbance, SLS, and refractive index (RI) detection. Thus, sample separation and analysis are combined in one single experimental setup. **Figure 4** shows a schematic setup with SEC being used exclusively for the preparative separation of different species such as detergent micelles and PDCs but not for analytical purposes, in particular, determination of molar masses. Thus, in contrast with conventional approaches, quantitative analysis does not rely on elution volumes, avoiding the need of calibration. Instead, the LS signal provides information on the molar masses of all scattering particles eluted in the course of an SEC run according to the Zimm equation [107]:

$$\Delta R_\Theta = Kc(MP_\Theta - 2A_2M^2cP_\Theta^2 + ...) \tag{1}$$

Here, ΔR_Θ is the so-called excess Rayleigh ratio, that is the Rayleigh ratio of the sample minus that of the solvent. The Rayleigh ratio is defined as the total intensity (I_Θ) of scattered light observed at an scattering angle Θ at distance r from the point of scattering, normalised with respect to the scattering volume V and the incident light intensity I_0:

$$R_\Theta = \frac{I_\Theta r}{I_0 V} \tag{2}$$

Furthermore, K is an optical constant, M the molar mass of the scattering particle in solution or suspension, and c its concentration. A_2 represents the second virial coefficient, which is the first and most important term accounting for interparticle interactions. P_Θ is the so-called particle scattering function, which reflects the angular dependency of the scattering intensity.

Coupling SLS with SEC leads to dilution of the sample to concentrations at which intermolecular interactions and, thus, the second term in parenthesis on the right-hand

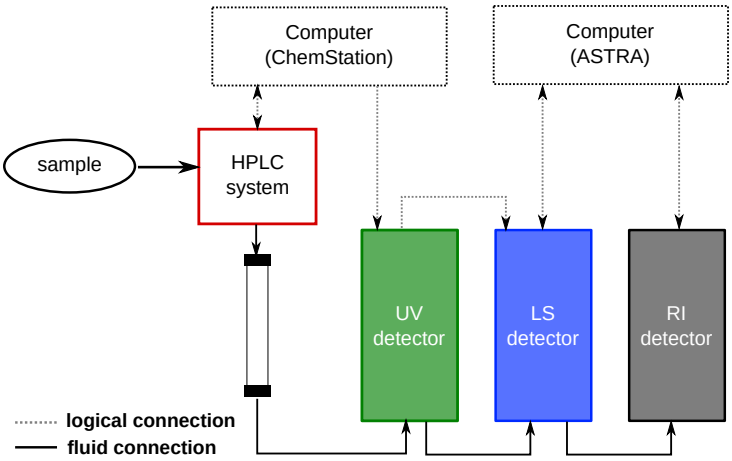

Figure 4: Schematic setup of triple-detection SEC. A liquid chromatography system is used to provide constant flow and an SEC column to separate different species. UV absorbance and RI detectors monitor changes in protein and detergent concentrations, while the LS detector follows changes in scattering intensity at multiple scattering angles. Data acquisition is controlled by a detector-dependent software package. Adapted and reprinted with permission from ref. [108].

side of **Equation 1** can safely be neglected. Moreover, in the so-called Rayleigh scattering regime, which is applicable for particles that are small in diameter (i.e., below $\lambda/20$) compared to the wavelength used (λ), scattering is isotropic. Thus, ΔR_Θ becomes angle-independent, and P_Θ approaches unity. This simplifies **Equation 1** to:

$$\Delta R = KMc \tag{3}$$

For vertically polarised light, K is given by

$$K = \frac{4\pi \left(\frac{\mathrm{d}n}{\mathrm{d}c}\right)^2 n_0^2}{N_\mathrm{A}\lambda_0^4} \tag{4}$$

where $\mathrm{d}n/\mathrm{d}c$ is the refractive index increment of the scattering particle, n_0 the refractive index of the solvent, N_A Avogadro's number, and λ_0 is the vacuum wavelength of the incident light.

For membrane proteins solubilised in detergent micelles, the accessible values of the $\mathrm{d}n/\mathrm{d}c$, c, and M refer to the entire PDC (comp). These quantities are related to those of pure protein (prot) and detergent (det) by the mass ratio of bound detergent to protein δ through the following equations:

$$M_\mathrm{comp} = (1+\delta) M_\mathrm{prot} \tag{5}$$

$$c_\mathrm{comp} = (1+\delta)\, c_\mathrm{prot} = \frac{\Delta \mathrm{UV}_{280\ \mathrm{nm}}}{\left(\left(\frac{1}{1+\delta}\right) A_{280\ \mathrm{nm,prot}} + \left(\frac{\delta}{1+\delta}\right) A_{280\ \mathrm{nm,det}}\right)} \tag{6}$$

and

$$\left(\frac{\mathrm{d}n}{\mathrm{d}c}\right)_{\mathrm{comp}} = \frac{\Delta\mathrm{RI}}{\Delta\mathrm{UV}_{280\ \mathrm{nm}}}\left(\left(\frac{1}{1+\delta}\right)A_{280\ \mathrm{nm,prot}} + \left(\frac{\delta}{1+\delta}\right)A_{280\ \mathrm{nm,det}}\right) \tag{7}$$

where $\Delta\mathrm{UV}_{280\ \mathrm{nm}}$ is the background-corrected UV absorbance signal, $A_{280\ \mathrm{nm}}$ is the absorbance coefficient at 280 nm (in ml/(g cm)), and ΔRI is the excess refractive index, that is the background-corrected refractive index of the sample minus that of the solvent.
Generally, δ is not known but can be calculated from measured quantities on the basis of the refractive index increments of the protein and the detergent $(\mathrm{d}n/\mathrm{d}c)_{\mathrm{prot}}$ and $(\mathrm{d}n/\mathrm{d}c)_{\mathrm{det}}$, respectively,

$$\delta = \frac{\left(\frac{\Delta\mathrm{RI}A_{280\ \mathrm{nm,prot}}}{\Delta\mathrm{UV}}\right) - \left(\frac{\mathrm{d}n}{\mathrm{d}c}\right)_{\mathrm{prot}}}{\left(\frac{\mathrm{d}n}{\mathrm{d}c}\right)_{\mathrm{det}} - \left(\frac{\Delta\mathrm{RI}A_{280\ \mathrm{nm,det}}}{\Delta\mathrm{UV}}\right)} \tag{8}$$

On the basis of **Equation 3**, the molar mass of the PDC can be determined and subsequent determination of δ allows decomposition into protein and detergent contributions. A more detailed review on LS theory and analysis of PDCs by triple-detection SEC can be found in **Section 2**.

1.7 Goals

The main goals of this thesis were:

- to establish triple-detection SEC for the use with high detergent and denaturant concentrations;
- to systematically characterise different detergent micelles regarding descriptive properties such as aggregation number, root-mean square radius, and shape in aqueous and urea-containing conditions;
- to determine the composition of PDCs under native and denaturing conditions.

To this end, it was essential to validate the performance of the triple-detection SEC setup in the presence of detergent and urea with well-known and well-characterised samples like the water-soluble protein bovine serum albumin (BSA), DDM micelles, and OmpLA–LDAO complexes. To allow for systematic analysis of detergent properties, the focus was directed at a homologous series with the same head group but with different alkyl-chain lengths and a detergent comprising a fluorocarbon instead of a hydrocarbon chain, which self-assembles into extended rod-shaped instead of spherical micelles. This enabled the systematic investigation of the role that detergents with different alkyl chain lengths exert on the aggregation behaviour and of micelle shape. Since Mistic has been shown

to completely unfold in the presence of denaturing agents, it was an ideal candidate to examine if the unfolded state, which was assumed as common reference state, is truly deprived of detergent.

2 Theory

2.1 Static light scattering

LS is based on the interaction of light with matter. Generally, all scattering processes are characterised by energy and momentum conservation but energy and momentum can be exchanged between all scattering partners. Depending on whether energy is transferred from the photon to internal degrees of freedom (Q) of the particle or not during this interaction, one distinguishes between inelastic and elastic scattering. Assuming an initially resting particle, the energy conservation of a scattering process is described by

$$\hbar c k_{\mathrm{i}} = \hbar c k_{\mathrm{f}} + \frac{1}{2} m v_{\mathrm{f}}^2 + Q \tag{9}$$

with $\hbar$ being the reduced Planck constant, c the speed of light, and m and v the mass and the velocity of the particle after the scattering. The absolute value of the wave vector $k = |\vec{k}|$ of the initial (i) or scattered (f) photon is given by

$$k = \frac{2\pi}{\lambda} \tag{10}$$

with λ being the wavelength.
In inelastic processes like Raman scattering, a loss of energy between incident and scattered light occurs because energy is transferred to the particle during the scattering process. The wavelength of the incident light is smaller than the wavelength of the scattered light. By contrast, in elastic scattering, the photon energy is conserved, and the frequencies or wavelengths of incident and scattered light are identical. In the framework of this thesis, I will focus on elastic scattering and, in particular, on SLS.
A full quantum-mechanical treatment of the scattering process would involve solving the Schrödinger equation for an ingoing plane wave and an outgoing radial wave. However, a detailed consideration is beyond the scope of this thesis but can be found in any basic physics textbook like, for example, reference [109]. From a semi-classical viewpoint, light can be described as an oscillating electro-magnetic field. Upon interaction with a neutral molecule, the oscillating field induces an oscillating dipole. The induced dipole itself now also emits electro-magnetic waves with properties depending on the molecule properties. This allows the characterisation of the molecule by analysing the scattered light and, thus, is the basis of all light scattering experiments. The ability of a molecule to be polarised and, thereby, to act as a dipole, depends on the ability of its electrons to be displaced

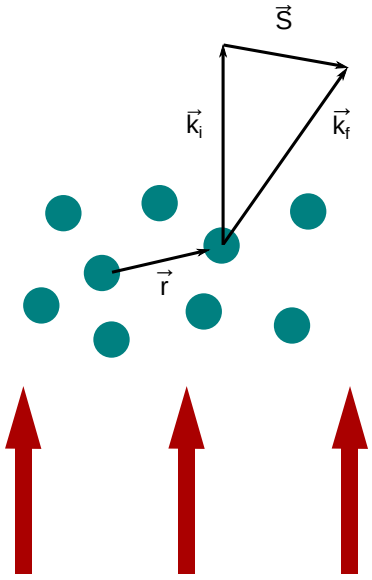

Figure 5: Geometrical relations between light and scattering system. Scattering particles in a volume V are depicted in distance $\vec{r}$ from each other with $\vec{k}_\mathrm{i}$ and $\vec{k}_\mathrm{f}$ being the unit vectors in the direction of the incident and the scattered light, respectively. The vector difference between the two unit vectors is $\vec{s}$.

from the equilibrium. A measure of this ability is the so called polarisability, which is directly proportional to $\mathrm{d}n/\mathrm{d}c$ [92].

Complementary to the phenomena described above, particles in solution are not isolated molecules but have to be treated as ensemble. The basic principle of oscillating dipoles is still applicable, but the observed scattered light is a superposition of the light emitted by all dipoles. Two important experimental approaches rely on elastic light scattering of ensembles. DLS that measures time-dependent scattered light intensity fluctuations, which are caused by random Brownian motion of the scattering particles, and by contrast, SLS that measures time-averaged scattering intensities at one or more scattering angles Θ. Generally, the theory presented in the following will focus on SLS.

The theoretical foundation of LS from macromolecular solutions were established by the works of Debye in 1944 [110] and Zimm from 1945–1948 [107, 111–113] and reviewed by Wyatt in 1993 [114]. In their considerations, each molecule is assumed to consist of η elements that are distributed within the molecule according to a distribution function $\rho(r)$. Each element is treated as a simple dipole scatterer that is excited and scatters independently of any other element of the molecule. This is generally true for most molecules in solution. The net scattering of the whole molecule into a direction Θ is obtained by simple summation over all elements. In addition, it is assumed that the particle solution contains N molecules in a volume V. As for the single elements, the net scattering of all particles in the solution into the direction Θ is described by summation over all molecules. As a result of this treatment, the excess scattering intensity or Rayleigh ratio (ΔR_Θ) at a given angle of a dilute solution upon illumination by a parallel beam of light is given by [107, 114]:

$$\Delta R_\Theta = \frac{K\eta^2 N^2}{V^2} \int \rho(r)\, \mathrm{e}^{-i\left(\vec{k}_\mathrm{f}-\vec{k}_\mathrm{i}\right)\vec{r}}\mathrm{d}^3 r = \frac{K\eta^2 N^2}{V^2} \int \rho(r)\, \mathrm{e}^{-i\vec{s}\cdot\vec{r}}\mathrm{d}^3 r \tag{11}$$

where Θ is the angle between incident and scattered light and $\vec{s}$ the vector difference

between the unit vectors in direction of the incident ($\vec{k}_\mathrm{i}$) and the scattered ($\vec{k}_\mathrm{f}$) light with a magnitude of $2\sin\left(\frac{\Theta}{2}\right)$ (**Figure 5**). The integration is performed over all orientations and magnitudes of $\vec{r}$ at constant $\vec{s}$.

Equation 11 holds only in the Rayleigh–Gans–Debye approximation, which considers that the incident light wave is essentially unaffected by the scattering molecule. Thus, the described theory is only valid if

$$|\frac{n}{n_0} - 1| \ll 1 \tag{12}$$

and

$$2ka \ll 1 \tag{13}$$

are satisfied. Here, n/n_0 is the ratio of the refractive index of the solvated molecule (n) relative to the refractive index of the solvent (n_0), $2a$ is the characteristic diameter of the molecule, and $k = {}^{2\pi n_0}/_{\lambda_0}$. The first inequality (**Equation 12**) corresponds to the condition that n is almost indistinguishable from n_0. The second inequality (**Equation 13**) represents the so-called dipole approximation and describes the assumption that the dimensions of the particle are considerably smaller than the wavelength. Hence, the dipole experiences no spatial variations in the electro-magnetic potential.

The excess scattering of a molecular solution depends on the radial distribution of dipole elements. This distribution can be separated into internal and external contributions, even for dilute solutions [107]. The internal part of the distribution function (ρ_int) refers to two elements in the same molecule, whereas the external contribution (ρ_ext) refers to elements in two different molecules and has to be normalised for the particle density. Hence,

$$\rho\left(r\right) = \left[\rho_\mathrm{int}\left(r\right) + \frac{N\rho_\mathrm{ext}\left(r\right)}{V}\right] \tag{14}$$

with both parts, internal (int) and external (ext), contributing to ΔR_Θ. The internal part can be represented in terms of the normalised intensity distribution function or particle scattering function P_Θ [107], which is defined as

$$P_\Theta = \int \rho_\mathrm{int}\left(r\right) \mathrm{e}^{-i\vec{s}\cdot\vec{r}} \mathrm{d}^3 r \tag{15}$$

In order to define an expression for the external part, two assumptions have to be made. First, two molecules mainly interact at only one point with each other (single contact assumption) [111]. And second, only highly diluted samples are considered. Thus, the expression for LS is valid to the second order of c. On the basis of these two considerations, Zimm [107] showed that the external probability contributes to the scattering by

$$\int \rho^*_\mathrm{ext}\left(r\right) \mathrm{e}^{-i\vec{s}\cdot\vec{r}} \mathrm{d}^3 r = \eta^2 X P^2_\Theta \tag{16}$$

where $\rho^*_{\text{ext}}(r)$ is the limit of $\rho_{\text{ext}}(r)$ as c approaches 0, and X is an integral representing short range interactions between pairs of elements.
Combining **Equations 11** and **14–16**, yields the basic light scattering relation [113] already presented in **Section 1.6.2**:

$$\Delta R_\Theta = KMc\left(P_\Theta + A_2 P_\Theta^2 c\right) \tag{17}$$

where A_2 is given by

$$A_2 = \frac{-N_\text{A}\eta^2 X}{2M^2} \tag{18}$$

For dilute solutions, terms that contain concentration contributions of higher order can be neglected. This can be safely assumed in all applications including SEC. Thus, **Equation 17** can be reduced to

$$\Delta R_\Theta \approx KMcP_\Theta \tag{19}$$

Additionally, P_Θ approaches unity if Θ approaches 0. Thus, for small angles **Equation 17** further simplifies to

$$\Delta R_\Theta \approx KMc \tag{20}$$

Generally, **Equation 20** also holds for dilute solutions of isotropically scattering particles, where the scattering intensity is direction-independent.
If more than a single molar mass species is present in the sample, M has to be replaced by the mass-average molar mass M_w (**Section 2.3**). Thus within the above mentioned approximations, M_w of any isotropically scattering particle in a dilute solution can be derived by

$$M_w = \frac{\Delta R_\Theta}{Kc} \tag{21}$$

In practice, ΔR_Θ of light scattered from a small volume V into a detector, which is set at an angle Θ with respect to the incident light, and collecting light scattered into a solid angle $\mathrm{d}\Omega$, might be expressed by means of light intensities as measured quantities:

$$\Delta R_\Theta = f\frac{\left[I(\Theta) - I_\text{sol}(\Theta)\right]}{I_0} \tag{22}$$

where $I(\Theta)$ is the intensity of light scattered by the sample, $I_\text{sol}(\Theta)$ is the intensity of light scattered by the pure solvent (sol), I_0 is the incident light intensity per unit projected area of V, and f is an absolute calibration constant derived from the detector geometry [100].

2.2 Multi-component systems

For scattering particles that are composed of two different molecular components like PDCs, both components contribute differently to all three detector signals, and the derived masses and concentrations refer to the entire complex. Thus, **Equation 20** can be rewritten as

$$\Delta R_\Theta = KMc = KM_{\text{comp}}c_{\text{comp}} \tag{23}$$

Then, the total mass of an PDC can be determined by

$$M_{\text{comp}} = \frac{\Delta R_\Theta}{Kc_{\text{comp}}} \tag{24}$$

The use of two concentration-sensitive detectors, which posses differential sensitivity towards detergent and protein concentrations, allows for concentration determination of each of the two components and, thus, their contribution to the entire complex. Conventionally in protein research, SEC is equipped with a concentration-sensitive UV absorbance detector, monitoring the solute concentration in the effluent. In triple-detection SEC, an RI detector acts as second concentration detector [17].

Absorption is caused by the excitation of electronic states in molecules. If a molecule contains π- or non-bonding electrons, these can be excited by absorbing light in the UV range. The absorption of proteins is caused by the three amino acids Trp, Tyr, and Phe, which posses delocalised π-electrons because of their aromatic ring structure and, thus, account for the an absorption maximum at 280 nm. An absorbance detector measures the absorbance (UV_λ) of the eluate, which is defined as the logarithm of the ratio of the intensities of the incident light and the transmitted light (I):

$$\text{UV}_\lambda = log\left(\frac{I_0}{I}\right) \tag{25}$$

According to Lambert and Beer, the fraction of radiation that is absorbed is independent of the intensity, and the amount of absorbed light is proportional to the amount of absorbing molecules. This can be translated into the Lambert–Beer law [115] that correlates absorbance and concentration the following:

$$\text{UV}_\lambda = log\left(\frac{I_0}{I}\right) = cA_\lambda L, \tag{26}$$

with A_λ being the absorbance coefficient at a certain wavelength λ and L the length of the measurement cell. For proteins, the absorbance coefficient at 280 nm ($A_{280\,\text{nm}}$) can be predicted directly from the amino acid sequence [116]. By contrast, many detergents commonly used in membrane-protein research, like the alkyl maltoside series, do not absorb in the UV range.

However, proteins and detergents do cause an RI signal with concentration-dependent in-

tensity. Concentration determination by RI detection uses the (mostly) linear dependence of the RI on the concentration. A higher solute concentration increases the RI according to:

$$n = n_0 + c\left(\frac{\mathrm{d}n}{\mathrm{d}c}\right) \tag{27}$$

By measuring the difference in RI between pure solvent and solute-containing solvent, one can determine the solute concentration as follows:

$$\Delta\mathrm{RI} = n - n_0 = \left(\frac{\mathrm{d}n}{\mathrm{d}c}\right) c \tag{28}$$

For multi-component complexes, the RI and UV signals contain contributions of all components. The detector responses in dependence on the concentration of, for example, a protein–detergent system are given by:

$$\Delta\mathrm{RI} = c_{\mathrm{comp}}\left(\left(\frac{\mathrm{d}n}{\mathrm{d}c}\right)_{\mathrm{prot}} w_{\mathrm{prot}} + \left(\frac{\mathrm{d}n}{\mathrm{d}c}\right)_{\mathrm{det}} w_{\mathrm{det}}\right) \tag{29}$$

and

$$\Delta\mathrm{UV} = A_{280\ \mathrm{nm,prot}} c_{\mathrm{prot}} + A_{280\ \mathrm{nm,det}} c_{\mathrm{det}} \tag{30}$$

where $w_{\mathrm{prot}} = c_{\mathrm{prot}}/c_{\mathrm{comp}}$ and $w_{\mathrm{det}}{=}c_{\mathrm{det}}/c_{\mathrm{comp}}$ the weight fractions and $A_{280\ \mathrm{nm,prot}}$ and $A_{280\ \mathrm{nm,det}}$ the absorbance coefficients of pure protein and pure detergent, respectively. The $\mathrm{d}n/\mathrm{d}c$ of an PDC can be expressed in terms of the $\mathrm{d}n/\mathrm{d}c$ of pure detergent and pure protein as

$$\left(\frac{\mathrm{d}n}{\mathrm{d}c}\right)_{\mathrm{comp}} = \left(\frac{\mathrm{d}n}{\mathrm{d}c}\right)_{\mathrm{prot}} w_{\mathrm{prot}} + \left(\frac{\mathrm{d}n}{\mathrm{d}c}\right)_{\mathrm{det}} w_{\mathrm{det}} \tag{31}$$

thus allowing to rewrite **Equation 29** as

$$\Delta\mathrm{RI} = c_{\mathrm{comp}}\left(\frac{\mathrm{d}n}{\mathrm{d}c}\right)_{\mathrm{comp}} \tag{32}$$

The chemical composition, that is, the relative component ratio, is obtained from the ratio between ΔRI and ΔUV.

$$\frac{\Delta\mathrm{RI}}{\Delta\mathrm{UV}} = \frac{c_{\mathrm{comp}}\left(\left(\frac{\mathrm{d}n}{\mathrm{d}c}\right)_{\mathrm{prot}} w_{\mathrm{prot}} + \left(\frac{\mathrm{d}n}{\mathrm{d}c}\right)_{\mathrm{det}} w_{\mathrm{det}}\right)}{A_{280\ \mathrm{nm,prot}} c_{\mathrm{prot}} + A_{280\ \mathrm{nm,det}} c_{\mathrm{det}}} \tag{33}$$

Because there are only two components in the studied complex, the sum of their weight fractions must equal unity, that is, $w_{\mathrm{prot}} + w_{\mathrm{det}} = 1$ and w_{det} can be rewritten as $1 - w_{\mathrm{prot}}$,

so that

$$\frac{\Delta \mathrm{RI}}{\Delta \mathrm{UV}} = \frac{\left(\frac{\mathrm{d}n}{\mathrm{d}c}\right)_{\mathrm{prot}} w_{\mathrm{prot}} + \left(\frac{\mathrm{d}n}{\mathrm{d}c}\right)_{\mathrm{det}} (1 - w_{\mathrm{prot}})}{A_{280\ \mathrm{nm,prot}} w_{\mathrm{prot}} + A_{280\ \mathrm{nm,det}} (1 - w_{\mathrm{prot}})} \tag{34}$$

Solving **Equation 34** for w_{prot} and calculating the ratio of w_{det} to w_{prot} yields δ as given in **Equation 8** in **Section 1.6.2**. This enables the determination of the contributions of protein and detergent to the total concentration, mass, and refractive index increment by **Equations 5–7** (**Section 1.6.2**) and, thus, a complete characterisation of the composition of PDCs.

2.3 Mass and size distribution

2.3.1 Molar-mass averages

In comparison with low-molar-mass compounds or proteins, macromolecules like detergents or polymers cannot be assigned to a single molar mass but show a distribution in mass and radius [92, 117]. The rate of occurrence of particular molar masses in a sample is described by the molar mass distribution that can be represented graphically by distribution curves and mathematically by distribution functions [92]. The molar mass distribution permits different averaging modes that will be briefly discussed in the following [117].

Number-average molar mass (M_n): The number-average molar mass (M_n) is the arithmetic mean and is given by

$$\bar{M_n} = \sum x_i M_i \tag{35}$$

where x_i is the mole fraction of molecules with mass M_i. x_i can be expressed as the ratio of the number of molecules (N_i) with mass M_i to the total number of molecules ($N = \sum N_i$)

$$x_i = \frac{N_i}{\sum N_i} = \frac{N_i}{N} \tag{36}$$

By applying **Equation 36**, M_n can be rewritten as

$$\bar{M_n} = \sum M_i \frac{N_i}{N} = \frac{\sum N_i M_i}{\sum N_i} = \frac{\sum c_i}{\sum \frac{c_i}{M_i}} \tag{37}$$

The last equality sign is based on the fact that the molal concentration of the i^{th} component is proportional to $n_i M_i$ [114].

Mass-average molar mass (M_w): The mass-average molar mass (M_w) is given by

$$\bar{M_w} = \sum w_i M_i \tag{38}$$

with w_i being the weight fraction of molecules with mass M_i. M_w relates the mass of all molecules with mass M_i ($N_i M_i$) to the total mass of all molecules $\sum N_i M_i$. Hence, analogous to x_i, one can write:

$$w_i = \frac{N_i M_i}{\sum N_i M_i} \tag{39}$$

Thus,

$$\bar{M_w} = \frac{N_i M_i^2}{\sum N_i M_i} = \frac{\sum c_i M_i}{\sum c_i} \tag{40}$$

***z*-average molar mass (M_z):** The z-average molar mass (M_z) (z stands for centrifugation; ger. *Zentrifuge*) is accessed by diffusion-based techniques like DLS or sedimentation-equilibrium measurements in AUC and is given by:

$$\bar{M_z} = \frac{\sum N_i M_i^3}{\sum N_i M_i^2} = \frac{\sum w_i M_i^2}{\sum w_i M_i} = \frac{\sum c_i M_i^2}{\sum c_i M_i} \tag{41}$$

Separation by SEC directly provides the size distribution curve of a sample. Although broadening effects may cause mixing of different mass species [100], it is generally assumed that each slice of the chromatogram contains molecules of a single or at least very narrowly distributed molar mass M_i. Hence, after separation the effective molar mass of a peak can be calculated following **Equations 37–41** [100, 114]. Due to the definitions of the different averages, the mutual relation of molar-mass averages is [117]:

$$\bar{M_n} < \bar{M_w} < \bar{M_z}$$

For non-disperse samples, the different molar-mass averages are identical [92]. In disperse samples, the homogeneity or heterogeneity of the mass distribution, which is reflected by the broadness of the distribution, is measured by the so-called polydispersity P and is calculated as the ratio of M_w to M_n [106, 118].

$$P = \frac{\frac{\sum c_i M_i}{\sum c_i}}{\frac{\sum c_i}{\sum \frac{c_i}{M_i}}} = \frac{\sum c_i M_i}{\sum c_i} \frac{\sum \frac{c_i}{M_i}}{\sum c_i} \tag{42}$$

If M_i is constant over the entire distribution, P approaches unity and indicates that the sample is homogeneous in mass.

2.3.2 Mean square radius

A second quantity that is often used to characterise a particle is the mean square radius R^2_{RMS}. It is a measure of a molecule's size weighted by the mass distribution around its centre of mass. For R^2_{RMS} a similar set of expressions like that for the different molar mass averages can be defined. However, the equations are not analogous. This is mainly caused by the fact that the molar-mass values directly provided by SLS measurements are mass-average values, whereas the mean square radius is obtained as z-average [119].

The **number-average mean square radius** ($R^2_{\mathbf{RMS},n}$) is given by

$$R^2_{\mathrm{RMS},n} = \frac{\frac{\sum R^2_{\mathrm{RMS,i}} c_i}{M_i}}{\sum \frac{c_i}{M_i}} \tag{43}$$

where M_i and $R^2_{\mathrm{RMS,i}}$ are molar mass and mean square radius of the i^{th} slice of concentration c_i of the distribution.

The **mass-average mean square radius** ($R^2_{\mathbf{RMS},w}$) is

$$R^2_{\mathrm{RMS},w} = \frac{\sum R^2_{\mathrm{RMS,i}} c_i}{\sum c_i} \tag{44}$$

and the ***z*-average mean square radius** ($R^2_{\mathbf{RMS},z}$) is given through

$$R^2_{\mathrm{RMS},z} = \frac{\sum R^2_{\mathrm{RMS,i}} c_i M_i}{\sum c_i M_i} \tag{45}$$

Both molar mass and mean square radius averages show differential sensitivities to low and high molar mass species depending on the averaging mode. Number averages are mainly sensitive to low-molar-mass fractions, whereas mass- and, to an even greater extend, z-averages are mainly sensitive to high-molar-mass fractions. That is especially important in analysing SLS data for mass and radius since the direct measures, $R^2_{\mathrm{RMS},z}$ and M_w are not identical regarding their averaging mode. However, results derived for the radius are more affected by high-molar-mass contributions than the corresponding mass values.

2.4 Conformation analysis

Particles that are larger than $\lambda/20$ in diameter, which is $\sim$35 nm for the setup used within this thesis, do not scatter isotropically but exhibit an angle-dependent scattering intensity. The exact scattering profile does not only depend on the size of the particle but also on its shape [107]. Therefore, the simplified expression for the scattering intensity (**Equation 20**) is no longer applicable, but the contribution of P_Θ has to be considered (**Equation 19**).

A general definition of P_Θ is given in **Equation 16**. For small angles this expression can be approximated to [92]

$$\lim_{\Theta \to 0} P_\Theta = 1 - \frac{16\pi^2}{3\lambda^2} R_{\mathrm{RMS}}^2 \sin^2\left(\frac{\Theta}{2}\right) \tag{46}$$

According to **Equation 46**, the plot of P_Θ against $\sin^2\left(\frac{\Theta}{2}\right)$ yields a straight line with the slope proportional to R_{RMS}^2. Hence, at $\Theta = 0$, the slope of the angle-dependent variation of the scattering intensity accounts for the root mean square radius (R_{RMS}). Information about the R_{RMS} of the scattering particles can be revealed only from the measurement of the angular variation of the scattering intensity and, thus, only for particles that are big enough to exhibit anisotropic scattering. The particle scattering function was calculated for various particle geometries, such as random coils, spheres, and rods [113, 114]. In principle, particle shapes can be determined by comparison of an experimentally determined scattering function and the calculated one. However, the estimation of the particle shape from the scattering function is limited by the fact that comparison of experimental and theoretical data requires a wide range of P_Θ values. Typically, this is given only for very large particles. For a more detailed description, see reference [92].
However, the rather limited ability of SLS to characterise shape and conformation of macromolecules can be enhanced by combination with a separation technique as given in triple-detection SEC. This provides the possibility to relate R_{RMS} and molar mass data. The so-called conformation plot is probably the most common method to determine the conformation of a scattering particle from the relation between R_{RMS} and M_w. For simple one-, two-, or three-dimensional objects like rigid rods, thin flat disks, or homogeneous spheres of constant density the relation between size and mass is given by the Euclidean dimension d. This means that for rigid rods, the mass scales with the first power of the radius of a circle circumscribing the rod ($d = 1$). The mass of a thin flat disk scales with the second power of the disk's radius ($d = 2$) and the mass of a hard sphere with the third power of the sphere's radius ($d = 3$) [101]. In general, this relation can be expressed by

$$R_{\mathrm{RMS}} = k M_w^{1/d} = k M_w^{\alpha} \tag{47}$$

which is the basis for LS-based conformation determination by a conformation plot. For this purpose, **Equation 47** is linearised as

$$\log R_{\mathrm{RMS}} = \alpha \log M_w + \log k \tag{48}$$

resulting in a log–log plot with α being the slope and, thus, indicative for the particle conformation. According to the relations described above, α varies between 0.33 for hard spheres, 0.5 for hollow spheres, ∼0.5–0.6 for linear random coils, and 1 for rigid rods [120].

3 Materials

3.1 Chemicals and enzymes

Agar-agar, ammonium hydroxide solution 32%, bacto-tryptone, BSA, $CaCl_2$, 1,4-dithio-DL-threitol (DTT), ethylenediamine tetraacetic acid (EDTA), HCl, imidazole, isopropyl-β-D-thiogalactopyranoside (IPTG), NaOH, peptone, sodium dodecyl sulphate (SDS), tris(hydroxymethyl)aminomethane (Tris), and yeast extract were from Carl Roth (Karlsruhe, Germany). Enterokinase (EK) and hydrochloric acid were purchased from Merck-Millipore (Darmstadt, Germany). *n*-dodecyl-*N*,*N*-dimethylamine-*N*-oxide (LDAO) was from Sigma–Aldrich (Steinheim, Germany). AnalaR Normapure NaCl was purchased from VWR International (Darmstadt, Germany). Benzonase and EDTA-free Complete were from Roche Applied Sciences (Penzberg, Germany). Urea was obtained from Affymetrix (High Wycombe, UK). *n*-nonyl-β-D-maltoside (NM), *n*-decyl-β-D-maltoside (DM), *n*-undecyl-β-D-maltoside (UM), and *n*-dodecyl-β-D-maltoside (DDM) were purchased from Glycon Biochemicals (Luckenwalde, Germany). Tridecafluoro-*n*-octyl-β-D-maltoside (F_6OM) was from Anatrace (Maumee, USA). Chloroform, ethanol (EtOH), and methanol were purchased from various companies. All chemicals were purchased in the highest available quality.

3.2 Proteins

3.2.1 Mistic

The nominal molar mass of Mistic is 12.8 kg/mol, the molar extinction coefficient at 280 nm is $\varepsilon_{280\,\mathrm{nm}} = 8480\,1/(\mathrm{M\,cm})$, and the absorbance coefficient at 280 nm is $\mathrm{Abs}_{280\ \mathrm{nm}} = 661\,\mathrm{mL}/(\mathrm{g\,cm})$ (ExPASy ProtParam http://expasy.org/tools/protparam.html was used to calculate all values). The refractive index increment is $\mathrm{d}n/\mathrm{d}c = 0.187\,\mathrm{mL/g}$ according to calculations with SEDFIT https://sedfitsedphat.nibib.nih.gov/default.aspx, which are based on the amino acid sequence. The amino acid sequence is:

M F C T F F E K H H R K W D I L L E K S T G V M E A M K V T S E E
K E Q L S T A I D R M N E G L D A F I Q L Y N E S E I D E P L I Q
L D D D T A E L M K Q A R D M Y G Q E K L N E K L N T I I K Q I L
S I S V S E E G E K E

3.2.2 OmpLA

The nominal molar mass of mature OmpLA is 30.8 kg/mol, $\varepsilon_{280\,\mathrm{nm}} = 82280\,1/(\mathrm{M\,cm})$, $\mathrm{Abs}_{280\,\mathrm{nm}} = 2667\,\mathrm{mL}/(\mathrm{g\,cm})$ (all values were calculated using ExPASy ProtParam), and $\mathrm{d}n/\mathrm{d}c = 0.194\,\mathrm{mL/g}$ according to amino acid sequence based calculations with SEDFIT. The amino acid sequence of the mature protein is:

Q E A T V K E V H D A P A V R G S I I A N M L Q E H D N P F T L Y
P Y D T N Y L I Y T Q T S D L N K E A I A S Y D W A E N A R K D E
V K F Q L S L A F P L W R G I L G P N S V L G A S Y T Q K S W W Q
L S N S E E S S P F R E T N Y E P Q L F L G F A T D Y R F A G W T
L R D V E M G Y N H D S N G R S D P T S R S W N R L Y T R L M A E
N G N W L V E V K P W Y V V G N T D D N P D I T K Y M G Y Y Q L K
I G Y H L G D A V L S A K G Q Y N W N T G Y G G A E L G L S Y P I
T K H V R L Y T Q V Y S G Y G E S L I D Y N F N Q T R V G V G V M
L N D L F

3.3 Detergents

Table 1 depicts characteristics of the detergents used in this study. The CMCs were taken from Broecker and Keller [81] and Frotscher et. al. [74]. Detailed information on structural properties of the detergents used in this thesis is summarised in **Figure 6**.

Table 1: Characteristics of detergents used in this study. CMCs from [81] and [74] in 50 mM Tris at pH 7.4 and 50 mM NaCl. The CMC of F_6OM was determined in H_2O. Tail length refers to the number of C-atoms in the tail. abbr., abbreviation.

detergent	abbr.	type	tail length (no. of C-atoms)	CMC (mM) buffer	CMC (mM) 8 M urea
n-nonyl-β-D-maltoside	NM	nonionic	9	6.85	24.6
n-decyl-β-D-maltoside	DM	nonionic	10	2.03	8.78
n-undeycl-β-D-maltoside	UM	nonionic	11	0.59	3.24
n-dodecyl-β-D-maltoside	DDM	nonionic	12	0.15	1.08
n-dodecyl-*N*,*N*-dimethyl-amine-*N*-oxide	LDAO	zwitterionic	12	1.8	–
tridecafluoro-*n*-octyl-β-D-maltoside	F_6OM	nonionic	8	0.7	–

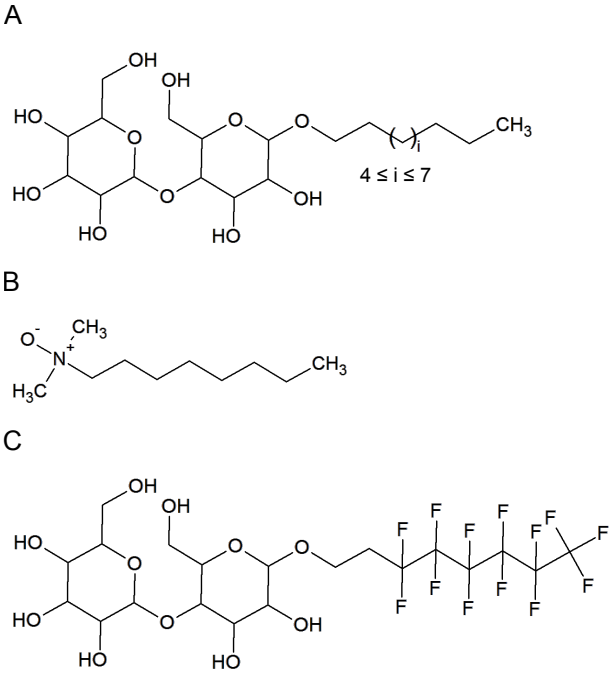

Figure 6: Structures of the detergents used in this study. (A) Alkyl maltosides consist of a maltose head group and a linear alkyl chain. Detergents with tails comprising 9–12 carbon atoms were used in this thesis. (B) LDAO consists of a zwitterionic dimethylamineoxid head group and a linear alkyl chain with 12 carbon atoms. (C) F_6OM consists of a maltose head group and a linear alkyl chain with 8 carbon atoms of which six are fluorinated.

4 Methods

4.1 Preparation of denaturants

Urea stock solutions were prepared in triple-distilled water by weight. Dissolved urea was deionized for 1 h with Amberlite IRN-150 mixed bead resin (Merck-Millipore, Darmstadt, Germany) to remove trace metal ions and cyanates [121]. Concentrations of urea stock solutions were determined on the basis of their refractive index [122] using an Abbemat 500 digital refractometer (Anton Paar, Ostfilden, Germany). Stock solutions were stored at −80 °C or supplemented with buffer components and used within a week.

4.2 Preparation of detergents

Generally, detergents were thawed at room temperature (RT) for at least 30 min before processing. Then, detergent solutions were prepared in triple-distilled water or buffer by weight. For structural and physichochemical properties of the detergents used within this thesis, see **Section 3.3**.

4.3 Production and purification of Mistic

Mistic was not produced within this thesis but purified Mistic was kindly provided by Bartholomäus Danielczak, M.Sc.. For the sake of completeness, Mistic was produced as described in the PhD thesis of Dr. Jana Bröcker [66]. Briefly, freshly transformed BL21(DE3) cells (Merck-Millipore) were grown in an overnight culture. 500 µL overnight culture were used to inoculate 50 mL LB medium and cells were again grown over night. Four 1-L cultures were inoculated with 12 mL of this culture and cells were grown to an optical density at 600 nm ($OD_{600\,nm}$) of 0.8–1.0. The $OD_{600\,nm}$ was monitored on a cell density meter 40 (Fisher Scientific, Schwerte, Germany) in disposal semi-micro plastic cuvettes (Rotilab, Dreieich, Germany) with an optical path length of 10 mm. Heterologous expression was induced with 0.5 mM IPTG and performed at 18°C for 18 h and monitored with SDS-polyacrylamide gel electrophoresis (NuPAGE, Thermo Fisher Scientific, Waltham, USA). Cells were harvested, washed, weighed, and stored at –80°C.
Mistic purification was performed according to the protocol established by Dr. Jana Bröcker [66]. Typically, 3 g bio wet mass (BWM) were thawed and solubilised in 30 mL breakage buffer (50 mM Tris at pH 7.4, 50 mM NaCl, 12 mM LDAO, 40 mM imidazole, 4 M

urea, and 2 mM $MgCl_2$). EDTA-free Complete and benzonase were added according to the manufacturer's instruction. Suspended cells were disrupted by sonification with a tip sonicator (Sonifier 250, Ultrasonics, Danbury, USA). Sonification was performed in four cycles of 10 min each with 10 min break in between at an amplitude of 40%. Cell debris was removed by centrifugation (6000 *g*, 60 min, 10°C). The supernatant (SN) was filtrated through a polyvinylidene fluoride membrane with a pore size of 0.45 µm (Carl Roth) and applied to a 5-mL HisTrap HP column (GE Healthcare) with a flow of 1 mL/min on an Äkta Purifier system (GE Healthcare). Purified fusion protein was eluted with 10 column volumes (CV) buffer containing 1 M imidazol and dialysed over night at RT against 50 mM Tris at pH 7.4, 50 mM NaCl, and 12 mM LDAO. Precipitates were spun down by centrifugation (6000 *g*, 10 min, 10°C), protein concentration was adjusted to 1 mg/mL, and the solution was supplemented with 4 mM $CaCl_2$ and 5 mM DTT prior to EK digest. EK was added in an 1:3000 (w/w) fusion protein/EK ratio and EK digest was performed for 23 h at RT and stopped by addition of EDTA-free Complete. The pH of the solution was adjusted to 8.0 and the protein was applied onto a 20-mL self-packed diethylaminoethanol (DEAE) anion exchange (AIX) column (GE Healthcare) with a flow of 5 mL/min at 8°C to remove DTT and to concentrate the protein. Bound compounds were eluted with buffer containing 1 M NaCl. Pooled protein-containing fractions were again loaded onto a 5-mL HisTrap HP column with a flow of 3 mL/min. The running buffer contained 50 mM Tris at pH 7.4, 50 mM NaCl, and 12 mM LDAO. Tag-free protein was eluted in the flow-through and tag and residual fusion protein were eluted with buffer containing 1 M imidazol. The protein solution was dialysed against 50 mM Tris at pH 7.4 containing 50 mM NaCl and 12 mM LDAO over night at RT and was then either stored at −20°C or transferred to detergent exchange (**Section 4.6**).

4.4 Production and purification of OmpLA

Production of OmpLA was not performed within this thesis and is described in detail elsewhere [6]. Purified and refolded OmpLA was kindly provided by Jessica Klement, M.Sc., and Michaela Herrmann, M.Sc.. Briefly, freshly transformed BL21(DE3) cells were grown in an overnight culture. This culture was used to inoculate 400 mL LB medium to an $OD_{600\,nm}$ of 0.1–0.2 and cells were grown at 37°C to an $OD_{600\,nm}$ of 0.6. Recombinant expression was induced by addition of 0.4 mM IPTG and performed at 37°C for 4 h. Expression progress was monitored with SDS-PAGE. Tag-free OmpLA was directly produced as inclusion bodies. Cells were harvested, washed, weighed, and stored at –80°C.
To isolate the inclusion bodies, cells were thawed on ice and resuspended in 10 mL ice-cold breakage buffer (50 mM Tris at pH 8.0, 40 mM EDTA, and 25% (w/v) sucrose) per 1 g BWM. Suspended cells were disrupted by sonification with a tip sonicator in two cycles of 10 min each with 10 min break in between at an amplitude of 40%. After addition of 0.01% (w/v) Brij-35 the solution was sonicated for 1 min. To harvest the inclusion bodies,

the lysate was centrifuged for 30 min at 4°C and 4500 *g*. The pellet was resuspended in 40 mL washing buffer (10 mM Tris at pH 8.0 and 1 mM EDTA), centrifuged for 30 min at 4°C and 4500 *g*, and dissolved in solubilisation buffer (20 mM Tris at pH 8.3, 2 mM EDTA, 8 M urea, and 100 mM glycine) under agitation for 3 h at 4°C. Unfolded OmpLA was separated from residual impurities by centrifugation for 30 min at 4°C and 4500 *g*. The solubilised and unfolded protein was then either stored at −80°C or directly refolded. For refolding, solubilised OmpLA was rapidly diluted by drop-dilution into refolding buffer consisting of 20 mM Tris at pH 8.3, 2 mM EDTA, and 35 mM LDAO. The temperature of the buffer was adjusted to 50°C to enhance refolding efficiency. Final protein and urea concentrations after dilution were 0.33 mg/mL and 0.87 M, respectively. Refolding was completed under agitation at 50°C over night. Afterwards, aggregates were spun down (15 min, 4°C, 7000 *g*). Folded and unfolded protein portions were separated by liquid chromatography on an Äkta Purifier system since the refolding procedure never yielded 100% folded protein. To this end, the SN was filtrated through a polyvinylidene fluoride membrane with a pore size of 0.45 µm and applied to a self-packed 20-mL DEAE AIX column with a flow of 2.5 mL/min. Unbound protein was removed from the column with 4 CV of 20 mM Tris at pH 9.5 containing 35 mM LDAO and 2 mM EDTA and folded protein was eluted with 5 CV buffer containing 100 mM KCl. Subsequently, unfolded protein was eluted with buffer containing 1.5 M KCl. The folded state of OmpLA was monitored by SDS-PAGE [39] and fractions containing >95% folded protein were pooled and dialysed against 20 mM Tris at pH 8.3, 2 mM EDTA, and 35 mM LDAO over night at RT. The dialysed protein solution was applied onto a 5-mL HiTrap Q HP AIX column (GE Healthcare) with a flow of 2 mL/min to concentrate the protein and to adjust the LDAO concentration to 12 mM. Bound compounds were eluted with buffer containing 1.5 M KCl. Protein-containing fractions were applied to a pre-equilibrated PD-10 desalting SEC column (GE Healthcare) to remove the KCl and then either stored at −80°C or transferred to triple-detection SEC (**Section 4.9.4**).

4.5 Determination of protein concentrations

Protein concentrations were determined spectrophotometrically on a NanoDrop 1000 (peqlab Biotechnology, Erlangen, Germany) or a Jasco V-630 spectrophotometer (Jasco, Gross-Umstadt, Germany). After blanking the system with protein-free buffer, the absorbance at 280 nm was measured and the concentration was calculated according to Lambert–Beer's law.

4.6 Detergent exchange

Detergent concentration and buffer composition were adjusted by AIX and SEC. A protein solution containing ∼10 mg protein was loaded manually onto a 1-mL HiTrap Q HP

column, which was pre-equilibrated with 5 CVs buffer containing 50 mM Tris at pH 8.3, 50 mM NaCl, and the target detergent at a concentration 5 mM above the CMC at 8 M urea ($c_{\mathrm{det,final}}$). Bound protein was washed with 10 CVs buffer and eluted with 7 CVs buffer additionally containing 1 M NaCl. The eluate was collected in 0.5-mL fractions and the protein concentration in each fraction was checked spectrophotometrically. The five fractions containing the highest protein concentrations were pooled and applied to a pre-equilibrated PD-10 desalting SEC column to adjust the NaCl concentration. The buffer contained 50 mM Tris at pH 7.4, 50 mM NaCl, and the target detergent at $c_{\mathrm{det,final}}$. Protein concentration in the final 3.5 mL of protein solution was determined as described in **Section 4.5**.

4.7 Thin-layer chromatography

Successful detergent exchange was routinely confirmed by thin-layer chromatography (TLC) [123]. Shortly, 5-µL samples of the protein sample, dilution series of the original and target detergent, and the desalting PD-10 SEC buffer were applied on a TLC silica-gel 60-F_{254} plate (Merck-Millipore). Plates were air-dried for ∼30 min and inserted into a solvent-equilibrated TLC tank. The solvent contained a mixture of chloroform, methanol, and a 32% ammonium hydroxide solution in a ratio of 63:35:5 ($v/v/v$). Chromatography was done vertically and stopped when the solvent front reached 1 cm from the upper end of the plate. Plates were again air-dried for ∼30 min. For staining, plates were placed into a sealed glass chamber saturated with ioded vapour for 20 min. For sealing, high-vacuum grease (Wacker Chemie, Munich, Germany) was used. After staining, plates were scanned immediately using a standard office scanner. The intensity of each spot was quantified using the software ImageJ [124].

4.8 Determination of refractive index increments

To determine $\mathrm{d}n/\mathrm{d}c$ for all detergents used within this thesis, the refractive indices of 10–15 different detergent concentrations, distributed below and above the detergents' CMCs, were recorded using an Abbemat 500 digital refractometer. The background corrected values ($\Delta n = n - n_0$) were plotted against the detergent concentration in g/mL and data were fitted by linear regression. The slope provides the $\mathrm{d}n/\mathrm{d}c$ in mL/g.

4.9 Triple-detection size-exclusion chromatography

Triple-detection size exclusion chromatography was performed using a Superdex 75 10/300 GL column (GE Healthcare) on an 1100/1200 Agilent HPLC system equipped with an G1312A quaternary pump (Agilent Technologies, Santa Clara, USA). $\mathrm{UV}_{280\,\mathrm{nm}}$ was recorded using a G1365B detector (Agilent Technologies), LS intensity at 41°, 90°, and

138° was measured on a miniDAWN TREOS (Wyatt Technologies, Santa Barbara, USA) operating at 658 nm, and RI was monitored with the aid of an Optilab T–rEX (Wyatt Technologies) operating at 660 nm. The refractive indices of all chromatography buffers were determined using an Abbemat 500 digital refractometer.
Prior to any measurement, the system was equilibrated for at least 3 h with chromatography buffer consisting of 50 mM Tris at pH. 7.4, 50 mM NaCl, and for detergent-containing samples target detergent at a concentration 2 mM above the respective CMC ($c_{\mathrm{det,sol}}$). In advance, all buffers were filtered through RC-filters with a pore size of 0.22 µm (Sartorius, Göttingen, Germany) to remove dust. For measurements studying the influence of urea, the buffer contained urea at the same concentration as the sample. After equilibration, 100 µL sample was injected into the system. All samples were centrifuged for 10 min at 20'000 g prior to injection to remove dust and aggregates. Flow was 0.4 mL/min and all experiments were performed at RT. Data were collected for 70 min with the ASTRA software package (Wyatt Technologies) at a data collection interval of 1.5 s. All measurements were performed as triplicates unless otherwise noted. Raw data were analysed using the protein conjugate procedure implemented in ASTRA or exported and analysed with the aid of a customised Python script based on LS theory for analysis of molecular complexes described in **Section 2.2**.

4.9.1 Detergents

Detergent samples were prepared in buffer containing 50 mM Tris at pH 7.4 and 50 mM NaCl and for the investigation of urea-induced effects 2–8 M urea as described in **Section 4.2**. The effect of concentration on micelle size and hydrodynamic behaviour of alkyl maltosides was measured with samples of 5 mM, 20 mM, 35 mM, and 50 mM micellar concentration. Measurements with urea were performed at 5 mM micellar concentration of the respective detergent and urea concentrations of 0–8 M for DDM and 0 M and 6 M for all other maltosides. F_6OM measurements were performed at 10 mM micellar detergent in the sample.

4.9.2 Bovine serum albumin

For BSA measurements, a protein stock with a concentration of ∼2–3 mg/mL was prepared. To this end, lyophilised protein was weighed and dissolved in chromatography buffer by volume. For measurements with DDM, the buffer contained additional 5 mM micellar DDM. For the investigation of urea influences sample and chromatography buffer were supplemented with 6 M denaturant. Deviating from the standard triple-detection SEC settings (**Section 4.9**), flow was 0.5 mL/min for both system equilibration and data collection.

4.9.3 Mistic

Prior to measurements, Mistic solutions were subjected to detergent exchange (**Section 4.6**), and protein concentration was adjusted to ∼1 mg/mL by dilution with 50 mM Tris at pH 7.4 containing 50 mM NaCl, 5 mM DTT, and 5 mM micellar concentration of the target detergent ($c_{\mathrm{det,sample}}$). For urea containing samples, dilution buffer additionally contained urea at its highest possible concentration to yield a final urea concentration in the protein sample of ∼6 M. Deviating from the standard triple-detection SEC settings (**Section 4.9**), all buffers were supplemented with 5 mM DTT immediately before they were used.

4.9.4 OmpLA

Prior to triple-detection SEC measurements, 1 mL of refolded OmpLA, with a protein concentration of ∼3 mg/mL, was dialysed for 24 h against 100–fold excess sample buffer containing 50 mM Tris at pH 8.3, 200 mM KCl, 20 mM $CaCl_2$, and 5 mM LDAO to adjust buffer composition and detergent concentration. Chromatography buffer for OmpLA–LDAO measurements consisted of 50 mM Tris at pH 8.3, 200 mM KCl, 20 mM $CaCl_2$, and 3 mM LDAO. The detergent concentration in the chromatography buffer was reduced compared with other membrane protein measurements, because OmpLA activity critically depends on detergent concentration [6]. However, detergent concentration was still high enough to ensure micelle integrity. For OmpLA-containing samples, the injection volume was reduced to 50 µL because of a higher extinction coefficient at 280 nm and a higher protein concentration compared with Mistic.

5 Results

The main goal of this thesis was to establish triple-detection SEC as a method for the mass determination of PDCs in total and the contributions of protein and detergent individually not only in aqueous buffer but also in difficult solvent systems. Such systems are, for example, buffer with high detergent and denaturant concentrations, which have been claimed to impede triple-detection SEC measurements [104]. Water-soluble BSA and DDM micelles, in both aqueous buffer and buffer containing high urea concentration, were characterised to verify the reliability and suitability of this technique for PDC analysis. Subsequently, the designed protocols were transferred to more complex systems, such as detergent micelles in high denaturant concentrations and PDCs. Finally, this work aimed at characterising the interaction of protein and detergent in the folded and unfolded state of the α-helical membrane protein Mistic.

5.1 Refractive index increments

Successful analysis of static light scattering data requires the knowledge of the refractive index increment of all scattering substances in the solution or suspension (**Equation 4** and **28**). However, the refractive index increment of a specific substance is not only wavelength dependent, as expected from dispersion laws, but also depends on the exact solvent composition [125]. Therefore, the refractive index increments of all detergents used within this study were determined for 50 mM Tris at pH 7.4 and 50 mM NaCl and, in the case of alkyl maltosides and LDAO, additionally for urea solutions of 2–6 M.

Figures 7 depicts the dependence of the refractive index of a solution of F_6OM on the detergent concentration. The refractive index increases linearly with concentration, as expected, and linear regression yields an $\mathrm{d}n/\mathrm{d}c$ value of 0.0632 mL/g.

In the presence of urea, the $\mathrm{d}n/\mathrm{d}c$ value of a certain substance is expected to decrease with increasing urea concentration because of the higher refractive index of the pure denaturant solution. Measurements with DM- and UM-containing samples (**Figure 8** and **9**) confirm this expectation, except for samples with 2 M urea. The refractive index increment of DM decreases from 0.1413 mL/g in the absence of urea to 0.1029 mL/g in the presence of 6 M. For UM, the decrease in the $\mathrm{d}n/\mathrm{d}c$ values with increasing urea concentration is less pronounced, and the obtained values are 0.1413 mL/g in the absence of denaturant and 0.1337 mL/g at 6 M urea. The values, partially measured by Bartholomäus Danielczak, M.Sc., of all detergents used within this study are summarised in **Table 2**.

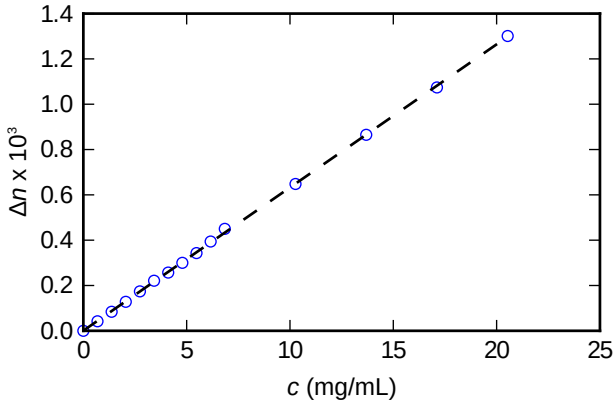

Figure 7: Evaluation of dn/dc of $\mathbf{F_6}$OM. The background-corrected refractive index Δn is plotted against various detergent concentrations (mg/mL) and fitted by a linear equation. Regression yields a slope of 0.06318 mL/g in is represented by the dashed line. The slope represents dn/dc. 50 mM Tris at pH 7.4 and 50 mM NaCl, RT.

Figure 8: Evaluation of dn/dc of DM in the presence of 0–6 M urea. The background-corrected refractive index Δn is plotted against various detergent concentrations (mg/mL) and fitted by a linear equation. Regression yields slopes of 0.1417 mL/g, 0.1623 mL/g, 0.1258 mL/g, and 0.1029 mL/g for 0 M, 2 M, 4 M, and 6 M urea, respectively. The slopes represent dn/dc. 50 mM Tris at pH 7.4 and 50 mM NaCl, RT.

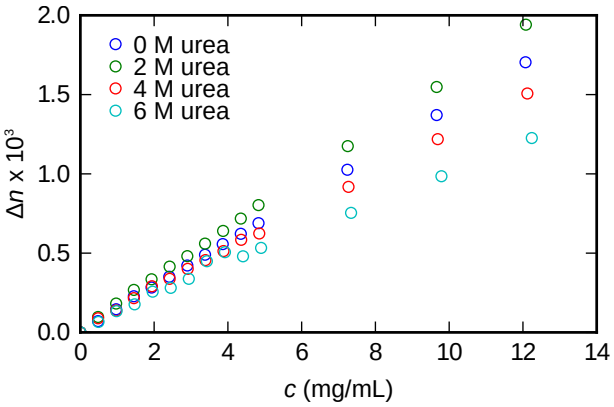

Figure 9: Evaluation of dn/dc of UM in the presence of 0–6 M urea. The background-corrected refractive index Δn is plotted against various detergent concentrations (mg/mL) and fitted by a linear equation. Regression yields slopes of 0.1413 mL/g, 0.1755 mL/g, 0.1327 mL/g, and 0.1337 mL/g for 0 M, 2 M, 4 M, and 6 M urea, respectively. The slopes represent dn/dc. 50 mM Tris at pH 7.4 and 50 mM NaCl, RT.

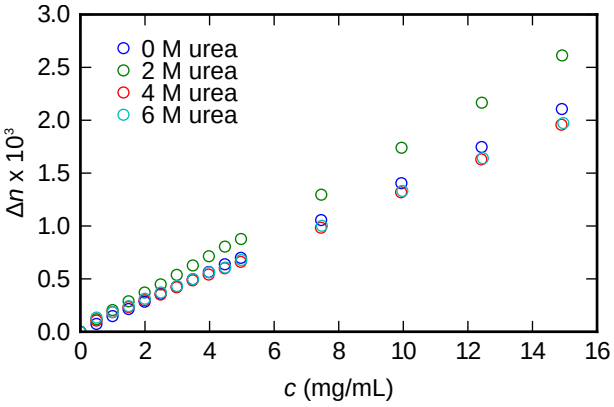

Table 2: Refractive index increments of detergents used in this study. dn/dc values in 50 mM Tris at pH 7.4 and 50 mM NaCl (buffer) and additionally with 2–6 M urea.

detergent	dn/dc (mL/g) buffer	dn/dc (mL/g) 2 M urea	dn/dc (mL/g) 4 M urea	dn/dc (mL/g) 6 M urea
NM	0.1461	0.1476	0.1575	0.1580
DM	0.1465	0.1623	0.1258	0.1029
UM	0.1444	0.1755	0.1329	0.1337
DDM	0.1449	0.1522	0.1640	0.1763
LDAO	0.1592	0.1789	0.2057	0.1624
F_6OM	0.0632	–	–	–

5.2 Molar mass determination by triple-detection SEC

BSA was subjected to triple-detection SEC to characterise the detector response to the passage of proteins and to verify data reproducibility. BSA is a good candidate for this purpose because it is not only well-characterised but also exhibits formation of dimers and higher oligomers in aqueous solution. This provides the possibility to test the resolution of the SEC column at the upper limit of its separation range and the setup's ability to distinguish between different protein oligomeric states.

5.2.1 Molar mass determination of water-soluble BSA

Figure 10 depicts the elution profile of BSA in aqueous buffer as monitored by UV absorbance, ΔR_Θ, and ΔRI and the molar masses derived according to **Equation 21**. Passage of the protein through the measurement cell leads to strong signals in all three detectors. The elution profile reveals two peaks, one very intense peak at ∼9.3 mL and a second smaller peak with a leading shoulder at ∼8.5 mL. Signal intensities of the smaller peak are decreased to roughly half of the intensity of the main peak for LS and to a quarter of the intensities of the UV and RI signal (**Figure 10 A**). The derived protein mass for the main peak amounts to (67.0±0.2) kg/mol for M_w and, thus, fits within <1% deviation the nominal mass of monomeric BSA of 66.4 kg/mol [126, 127]. This is especially remarkable because the two peaks do not show baseline resolution, meaning that the signal does not reach baseline level before it rises again. Analysis of the peak maximum of the smaller peak yields an M_w of 130–140 kg/mol, which accordingly agrees with the molar mass of BSA dimers but is slightly shifted towards higher molar masses. For the leading wing of the peak, reliable molar mass determination was not possible. This is owed to the poor separation of higher-molar-mass aggregates of BSA, which is expected for particles of this size and the used SEC column. The imperfect separation is also reflected in the steep drop at ∼8 mL and, less pronounced, the sloping of the molar-mass values at around 8.5 mL

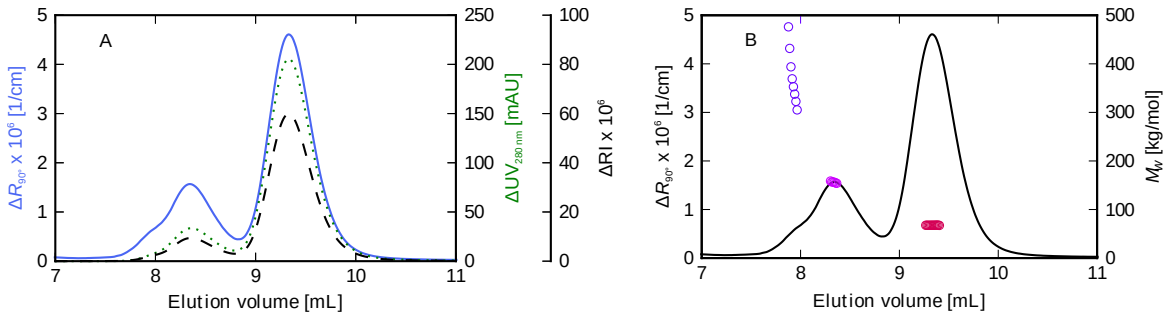

Figure 10: (A) Elution profile and (B) molar mass of BSA. (A) Excess Rayleigh ratio at 90°, UV absorbance at 280 nm, and excess RI values are depicted as functions of elution volume. (B) Excess Rayleigh ratio at 90° and derived molar masses of different oligomerisation states (monomer, dimer, higher oligomers) of BSA are depicted as functions of elution volume. 2 mg/mL BSA in 50 mM Tris at pH 7.4 and 50 mM NaCl; flow 0.5 mL/min, RT.

(**Figure 10 B**). By comparison, molar-mass values derived for the monomer peak show no inclination across the entire analysis range.

As expected, protein passage through the detection volume causes response in all three detectors. Slight overlap of two peaks still allows data analysis with sufficiently high accuracy, whereas simultaneous or almost simultaneous elution of two species with different molar masses impedes accurate mass determination but results in average values. However, differentiation between different oligomeric states might still be possible.

5.2.2 Sample-to-sample reproducibility

Three independent measurements of 100-µL samples of 2 mg/mL BSA were performed to challenge sample-to-sample reproducibility of triple-detection-based molar mass determination. **Figure 11** depicts the elution profiles as monitored by SLS in terms of ΔR_Θ at a scattering angle of 90° ($\Delta R_{90°}$) and the derived molar masses for each data point across the entire BSA monomer peak (**Section 5.2.1**) at 9.3 mL. Using the RI signal for concentration determination, the best-fit values of M_w are (67.7±0.3) kg/mol, (66.8±0.3) kg/mol, and (66.6±0.3) kg/mol for the three independent measurements. The nominal mass of BSA is has been reported as being 66.4 kg/mol, with an uncertainty of 0.0013 kg/mol [126, 127]. Hence, these measurements reproduce the reference value within an accuracy of 2% and a precision of 0.9 kg/mol. This is perfectly within the range of an average accuracy of 5% and a precision of 1 kg/mol, as reported for soluble proteins [18]. Using the 280-nm absorbance signal for concentration determination yields M_w values of (65.0±0.3) kg/mol, (66.5±0.3) kg/mol, and (67.0±0.3) kg/mol instead. This corresponds to an accuracy of ∼1% and a precision of 0.8 kg/mol, turning mass determination on the basis of UV-absorbance-based concentration determination slightly more accurate. Nevertheless, both approaches can be considered equal in terms of reproducibility.

Additionally, concentration-normalised elution profiles superpose well in the range of 8.5–11 mL but vary drastically at lower retention volumes. Since the exclusion limit of this

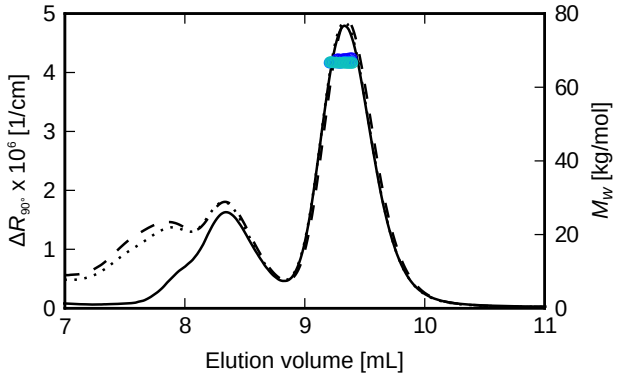

Figure 11: Elution profiles and molar masses of BSA. Excess Rayleigh ratios at 90° and deduced molar mass distributions of three independent BSA samples, which are indicated by different line styles ($\Delta R_{90°}$) and different shades of blue (M_w), are depicted as functions of elution volume. Raw LS data were transformed into excess Rayleigh ratios and normalised for slight differences in protein concentration. 2 mg/mL BSA in 50 mM Tris at pH 7.4 and 50 mM NaCl; flow 0.5 mL/min, RT.

column has been reported to be ∼8 mL, inaccuracies <8.5 mL can be neglected and might occur because of insufficient separation of high-molar-mass particles (**Section 5.2.1**).

5.3 Behaviour of detergents in triple-detection SEC

When studying membrane proteins, detergents are omnipresent substances in many applications since they are commonly used in stabilising the proteins in aqueous environments as so called PDCs. Hence, triple-detection SEC studies of membrane proteins are typically studies of PDCs. Thus, data generally contain contributions of protein and detergent in the PDC and very often of detergent micelles that are formed by excess detergent in the sample or the buffer. To be able to differentiate between protein and detergent contributions, it is necessary to know the behaviour of pure detergent micelles. To this end, data reproducibility in molar mass determination of DDM micelles was studied. The detector response in dependence on sample concentration and the influence of alkyl chain length on micelle properties, such as elution profile, micelle mass, and aggregation number, were tested with concentration series of different alkyl maltosides.

5.3.1 Investigation of DDM micelles

A sample of 5 mM micellar DDM and a sample without detergent, but in all other respects identical, were subjected to triple-detection SEC, equilibrated with buffer containing DDM at a concentration slightly above its CMC of 0.15 mM. In both cases, the elution profile was recorded with all three detectors as depicted in **Figure 12**. The upper panel shows the elution profile of DDM micelles, whereas the lower panel depicts the detector signals caused by the absence of detergent in the sample. DDM micelles show positive LS and RI signals but no noteworthy absorbance at 280 nm at an elution volume of 9.8 mL

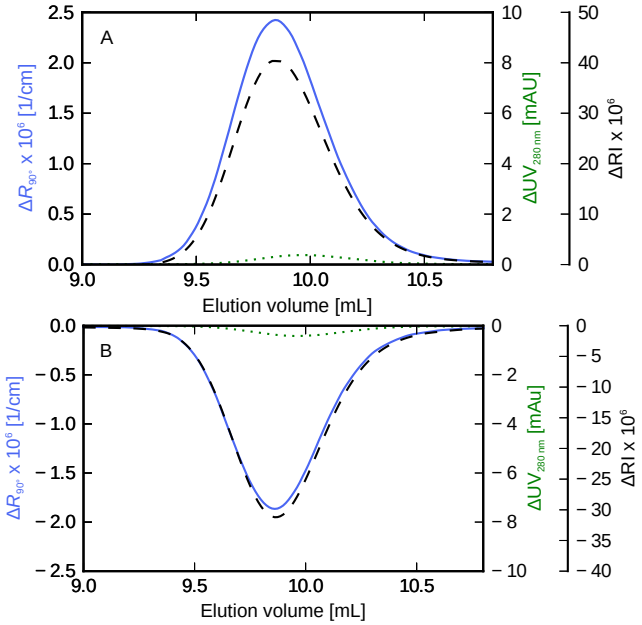

Figure 12: Elution profile of DDM micelles. Excess Rayleigh ratio at 90°, UV absorbance at 280 nm, and excess RI values of (A) 35 mM micellar DDM and (B) a sample without DDM are depicted as functions of elution volume. DDM in 50 mM Tris at pH 7.4, 50 mM NaCl, and $c_{\mathrm{det,sol}}$; flow 0.5 mL/min, RT.

(**Figure 12 A**). In the absence of detergent, the detector responses are reflected with respect to the x-axis; thus, showing negative signals of similar intensities (**Figure 12 B**). This behaviour is owed to a local detergent depletion by the detergent-free sample [19].
For verifying the reproducibility of the determined molar masses for independent measurements of detergent micelles and the influence of concentration, two samples with 5 mM and 35 mM micellar DDM were measured twice each. Excess Rayleigh ratios and the calculated molar mass for each data point are depicted in **Figure 13** in course of the elution volume. As for BSA (**Section 5.2.1**), excess Rayleigh ratios superpose well across the entire peak in both cases. This perfect superposition can also be observed for the molar mass distribution of the 35-mM sample (**Figure 13 B**). For the 5-mM sample, the two molar mass distributions are similar but not as perfectly superposed as for the higher-concentrated sample, which might basically be due to lower signals in the case of lower concentration. The best-fit M_w values are (66.8±0.3) kg/mol and (67.8±0.3) kg/mol for the high-concentration sample and (65.0±0.5) kg/mol and (67.3±0.5) kg/mol for the low-concentration sample. Therefore, the deviation between two measurements corresponds to <2% and 3.4%, depending on signal intensities, which demonstrates that concentration does also matter to assure good data quality.
Alkyl maltosides produce pronounced signals in LS and RI detectors, but miss absorbance at 280 nm, which clearly distinguishes them from proteins. Like for BSA, the reproducibility between independent measurements is within 2% discrepancy for a sample ideally suited for triple-detection SEC and still ∼3–4% for samples of low concentration.

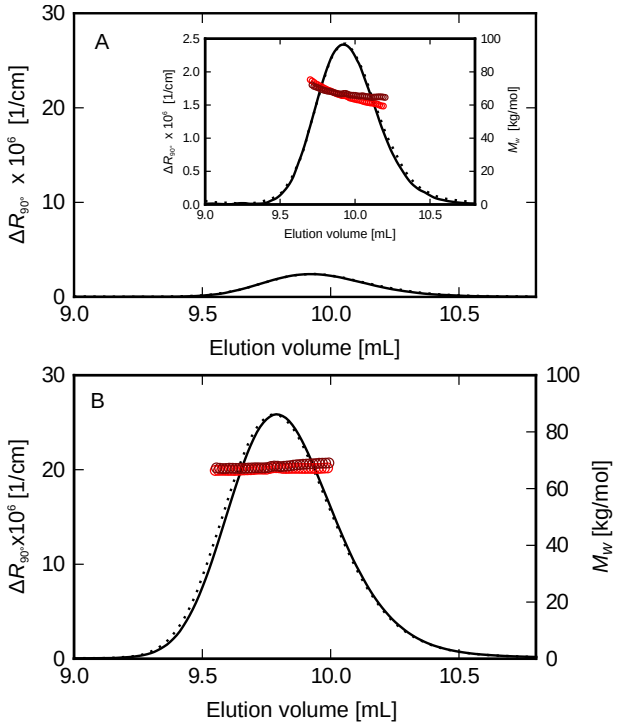

Figure 13: Elution profiles and molar masses of DDM at different concentrations. Excess Rayleigh ratios at 90° and deduced molar masses of DDM micelles at a concentration of (A) 5 mM and (B) 35 mM are depicted as functions of the elution volume. In each case, data from two independent measurements, which are indicated by different line styles ($\Delta R_{90°}$) and different shades of red (M_w), are shown. The inset in (A) shows a zoom-in. DDM ($c_{\mathrm{det,sample}}$) in 50 mM Tris at pH 7.4, 50 mM NaCl, and $c_{\mathrm{det,sol}}$; flow 0.5 mL/min, RT.

5.3.2 Concentration series of alkyl maltosides

Concentration series from 5 mM to 50 mM micellar concentration of alkyl maltosides with chain lengths ranging from 9 to 12 carbon atoms (NM, DM, UM, and DDM) were analysed with triple-detection SEC to investigate the influence of detergent concentration on detector response and micelle size. Additionally, different molar-mass averages of the investigated detergents were obtained, and the dependence of micelle size on alkyl chain length was analysed.

Elution profiles

The chromatograms as monitored by SLS are depicted in **Figure 14A–D**. Elution profiles of DDM, UM, DM, and NM show one characteristic peak each after 9.8 mL, 10.3 mL, 10.8 mL, and 11.5 mL, respectively. Signal intensities decrease linearly with decreasing concentration. Generally and concentration independent, the elution peak broadens with decreasing alkyl chain length. Additionally, the DM and, even more pronounced, the NM chromatograms show asymmetric peaks with distinct tailing at all concentrations. In all measurements, the elution volumes of the low-concentration peaks, mainly the 5-mM peaks, are slightly shifted towards higher volumes. This effect is also more pronounced for the shorter-chain-length maltosides.

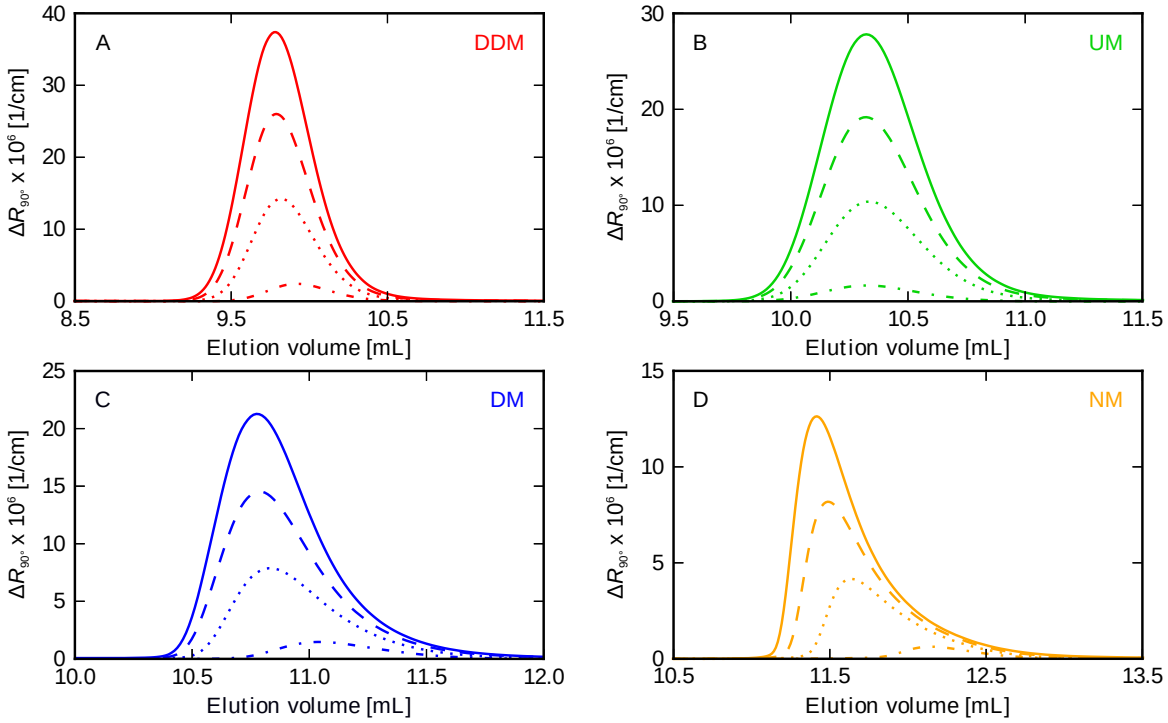

Figure 14: Elution profiles of DDM, UM, DM, and NM at different micellar concentrations. Excess Rayleigh ratios at 90° of (A) DDM, (B) UM, (C) DM, and NM are depicted as function of elution volume. Samples of 5 mM (dash–dotted line), 20 mM (dotted line), 35 mM (dashed line), and 50 mM (solid line) micellar concentration of each detergent in 50 mM Tris at pH 7.4, 50 mM NaCl, and $c_{\mathrm{det,sol}}$; flow 0.5 mL/min, RT.

Different molar-mass averages

For all four detergents and all investigated concentrations, data were analysed regarding different averaging modes. The best-fit values of M_n, M_w, and M_z for each sample were derived and are depicted in **Figure 15 A–D**. Each panel contains M_n, M_w, and M_z values for 5 mM, 20 mM, 35 mM, and 50 mM micellar DDM, UM, DM, and NM, respectively. The depicted uncertainties are based on standard deviations of the molar-mass values derived for each slice of the peak and were calculated by rules of error propagation. They represent only statistical uncertainties. Systematic errors that may be present are not considered.

In all samples, the different averaging modes yielded identical molar masses within statistical uncertainties (**Table 3**). However, for DDM and UM, the precision of the derived values increases with concentration up to 35 mM and 20 mM, respectively (**Figure 15 A** and **B**). This might be owed to low signal intensities of the low-concentrations samples, which adversely affect data quality (**Section 5.3.1**). For all samples, M_n and M_w are identical or almost identical, which results in a polydispersity of one and indicates a non-disperse mass distribution for all investigated maltoside micelles.

Although absolute uncertainties throughout the whole series of measurements are very similar, relative uncertainties regarding all molar-mass averages increase with decreasing micelle size. Hence, they are higher for DM and NM in comparison with DDM and UM.

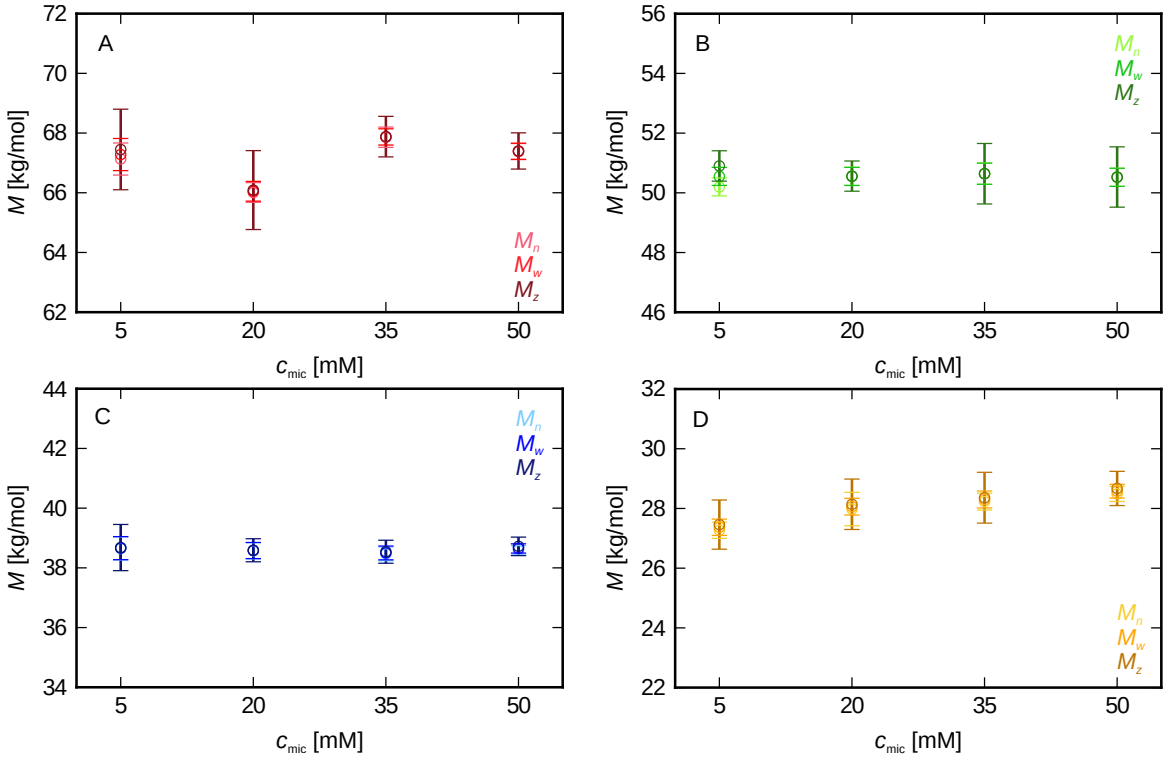

Figure 15: Molar masses of DDM, UM, DM, and NM. Number-average (M_n), weight-average (M_w), and z-average (M_z) molar masses of (A) DDM, (B) UM, (C) DM, and (D) NM are related to micellar concentration. Error bars are poorly statistically (see main text). c_{mic} = 5 mM, 20 mM, 35 mM, and 50 mM in 50 mM Tris at pH 7.4, 50 mM NaCl, and $c_{det,sol}$; flow 0.5 mL/min, RT.

Additionally, the calculated uncertainties of M_n and M_w are identical, whereas M_z shows systematically higher deviations. This is based on the mathematical determination procedure (**Section 2.3**). Nevertheless, in the screened conditions, the derived molar masses depend significantly neither on the averaging procedure nor on concentration. Thus, and because it is the direct measure provided by SLS experiments, M_w is used exclusively in the following to express average molar masses of micelles and PDCs unless noted otherwise.

Micelle size in dependence on alkyl chain length

Based on the findings above (**Section 5.3.2**), the best-fit average values for the M_w of DDM, UM, DM, and NM in buffer containing 50 mM Tris at pH 7.4 and 50 mM NaCl can be summarised as 67 kg/mol, 51 kg/mol, 39 kg/mol, and 28 kg/mol, respectively. Dividing these values by the mass of the monomer of the corresponding detergent yields aggregation numbers of 129, 103, 80, and 60 monomers per micelle. This represents an increase of ~20 detergent molecules per micelle per additional methylene group in the alkyl chain. M_w values and aggregation numbers are summarised in **Table 4**. Micelle masses as function of alkyl chain length in terms of carbon atoms are additionally presented in **Figure 16**, which again illustrates the linear dependence.

Table 3: Molar-mass averages of alkyl maltosides. Number-, weight-, and z-average molar masses of DDM, UM, DM, and NM micelles at 5 mM, 20 mM, 35 mM, and 50 mM micellar concentration and corresponding statistical errors; c_{mic}: micellar concentration, M_n: number-average molar mass, M_w: weight-average molar mass, M_z: z-average molar mass.

c_{mic} [mM]	M_n [kg/mol]	M_w [kg/mol]	M_z [kg/mol]	c_{mic} [mM]	M_n [kg/mol]	M_w [kg/mol]	M_z [kg/mol]
DDM				**UM**			
5	67.1±0.8	67.3±0.8	67.5±2.0	5	50.2±0.3	50.6±0.3	50.9±0.5
20	66.0±0.5	66.1±0.5	66.1±2.0	20	50.6±0.3	50.6±0.3	50.6±0.5
35	67.9±0.5	67.9±0.4	67.9±1.0	35	50.6±0.4	50.6±0.4	50.6±1.0
50	67.4±0.4	67.4±0.4	67.4±0.9	50	50.5±0.1	50.5±0.1	50.5±1.0
DM				**NM**			
5	38.7±0.4	38.7±0.4	38.7±0.8	5	27.3±0.3	27.4±0.3	27.5±0.8
20	38.6±0.3	38.6±0.3	38.6±0.4	20	28.0±0.6	28.1±0.3	28.1±0.8
35	38.5±0.2	38.5±0.2	38.5±0.4	35	28.2±0.3	28.3±0.3	28.4±0.9
50	38.6±0.2	38.7±0.2	38.7±0.3	50	28.5±0.3	28.6±0.2	28.7±0.6

Table 4: Molar masses and aggregation numbers of maltosides in the absence and presence of urea. Mean mass-average molar masses M_w and derived aggregation numbers (agg. no.) of DDM, UM, DM, and NM for 0 M and 6 M urea.

	0 M urea		6 M urea	
detergent	M_w [kg/mol]	**agg. no.**	M_w [kg/mol]	**agg. no.**
DDM	67	129	30	59
UM	51	103	27	54
DM	39	80	20	41
NM	28	60	7	15

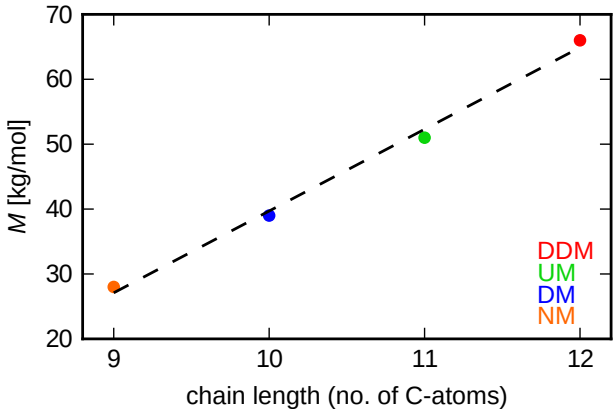

Figure 16: Average molar masses of maltoside micelles. Average M_w values of DDM, UM, DM, and NM are depicted as function of alkyl chain length. The dashed line is there to guide the eye.

5.4 Triple-detection SEC in the presence of urea

High denaturant concentrations are used to analyse chemically denatured proteins. Urea is one of the denaturants commonly used for this purpose. It increases the viscosity and the refractive index of a solvent, changes the micellisation behaviour of detergents, and additionally alters the structure of a protein by (partial) unfolding. Hence, it is likely that the performance of triple-detection SEC in the presence of urea will be influenced. To characterise these influences, BSA and alkyl maltosides were subjected to triple-detection SEC in the presence of high urea concentrations.

5.4.1 BSA in the presence of urea

Figure 17 depicts the elution profile and molar mass distribution of BSA in buffer supplemented with 6 M urea. As in urea-free buffer (**Figure 10**), the chromatograms show two peaks. However, in this case they are shifted to lower elution volumes and are separated less well. Nevertheless, global analysis results in best-fit values for M_w of 64 kg/mol for the peak at 8 mL and 135 kg/mol for the peak at 7.5 mL, which assigns the two peaks to monomeric and dimeric BSA, respectively, and reflects urea-free data. However, the BSA monomer/dimer equilibrium seems to be shifted in the direction of the dimer, as indicated by the ratio of the LS signal intensities, which was 1/2–1/3 in aqueous buffer and is ∼1 here. The distinct deviation and drop of molar mass from 160–136 kg/mol at the beginning of the first peak is due to influences of higher oligomers in the wing region of the peak. These aggregates cause no UV and RI detector response because of their low concentration but can be recognised by the LS detector because of their high mass (**Figure 17 A**).

Data reproducibility was investigated as in urea-free conditions. For two of three measurements, excess Rayleigh ratios and molar mass distributions are as similar as in urea-free measurements (**Section 5.2.2**). However, one measurement shows a slight broadening of the peak compared with the other data, which is also reflected in a deviation of the molar mass distribution (**Figure 18**). M_w values for monomeric BSA were determined to (56±0.6) kg/mol, (63.7±0.6) kg/mol, and (64.6±0.5) kg/mol for the three measurements. Hence, they are in general slightly below the values determined in urea-free measurements. Moreover, the relative uncertainty is increased from 0.5% to 1%.

The measurements with BSA, described in this section, show that urea is not a hindrance in protein analysis by triple-detection SEC but slightly impairs accuracy and certainty of data analysis for soluble proteins. However, the average M_w of BSA was determined to ∼65 kg/mol and, thus, is still in good agreement with the protein's nominal mass. The urea-induced shift in the elution volume does not negatively influence mass determination but impairs chromatographic separation.

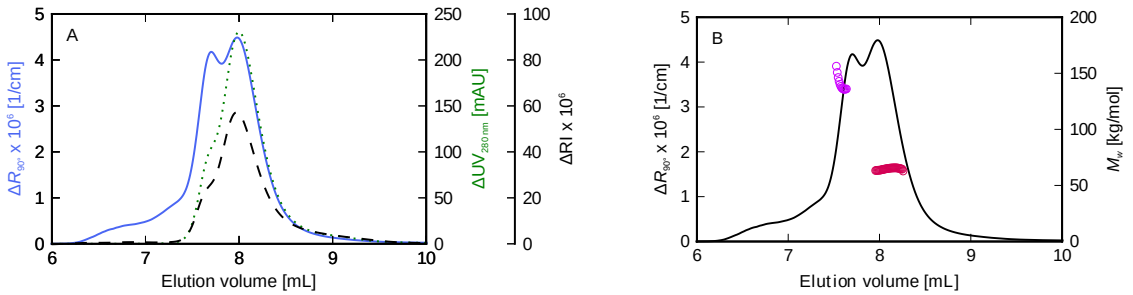

Figure 17: Elution profiles and determined molar masses of BSA in the presence of urea. (A) Excess Rayleigh ratio, UV absorbance, and excess RI values are depicted as functions of the elution volume. (B) Excess Rayleigh ratios at 90° and deduced molar mass distributions of monomeric and dimeric BSA are plotted as function of the elution volume. 2 mg/mL BSA in 50 mM Tris at pH 7.4, 50 mM NaCl, and 6 M urea; flow 0.4 mL/min, RT.

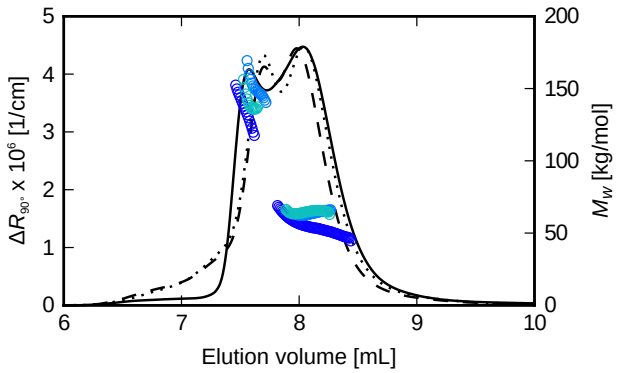

Figure 18: Elution profiles and molar masses of BSA at 6 M urea. Excess Rayleigh ratios at 90° and deduced molar mass distributions of three independent BSA samples, which are indicated by different line styles (ΔR_Θ) and different shades of blue (M_w), as functions of elution volume. Raw LS data were transformed into excess Rayleigh ratios and normalised for slight differences in protein concentration. 2 mg/mL BSA in 50 mM Tris at pH 7.4, 50 mM NaCl, and 6 M urea; flow 0.4 mL/min, RT.

5.4.2 Alkyl maltoside micelles in the presence of urea

DDM micelles in the presence of different urea concentrations

On the basis of the measurements presented in **Section 5.3.1**, 5.15 mM DDM in the presence of 0–8 M urea were subjected to triple-detection SEC. An overview of the corresponding elution profiles, as monitored in terms of excess Rayleigh ratios, is depicted in **Figure 19**. The position of the main peak is shifted gradually to lower retention volumes with increasing urea concentration. It arises after 10 mL in the absence of urea compared with 9.3 mL in the presence of 8 M urea. Additionally, the peak height decreases stepwise with increasing denaturant concentration, which leads to a lower signal-to-noise ratio (S/N) for the already small signals. The additional peak, rising with increasing urea concentration, after 8.3 mL might represent a so-called system peak since it is only visible in the LS signal. System peaks are due to injected air or shedding of the column and give rise to a peak close to the column's exclusion limit. Moreover, for the 4–8 M urea measurements, baseline subtraction was imperfect because of oscillations, mainly in the RI baseline, which interferes with the baseline subtraction procedure. This is indicated by the offset in y-direction.

Mass determination of DDM micelles results in lower masses at higher urea concentrations (**Figure 20** and **Table 5**), which is counter-intuitive to the observed shift of the elution volume. Typically, the elution volume in SEC decreases with increasing hydrodynamic radius (R_H) of the eluting particles, which is typically assumed to be proportional to their mass. However, SLS-based molar mass determination shows the reverse effect for DDM micelles in the presence of urea. All measurements were performed as triplicates allowing for investigation of sample-to-sample reproducibility. It is apparent that chromatograms and molar mass distributions superpose well up to a urea concentration of 6 M, when comparing the different panels in **Figure 20**. Measurements in the presence of 8 M urea, however, deviate from each other in both quantities. Furthermore, precision is also diminished among the measurements at lower concentration, leading to a more pronounced effect with increasing urea concentration. Global analysis yields best-fit values for M_w of DDM micelles of (67 ±0.3) kg/mol in the absence of urea and (50±0.5) kg/mol, (40–42±0.4) kg/mol, (25–29±0.6) kg/mol, and (30–37±1) kg/mol in the presence of 2 M, 4 M, 6 M, and 8 M urea, respectively. The corresponding aggregation numbers are 129, 98, 78–82, 49–57, and 59–72 (**Table 5**). In addition to the increased deviation between values determined for identical samples, polydispersity was calculated to ∼1 for all measurements up to a urea concentration of 6 M but increases to 1.2–2.3 for the measurements in the presence of 8 M urea. An increase of the polydispersity of the size distribution of detergent micelles upon treatment with urea has been also observed in DLS measurements [81].

Mass determination of DDM micelles is accurate and precise for urea concentrations up to 4–6 M. However, baseline instabilities and low signal intensities impede precise analysis

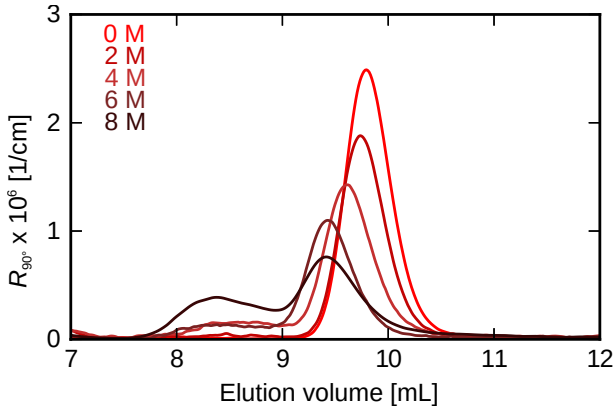

Figure 19: SEC of DDM micelles in the presence of different urea concentrations. Excess Rayleigh ratios at 90° ($\Delta R_{90°}$) for protein-free DDM micelles are depicted as functions of the elution volume. The SEC elution profiles were recorded in the presence of 0 M, 2 M, 4 M, 6 M, and 8 M urea. 5.15 mM DDM in 50 mM Tris at pH 7.4, 50 mM, $c_{\mathrm{det,sol}}$, and c_{urea}; flow 0.4 mL/min, RT.

Table 5: Molar masses and aggregation numbers of DDM in the presence of urea. Mean M_w in kg/mol and derived agg. no. of DDM for 0 M, 2 M, 4 M, 6 M, and 8 M urea are given.

0 M urea		2 M urea		4 M urea		6 M urea		8 M urea	
M_w	agg. no.	M_w	agg. no.	M_w	agg. no.	M_w	agg. no.	M_w	agg. no.
66	129	50	98	40–42	78–82	25–29	49–57	30–37	59–72

the more the urea concentration increases. Taking these errors into account, it is still obvious that the micelle sizes in terms of mass and the resultant aggregation numbers decrease with increasing urea concentrations.

Homologous series of maltosides in the presence of 6 M urea

Based on the findings above, the influence of urea on the micellisation behaviour of alkyl maltosides with chain lengths of 9–12 carbon atoms was studied with at most 6 M urea. **Figure 21 A** shows elution profiles in terms of excess Rayleigh ratios of DDM, UM, DM, and NM in the absence and **Figure 21 B** in the presence of 6 M urea. Without urea, molar mass determination yields 66 kg/mol, 50 kg/mol, 38 kg/mol, and 26 kg/mol for DDM, UM, DM, and NM, respectively (**Section 5.3.2**). Masses derived in the presence of 6 M urea are significantly lower, with 30 kg/mol, 27 kg/mol, 20 kg/mol, and 7 kg/mol. Despite the pronounced mass reduction caused by urea, the elution volumes decreased slightly under denaturing conditions for all detergents except NM. The decrease in retention volume was already observed for DDM micelles at increasing urea concentrations (**Figure 19**). Following the micelle masses, aggregation numbers are also smaller and yield values of 59, 54, 41, and 15 for DDM, UM, DM, and NM, respectively (**Table 4**). Hence, the decrease in aggregation number with reduction of alkyl chain length is not equidistant as in the

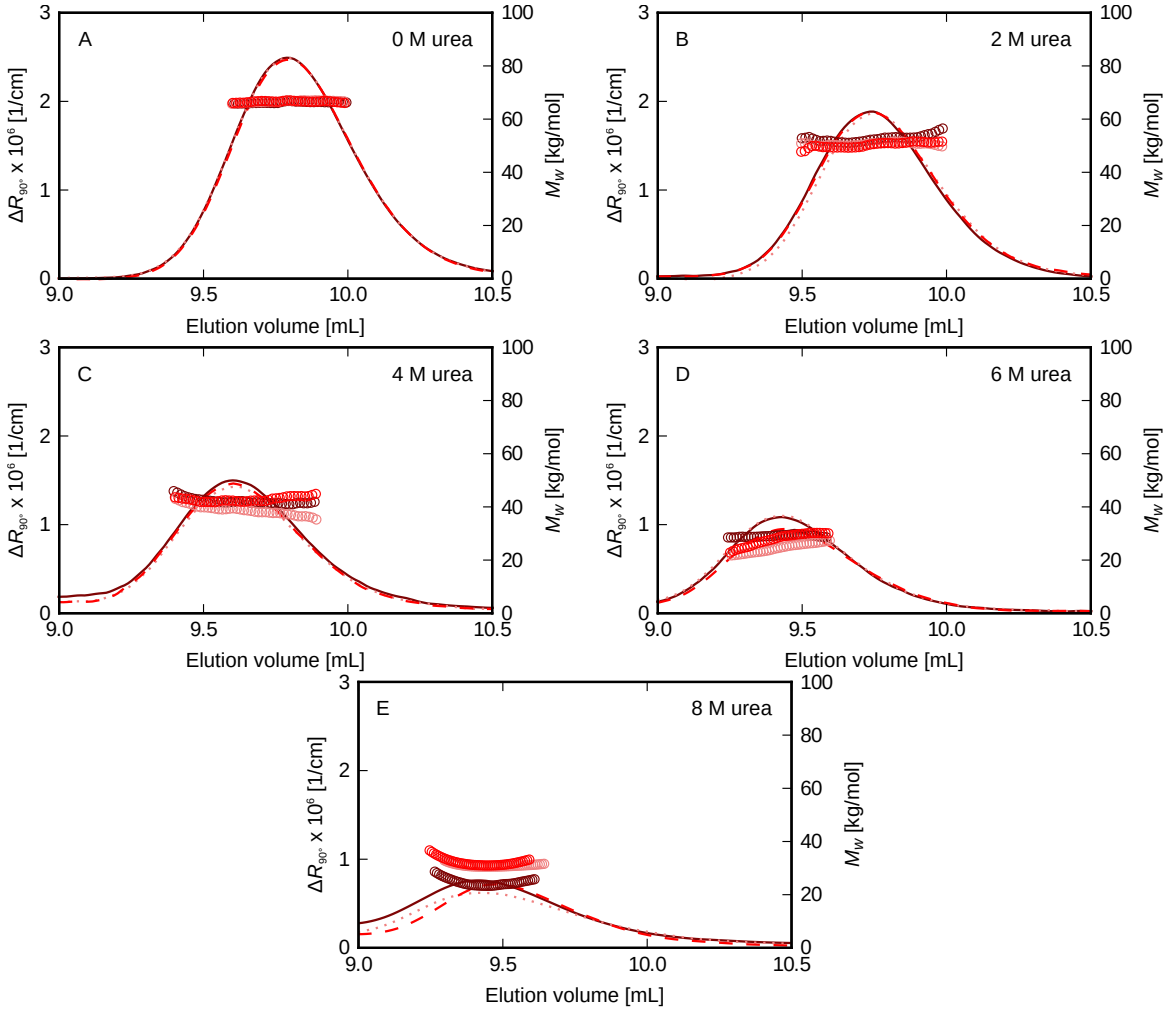

Figure 20: Elution profiles and molar masses of DDM in the presence of different urea concentrations. Excess Rayleigh ratios and derived molar masses of DDM are depicted as functions of the elution volume. Chromatograms were recorded in the presence of (A) 0 M, (B) 2 M, (C) 4 M, (D) 6 M, and (E) 8 M urea. Each panel depicts three independent measurements, which are distinguished by colour and line style (ΔR_Θ), and corresponding derived mass data. 5.15 mM DDM in 50 mM Tris at pH 7.4, 50 mM NaCl, $c_{\mathrm{det,sol}}$, and c_{urea}; flow 0.4 mL/min, RT.

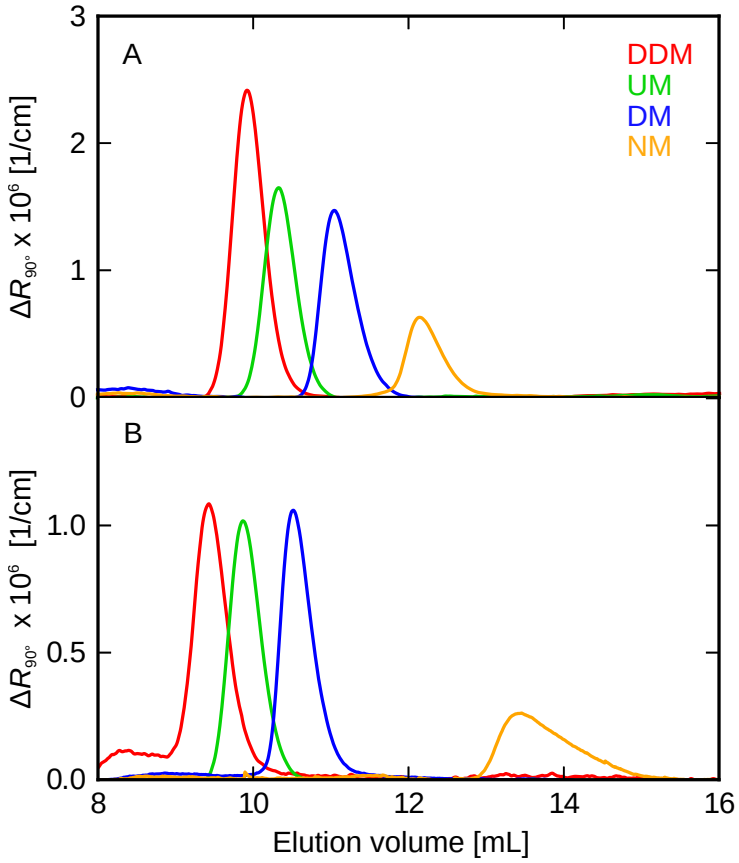

Figure 21: SEC as monitored by static light scattering of different alkyl maltosides in the (A) absence and (B) presence of 6 M urea. Excess Rayleigh ratios at 90° and molar masses of DDM, UM, DM, and NM are depicted as functions of elution volume. 5 mM micellar detergent in 50 mM Tris at pH 7.4, 50 mM NaCl, $c_{\mathrm{det,sol}}$, and c_{urea}; flow 0.4 mL/min, RT. Reprinted with permission from ref. [108].

absence of denaturant.

Micelle masses and, thus, aggregation numbers can be determined precisely in the absence of urea, whereas with increasing urea concentration the uncertainty in mass determination increases and data reproducibility decreases. Generally, the presence of urea leads to a decrease in micelle size and elution volume for all screened alkyl maltosides. Up to a concentration of ∼6 M urea, reliable and reproducible measurements and data interpretation are possible. For increasing denaturant concentrations, however, they are more complicated.

5.5 Separation and characterisation of PDCs and protein-free micelles

To determine the performance of triple-detection SEC in protein-conjugate analysis, BSA and DDM were injected simultaneously (**Section 5.5.1**). The β-barrel protein OmpLA solubilised in LDAO micelles (**Section 5.5.2**) was analysed as a well-characterised rep-

resentative for PDCs. Additionally, the established protocol was transferred to measurements on the detergent-solubilised α-helical membrane protein Mistic in the presence of 0 M (**Section 5.5.3**) and 6 M urea (**Section 5.5.4**).

5.5.1 BSA in the presence of DDM micelles

The elution profile as monitored by UV absorbance, excess Rayleigh ratio, and excess refractive index of BSA in the presence of DDM (**Figure 22 A**) exhibits two poorly separated peaks after 9.3 mL and 9.8 mL, which resemble the retention volumes of the pure substances (**Figure 10** and **12**). Global analysis of the peak at 9.3 mL, with the assumption of an BSA–DDM complex, yields a molar mass of 72 kg/mol for the complex, which is distributed as 54 kg/mol and 18 kg/mol between BSA and DDM, respectively. Assuming that the peak contains BSA only, the M_w amounts to 67 kg/mol. If the same approach is applied to the second peak, global analysis results in 66 kg/mol as molar mass of an assumed PDC, which is distributed as 6 kg/mol and 60 kg/mol between BSA and DDM. Assumption of a peak containing only DDM yields a molar mass of 66 kg/mol.
Analogous measurements were performed in the presence of 6 M urea. The chromatogram depicted in **Figure 22 C** again perfectly resembles an overlap of the DDM-free BSA and the BSA-free DDM measurement under identical conditions. Analysis identifies the peak at 8 mL as containing solely BSA monomers with a best-fit M_w of 71 kg/mol and the peak at 9.5 mL as containing solely DDM micelles with a best-fit M_w of 32 kg/mol. This is again similar to results obtained for the pure substances (**Table 3**).
Because of the different UV activities of the detergent and the protein, it is possible to distinguish between protein and detergent contributions on the basis of data analysis even without prior knowledge of sample contribution and to determine the molar masses of both substances individually. However, imperfect separation of closely eluting species impedes reliable assignment of different particles to the overall signals, thus leading to erroneous protein and detergent masses.

5.5.2 LDAO-solubilised OmpLA

Figure 23 A shows the elution profile of presumably monomeric OmpLA, refolded in LDAO, as monitored by UV absorbance, SLS, and RI detection. The elution profile reveals two distinct peaks at ∼9 mL and ∼10.8 mL. Strong signals in all three detectors identify the first peak as protein-containing since LDAO shows no noteworthy absorbance at 280 nm. The absence of a noticeable 280-nm absorbance signal indicates that the second peak reflects protein-free LDAO micelles. Mass and composition of both peaks were determined independently (**Figure 23 B**). The resulting best-fit value of M_w of OmpLA is (29±0.2) kg/mol, which corresponds to a deviation of 6% from the nominal mass of 31 kg/mol of the monomeric protein. Hence, the measurement is less accurate than measurements on the water-soluble BSA. The mass ratio of bound LDAO was calculated as

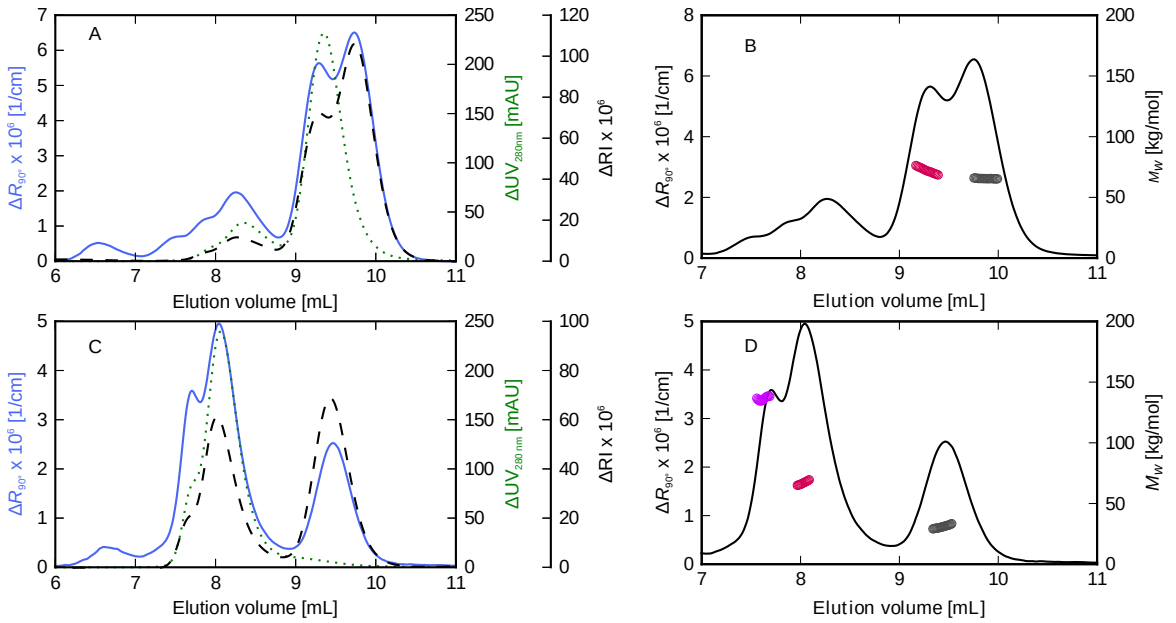

Figure 22: Elution profiles and determined molar masses of BSA in the presence of DDM and urea. (A and C) Excess Rayleigh ratio, UV absorbance, and excess RI values and (B and D) excess Rayleigh ratios at 90° and deduced molar mass distributions of BSA and 10 mM DDM are depicted as functions of the elution volume in (A and B) 0 M and (C and D) 6 M urea. 2 mg/mL BSA in 50 mM Tris at pH 7.4, 50 mM NaCl, $c_{\mathrm{det,sol}}$, and c_{urea}; flow 0.4 mL/min, RT.

1.15, meaning that 1.15 g detergent is bound per 1 g protein. The protein fraction in the PDCs corresponds to 46% of the total mass. This yields a detergent contribution of (33±0.3) kg/mol to the overall molar mass of the PDC, which amounts to 62 kg/mol.
Analysis of the protein-free peak yields a molar mass of (17±0.3) kg/mol for the assumed micelle peak and, thus, reproduces well the results for micellar LDAO measured in the absence of OmpLA (**Figure 24**). These measurements were performed with micellar concentrations of 5–50 mM and yielded M_w values of (18±0.18) kg/mol independent of the applied concentration.
Generally, it was possible to successfully separate PDCs and protein-free LDAO micelles with the aid of triple-detection SEC. Molar masses of both species and the composition of the OmpLA–LDAO complex could be determined without introducing any prior knowledge about elution behaviour or sample composition in the analysis procedure.

5.5.3 Detergent-solubilised Mistic

For studying equilibrium unfolding, Mistic was solubilised in a homologous series of alkyl maltosides with chain lengths ranging from 8–12 carbon atoms [128]. To ensure the presence of detergent micelles under all experimental conditions, an excess of detergent was added to the sample [14]. However, as for most membrane proteins, the actual detergent concentration needed to stabilise the protein is unknown. Therefore, the composition of Mistic–maltoside complexes was investigated with the aid of triple-detection SEC.

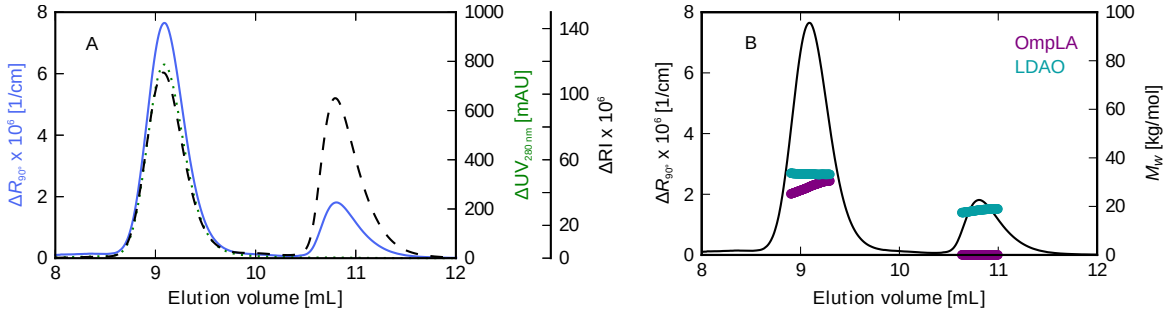

Figure 23: (A) Elution profile and (B) molar masses of OmpLA/LDAO complexes. (A) Excess Rayleigh ratio at 90°, UV absorbance at 280 nm, and excess RI values are depicted as functions of the elution volume. PDC and protein-free detergent micelles elute as two separate peaks at 9 mL and 11 mL, respectively. (B) Excess Rayleigh ratios at 90° and derived molar masses of OmpLA and LDAO in PDCs and micelles are plotted as functions of elution volume. 3 mg/mL OmpLA and 5 mM LDAO in 50 mM Tris at pH 8.3, 100 mM KCl, 2 mM EDTA, and $c_{\mathrm{det,sol}} = 4$ mM; flow 0.4 mL/min, RT. Adapted and reprinted with permission from ref. [108].

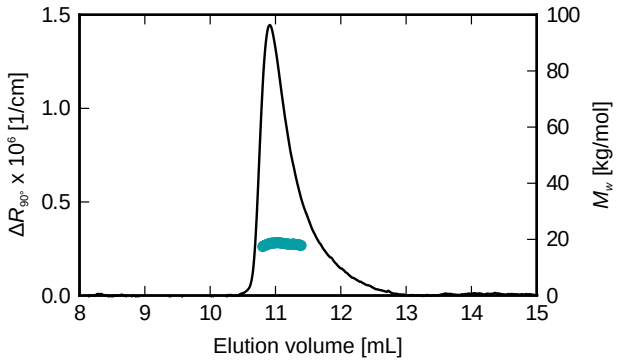

Figure 24: Elution profile and derived molar masses of LDAO micelles. Excess Rayleigh ratio at 90° and derived molar masses of LDAO micelles are plotted as function of the elution volume. The mass of LDAO micelles was calculated to 18 kg/mol. 20 mM micellar LDAO in 50 mM Tris at pH 8.3, 100 mM KCl, and 2 mM EDTA; flow 0.4 mL/min, RT.

Figure 25 A shows the excess Rayleigh ratio at 90° scattering angle of Mistic in alkyl maltosides with chains containing 9–12 carbon atoms in the absence of denaturant, that is, native conditions. Measurements in *n*-octyl-β-D-maltopyranoside were impeded by the detergent's impurity leading to distorted signals. As in the case of protein-free alkyl maltoside micelles (**Section 5.3.2**), the elution volume of the PDC depends on the alkyl chain length, with complexes consisting of protein and shorter-chain maltosides eluting later. Chromatograms of Mistic–NM and Mistic–DM show two distinct peaks each at 10.5 mL and 11.5 mL and at 10.3 mL and 10.8 mL, respectively. The chromatograms of Mistic–UM and Mistic–DDM instead exhibit only one peak each at 10 mL and 9.8 mL, respectively. For Mistic–NM, analysis of the first peak yields molar masses of 13 kg/mol for the protein contribution and 12 kg/mol for the modifying detergent. Analysis of the second peak yields a molar mass of 28 kg/mol, which is in good agreement with the values obtained for protein-free NM micelles (**Section 5.3.2**). Similarly, the analysis of the first peak in the chromatogram of Mistic associated with DM revealed a protein contribution of 13 kg/mol and a detergent contribution of 20 kg/mol to the molar mass of the total complex. Here, the two peaks were less separated. However, independent analysis of the second peak was possible, yielding a molar mass of 38 kg/mol and, thus, agrees well with protein-free DM micelles (**Section 5.3.2**). For samples containing UM and DDM, the molar mass of the single peak was identified as 47 kg/mol and 53 kg/mol, respectively. The masses of the corresponding PDCs are built up by 13 kg/mol for the protein contribution and 34 kg/mol for UM and 40 kg/mol for DDM. With these values at hand, the mass ratio of bound detergent/protein appears to increase from ∼1 for the Mistic–NM complex to ∼2 for Mistic–DM and further to ∼3 for Mistic–UM and Mistic–DDM.
The molar mass of Mistic could be determined reproducibly and reliably for all tested alkyl maltosides. Additionally, the masses of NM and DM micelles mirror the results obtained in pure detergent measurements. For UM and DDM, separation of PDCs and protein-free detergent micelles was not possible, and simultaneous elution might explain the observed increase in the detergent/protein ratio.

5.5.4 Detergent-solubilised Mistic in 6 M urea

Comparative folding studies rely on the unfolded state as the reference state. Thereby, it is implied that the unfolded state is independent of the used membrane-mimetic system [15]. When comparing protein stabilities among different detergent micelles, this means that the protein in the unfolded state has no detergent bound, which is referred to as detergent-free. Mostly, the absence of bound detergent is verified by indirect methods such as turbidity measurements. To introduce triple-detection SEC as direct method for the verification if a protein is completely deprived of detergent in its unfolded state, detergent-solubilised Mistic in the presence of 6 M urea was subjected to triple-detection SEC.

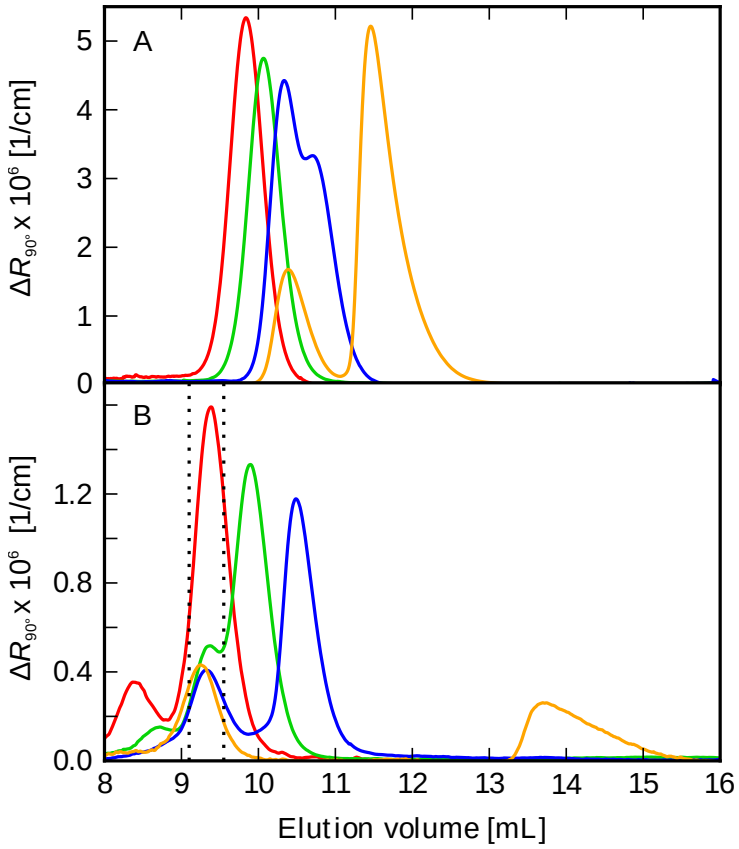

Figure 25: SEC of Mistic solubilised in different alkyl maltosides in the (A) absence and (B) presence of 6 M urea as monitored by static light scattering. Excess Rayleigh ratios at 90° ($\Delta R_{90°}$) for Mistic solubilised in DDM, UM, DM, and NM are depicted as functions of the elution volume. (A) In the absence of urea, the traces of NM and DM show two peaks, whereas the traces of UM and DDM exhibit only one single peak. (B) At 6 M urea, for all detergents except DDM, chromatograms show two peaks. The elution volume of pure Mistic is enclosed by the two dotted lines and at ∼9.3 mL for all measurements, whereas the elution volumes of detergent micelles change according to their size. Additional peaks in the SLS signal at 8.5 mL in the DDM and UM traces are system peaks, as they do not show up in UV and RI signals. 1 mg/mL Mistic and $c_{\mathrm{det,sample}}$ in 50 mM Tris at pH 7.4, 50 mM NaCl, 5 mM DTT, $c_{\mathrm{det,sol}}$, and c_{urea}; flow 0.4 mL/min, RT. Adapted and reprinted with permission from ref. [108].

Homologous series of alkyl maltosides

For all alkyl maltosides except DDM, the elution profiles in the presence of urea, depicted in **Figure 25 B**, exhibit two distinct peaks. By contrast, DDM-solubilised Mistic causes only one peak beside the system peak at ∼8.3 mL. The first peak arises at 9.3 mL and is common for all samples. UM-, DM-, and NM-containing measurements show a second peak after 10 mL, 10.8 mL, and 13.5 mL, respectively. Quantitative analysis yields a protein mass of 12–13 kg/mol for the peak at 9.3 mL and demonstrates the absence of detergent from this peak for all detergents except DDM. For the latter one, global analysis results in physically unrealistic masses of 9 kg/mol for the protein and 11 kg/mol for the detergent. More detailed considerations about this case are presented in in the next paragraph. Additionally, analysis of the peaks eluting at higher volumes yields masses very close to those observed in measurements of the corresponding detergent without protein (**Section 5.4.2**), namely, 23 kg/mol for UM, 19 kg/mol for DM, and 9 kg/mol for NM (**Table 4**). Moreover, the analysis also confirmed the absence of detergent. Hence, the peak at 9.3 mL can be assigned to unfolded detergent-free Mistic, whereas the second peak at higher elution volume represents protein-free detergent micelles.

DDM-solubilised Mistic

As mentioned above, global analysis of the data from DDM-solubilised Mistic yields physically unrealistic values. However, comparison of UV absorbance and LS profiles of protein-free DDM micelles at 6 M and unfolded Mistic in the presence of, for example, NM (**Figure 26 B**) reveals a common peak at 9.3 mL. In the presence of NM, protein and detergent elute as two separate peaks after ∼9.3 mL and ∼13.5 mL, and DDM micelles also elute after ∼9.3 mL. Additionally, the peak produced by DDM-solubilised Mistic also occurs after ∼9.3 mL (**Figure 26**) and comprises UV absorbance indicating the presence of protein. Since Mistic–NM and protein-free DDM measurements provide data that are influenced by only one of the species of interest, namely unfolded Mistic and DDM micelles in the presence of urea, it is possible to derive the influences of those two particles on the total signal. The first peak of the NM measurement comprises only Mistic, as described above, thus

$$\mathrm{LS}_{\mathrm{total,Mistic–NM}} = \mathrm{LS}_{\mathrm{Mistic}} \tag{49}$$

$$\mathrm{RI}_{\mathrm{total,Mistic–NM}} = \mathrm{RI}_{\mathrm{Mistic}} \tag{50}$$

$$\mathrm{UV}_{\mathrm{total,Mistic–NM}} = \mathrm{UV}_{\mathrm{Mistic}} \tag{51}$$

Therefore, the RI/UV and LS/UV ratios for Mistic only can be calculated from this peak to 0.0003 and 0.033, respectively. Analogously, the LS/RI ratio of DDM can be

calculated from the pure DDM measurement to 300. In the DDM–Mistic measurement, the UV signal is solely due to the UV activity of Mistic; therefore, the Mistic contribution to the total RI signal can be calculated by

$$\mathrm{RI}_{\mathrm{Mistic}} = \frac{\mathrm{RI}_{\mathrm{Mistic}}}{\mathrm{UV}_{\mathrm{Mistic}}} \mathrm{UV}_{\mathrm{total,Mistic–DDM}} \tag{52}$$

In the same way, the contribution of the protein to the LS signal can be calculated by multiplication of the UV signal with the LS/UV ratio.

$$\mathrm{LS}_{\mathrm{Mistic}} = \frac{\mathrm{LS}_{\mathrm{Mistic}}}{\mathrm{UV}_{\mathrm{Mistic}}} \mathrm{UV}_{\mathrm{total,Mistic–DDM}} \tag{53}$$

The total RI signal is the linear combination of the RI signal of Mistic and the RI signal of DDM micelles, thus

$$\mathrm{RI}_{\mathrm{DDM}} = \mathrm{RI}_{\mathrm{total,Mistic–DDM}} - \mathrm{RI}_{\mathrm{Mistic}} \tag{54}$$

Subsequently, the DDM LS signal is calculated by multiplication of $\mathrm{RI}_{\mathrm{DDM}}$ with the LS/RI ratio of DDM obtained from the pure DDM measurement. Summation of the two calculated LS signals perfectly resembles the experimental data (**Figure 27**). This demonstrates that the LS signal equals the sum of two overlapping peaks, which are detergent-free Mistic and protein-free DDM micelles (**Figure 27**). Thus, it is shown that also DDM-solubilised Mistic is detergent-free in its unfolded state.

5.6 Fluorinated octyl maltoside

Like hydrogenated detergents, fluorinated surfactants are amphiphilic and form micelles in an aqueous environment. Moreover, it has been reported [74] that one of the two commercially available fluorinated surfactants, namely F_6OM, acts like a detergent and builds up large rod-like micelles. This renders F_6OM the perfect candidate for the investigation of micelle shape by triple-detection SEC.

5.6.1 Mass and shape determination

The elution profile of 10 mM micellar F_6OM is depicted in **Figure 28 A**. The surfactant elutes after ∼7.3 mL with slight tailing. In contrast with maltoside micelles, F_6OM micelles show an angle-dependent scattering intensity allowing for the determination of the micelles' R_{RMS}. Thus, the micelles' conformation can be estimated by analysis of the relation between the R_{RMS} and the M_{w}. **Figure 28 B** depicts the excess concentration, that is, the difference in concentration between sample and chromatography buffer, of F_6OM as derived from the RI signal, R_{RMS}, and M_{w} as functions of the elution volume. Unlike alkyl maltoside micelles, the molar mass of F_6OM micelles is not constant in the course of the elution volume but rises steeply from ∼600 kg/mol in the beginning to

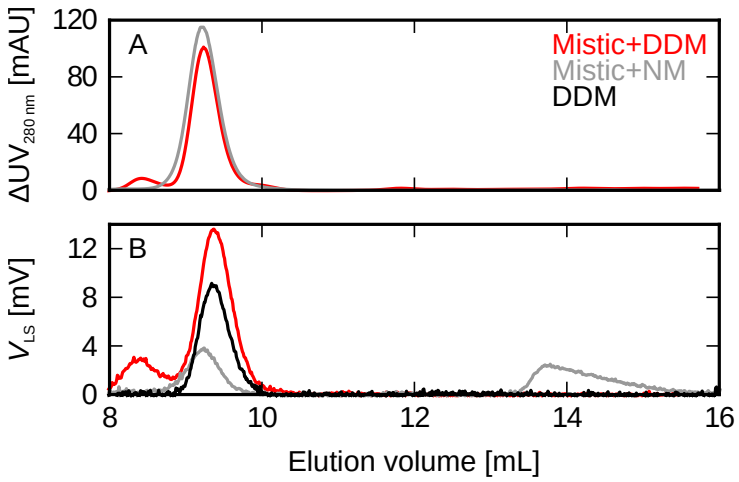

Figure 26: Triple-detection SEC of Mistic solubilised in DDM or NM in the presence of 6 M urea. (A) Absorbance at 280 nm and (B) voltage of 90° light scattering detector (V_{LS}) versus the elution volume. 1 mg/mL Mistic in $c_{\mathrm{det,sample}}$ in 50 mM Tris at pH 7.4, 50 mM NaCl, $c_{\mathrm{det,sol}}$, and 6 M urea; flow 0.4 mL/min, RT. Reprinted with permission from ref. [14]. Copyright 2014 American Chemical Society.

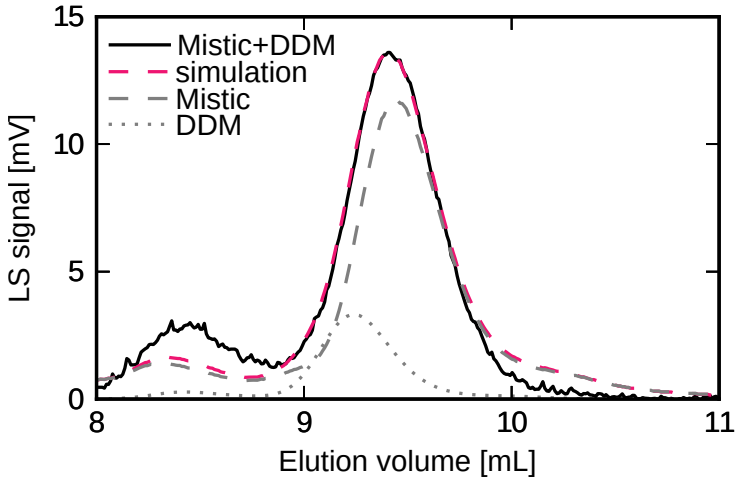

Figure 27: SEC of Mistic as monitored by right-angle light scattering. SEC of Mistic and DDM in the presence of 6 M urea. The simulated chromatogram (sim) represents the sum of the scattering contributions from detergent-free Mistic and protein-free DDM micelles. Reprinted with permission from ref. [14]. Copyright 2014 American Chemical Society.

∼1150 kg/mol with increasing concentration and declines again as the concentration does. The steep drop in molar mass at an elution volume <7.3 mL is most likely an artefact due to low excess concentration. Contrary to general expectations, the R_{RMS} seems to decrease with increasing micelle mass. As in mass determination, R_{RMS} values at elution volumes <7.3 mL can be neglected because of high uncertainties in their determination. The same holds true for the zero R_{RMS} values after ∼7.8 mL. Low micelle concentrations cause low LS signals despite the relatively high micelle mass and, thus, impede reliable R_{RMS} determination. In contrast with the M_w, the R_{RMS} decreases constantly in the course of the elution volume from 50 nm in the beginning to 10 nm towards the end of the peak.

The conformation plot for R_{RMS}–M_w pairs in the range between 7.3 mL and 7.8 mL is shown in **Figure 29 A**. The colour gradient is used to distinguish between the different parts of the plot. The two main regions in the conformation plot, with significantly different slopes, impede meaningful analysis of the peak in its entirety. Therefore, the two regions were fitted separately with linear equations. The first, mainly "blue" part (**Figure 29 B**) is characterised by a shallow decaying straight line with a slope of −1.03±0.01, the error being the standard deviation of the linear fit. The second, mainly "red" part belongs to data <7.5 mL and can safely be neglected. The absolute value 1.03 of the slope implies a rod-like structure of the micelles (**Section 2.4**). The decline of the slope is caused by the fact that the R_{RMS} of the micelles decreases more strongly than their molar mass.

In contrast with the other micelles investigated in this work, F_6OM micelles are not homogeneous in size but show a concentration-dependent variation in mass, which is accompanied by a decrease in R_{RMS}. Analysis of micelle conformation by a log–log plot of the R_{RMS} versus the M_w indicates a rod-like micelle structure.

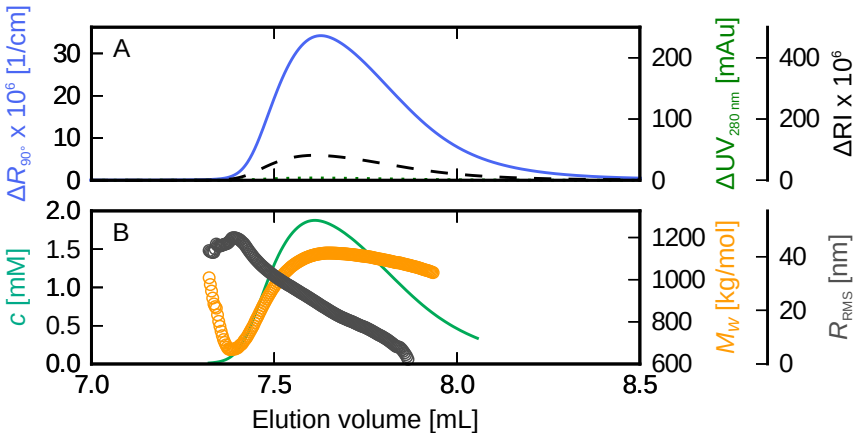

Figure 28: (A) Elution profile and (B) concentration, molar mass, and root mean square radii of F_6OM. (A) Excess Rayleigh ratio at 90°, UV absorbance at 280 nm, and excess RI values are depicted as functions of the elution volume. (B) Derived concentration, molar mass, and R_{RMS} of 10 mM micellar F_6OM in 50 mM Tris at pH 7.4, 50 mM NaCl, and $c_{det,sol}$; flow 0.4 mL/min, RT.

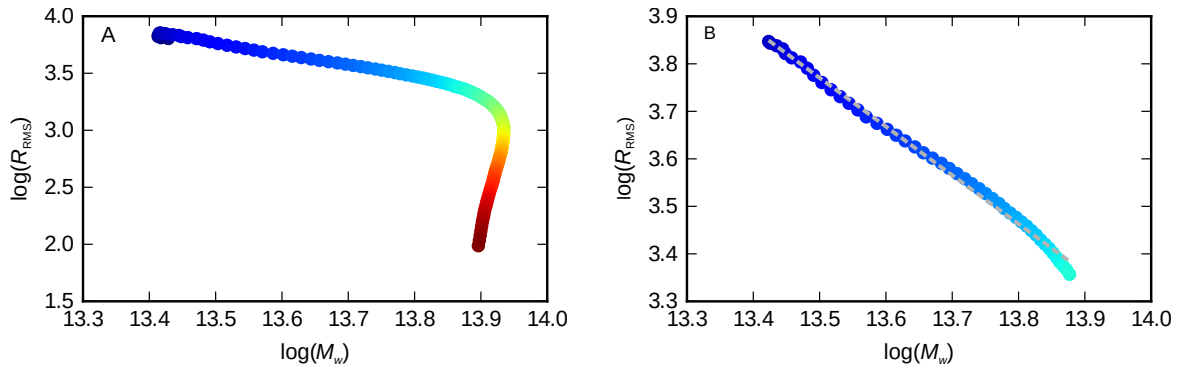

Figure 29: Conformation plots of F_6OM. R_{RMS} and M_w are plotted as log–log plot and fitted by linear regression. The colour gradient assigns values to their position in the elution profile with blue indicating high and red low elution volume. (A) Conformation plot over the entire peak. (B) Conformation plot data between 7.5 mL and 7.8 mL. The dashed line depicts the linear regression curve.

5.6.2 F_6OM mass and shape: theoretical considerations

The results obtained by triple-detection SEC are very error-prone because of the low signal intensities. Moreover, SLS was performed with only three different angles, which is the minimum number of detection angels allowing for shape estimation. This further decreases data reliability. To verify the validity of the obtained results, negative-staining transmission-electron-microscopy (TEM) figures, obtained by Dr. Anette Meister [74], were re-evaluated in terms of micelle dimensions. Based on this data, the micelle aggregation number for F_6OM was estimated with the help of simple geometric considerations [73].

The length and diameter of different F_6OM micelles were determined from the TEM pictures with the aid of the program measureIT (Olympus Soft Imaging Solutions, Münster, Germany), and the volume of the detergent micelles was estimated by considering an ellipsoidal shape. The number of detergent monomers fitting in that volume was calculated according to Tanford [73]. His considerations are based on two assumptions: The HC core consists only of portions of hydrocarbon chains; only one or two methylen groups near the head group may not be part of the HC core. No solvent enters the core. And, the volume V in Å^3/chain of an HC chain of n_c carbon atoms that is embedded in the HC core is given by

$$v_H = 27.4 + 26.9 n_c \tag{55}$$

if the temperature T is near RT. Since fluorocarbon tails are bulkier than hydrocarbon tails, the expression for v has to be adapted to [129]

$$v_F = 42.4 + 41.6 n_c \tag{56}$$

with n_c being the the total number of carbon atoms in the tail, reduced by one since the CF_2-group attached to the polar head is considered as being part of the hydration sphere.

Analysis of TEM pictures yielded a constant micelle diameter of 4±0.5 nm and micelle length varying between 23 nm and 48 nm. The micelles' diameter can be determined within 1 nm deviation. The micelles' length, however, is not so clearly defined and an uncertainty of up to 10 nm has to be considered. The curvature of the ellipsoid is given by the maximum length (l_{max}) of the fluorocarbon chain, which is estimated by [129]

$$l_{\mathrm{max}} = 2.04 + 1.30 n_{\mathrm{c}} \tag{57}$$

Assuming the volume of an ellipsoid and dividing it by the volume of one fluorocarbon chain yields micelle masses of 795 kg/mol–1660 kg/mol. This is higher than both the lower and upper limit of molar masses determined by triple-detection SEC. However, one might assume that the micelle diameter is slightly overestimated in the TEM figures because of staining and binding of the uranyl ion to the detergent head groups [130]. To correct for this overestimation, the micelle diameter is estimated to be on average one nanometre less. Micelle lengths were not corrected because of their anyway wide distribution. This correction reduces the minimum mass of a F_6OM micelles to 477 kg/mol and the maximum mass to 933 kg/mol. Thus, the boundaries derived with triple-detection SEC are in between the two extreme values.

It can be assumed that, in the case of structures like F_6OM micelles, LS detection with three detectors is sufficient to at least give an estimate on the micelle mass and shape. Additionally, it was shown that the polydispersity observed in micelle mass and shape is not exclusively an artefact based on low signal intensities but represents the diverse structure of F_6OM micelles regarding their length. This is a commonly observed effect for rod-like or cylindrical micelles since their growth in length is not limited by any unfavourable energetics [73].

6 Discussion

The goal of this thesis was to refine standard experimental and data-analysis procedures of triple-detection SEC for challenging membrane-protein samples, which so far elude routine approaches. SLS and, to almost the same extent, triple-detection SEC are common techniques for the characterisation of polymers regarding mass and shape [100, 114, 131–134], but their potential in the field of membrane-protein analysis is still not exploited. The applicability of triple-detection SEC to the mass determination of membrane proteins was described already in 1982 [135]. Moreover, there are several publications on the application of triple-detection SEC on PDCs and its ability to determine the contribution of each component, that is, protein and detergent individually [14, 16–20]. However, up to now, triple-detection SEC still lacks applicability to complex systems such as membrane proteins in the presence of high denaturant concentrations as analysed in the course of this work.

6.1 Influence of urea on triple-detection SEC

Urea, especially at high concentrations, substantially changes solvent properties such as the refractive index [122] and the viscosity [136]. Hence, it is likely that its presence has an influence beyond the denaturant's direct effect on proteins and detergents.

6.1.1 Changes in elution behaviour

The probably most obvious effect caused by the presence of urea in the measurements presented here is a shift in elution volume to lower volumes. The BSA monomer peak elutes at lower elution volumes and is moved towards the dimer peak (**Section 5.4.1**). Consequently, the two peaks are no longer separated as well as under urea-free conditions. DDM micelles show a gradual shift to lower elution volume with increasing urea concentrations that is accompanied by increased peak broadening (**Section 5.4.2**). Finally, all alkyl maltoside micelles, except NM, elute earlier in the presence of 6 M urea despite the pronounced size reduction (**Section 5.4.2**).
For BSA, it is most likely to assign the change in hydrodynamic behaviour to urea-induced structural changes. At 6 M urea, BSA is at least partially unfolded [137], which causes a decrease in compactness and, thus, significant deviation from a theoretically assumed globular protein structure. This is expressed in an increased R_{H}, which is accompanied

by a reduced retention volume based on the separation principle of SEC. The fact that SEC does not separate particles on the basis of their mass but rather on the basis of differences in hydrodynamic volume is commonly used to follow the unfolding of proteins by liquid chromatography [138–140]. It has been shown [138, 141, 142] that upon unfolding the Stokes radius of the protein increases drastically, and this increase can be followed by SEC. Generally, the unfolded state exhibits a higher R_H and, thus, a lower elution volume. This effect has been observed for both chemical and thermal unfolding [138]. In addition, not only the unfolding process upon increase of urea concentration can be examined, but SEC is also applicable to studying changes in the hydrodynamic volume upon protein refolding, where the R_H is decreased by dilution of the urea concentration and the elution volume is shifted back to higher volumes with the protein adopting its native fold [140]. These observations confirm that conformational changes of BSA in the presence of 6 M urea are responsible for the observed shift in retention to lower volumes. As a side effect, this shift moves the BSA monomer peak close to the column's void volume of ∼8 mL, where the resolution of the column is decreased. Thus, BSA monomers and higher oligomers cannot be separated, which impedes high-precision M_w determination.
For alkyl maltosides, it has been reported by Broecker and Keller [81] that the micelles' hydrodynamic volume decreases with increasing denaturant concentration. This would, at first glance, cause an increase in elution volume rather than a decrease, analogous to what has been observed for protein refolding [140]. However, high amounts of urea drastically increase the viscosity of both sample and chromatography buffers [136]. Furthermore, the solvent's viscosity and the diffusion coefficient of a solute are inversely related [143], meaning that an increase in viscosity decreases the diffusion coefficient. Additionally, the Stokes–Einstein equation correlates the diffusion coefficient and the R_H of a particle such that a higher particle radius causes a smaller diffusion coefficient [144]. In DLS measurements, viscosity effects are factored out by the conversion of diffusion coefficients into R_H [145]. Thus, a viscosity-independent R_H can be determined. Moreover, if the R_H of a scattering particle is known, this knowledge can be used to determine the solvent's viscosity by the difference between the expected and the measured diffusion coefficients [146, 147]. By contrast, SEC cannot compensate for increased viscosity and, thus, reduced diffusion coefficients, which might result in a higher apparent R_H and, thus, in the observed decrease in retention volume [99]. This effect should influence all samples investigated in highly viscous solvents, and has to be corrected by calibrating the column at different urea concentrations, that is, different solvent viscosities if the elution volume matters for data analysis, as it is the case in analytical SEC. In triple-detection SEC, it can be neglected if it does not impede separation.
The increasing peak broadening at higher urea concentrations, observed particularly for DDM micelles at varying denaturant concentrations, can also be assigned to a higher solvent viscosity [142, 143]. The main source of band broadening in liquid chromatography is the so-called resistance to mass transfer [148], which is caused by limited particle dif-

fusion between mobile and stationary phase. The particles permanently switch between the two phases. Molecules that are located near the phase boundary can change quickly; those that are located at a greater distance require more time. During that time, analyte molecules in the mobile phase are transported further along the column, and since the mass transfer between the two phases is not instantaneously completed, a full equilibrium cannot establish under standard separation conditions [149]. Thus, the analyte concentration in the stationary phase is always displaced slightly behind the equilibrium position, while it is slightly ahead in the mobile phase. This leads to a symmetric peak broadening around the equilibrium position [150]. The resistance to mass transfer is increased if the exchange of particles between mobile and stationary phases is further impaired. Higher solvent viscosity is such a limiting effect, since it decreases the particles' diffusion coefficient [151].

Elution of NM micelles

In comparison with all other alkyl maltosides, NM micelles exhibit higher retention volumes in the presence of 6 M urea (**Section 5.4.2**). That is the behaviour typically expected for a decrease in size. However, the increase in elution volume is not as pronounced as expected. The apparently different behaviour of NM micelles might be caused by the extreme size reduction. Since the decrease in micelle size upon exposure to urea is more pronounced for NM than for any other investigated detergent, elution is shifted to higher volumes compared with measurements in the absence of urea. However, compared with particles of similar size, the retention volume is still lower than expected. Thus, it is in line with the longer-chain alkyl maltosides.

6.1.2 Effect on data reproducibility

Urea does not only influence the hydrodynamic behaviour of all kinds of investigated macromolecules but was also shown to affect data quality. The urea-induced influences on the hydrodynamic behaviour did not impede data analysis in triple-detection SEC; however, investigations of BSA at 6 M (**Section 5.4.1**) and DDM micelles at 0–8 M urea (**Section 5.4.2**) exhibit an increased uncertainty in the derived data as well as reduced sample-to-sample reproducibility. Both effects are more pronounced with increasing urea concentration, and can be attributed mainly to disturbed RI detection.
The RI detector is most sensitive to external, that is, non-sample-induced influences. Such influences are all effects that change n_0, for example, changes in temperature or pressure, which change the density of a solution [152]. Furthermore, local inhomogeneities in solvent composition can occur, if using salt or denaturant concentrations in the molar range in SEC. This is also accompanied by local changes in n_0. The first two effects cause mainly drifting baselines, whereas solvent inhomogeneity leads to a fluctuating base-

line. Additionally, viscosity [122] and compressibility [153, 154] in highly concentrated urea buffers are different from mainly aqueous solvents, increase with urea concentration, and might lead to changes in the back pressure in the chromatographic system, since the pressure drop across the column is viscosity-dependent [150]. A non-constant pressure drop introduces flow pulsations due to the compressibility compensation mechanism of the pump [155]. This pulsation also causes fluctuations in the RI baseline. While constantly drifting baselines can be well compensated by background-correction procedures, fluctuating baselines interfere with the baseline correction. If background corrections are non-identical for all signals, the signals become distorted with respect to each other. Here, it is the RI signal that is deviating from the LS signal. This leads to inaccuracies in concentration determination, which in turn result in varying masses across the peak, as it is observed for BSA (**Figure 17**) and DDM (**Figure 19**).
For DDM micelles, it has to be considered additionally that the CMC of DDM increases with urea concentration [81]. Hence, the total number of micelles and, thus, scattering particles, is reduced if the total detergent concentration is kept constant, as in **Section 5.4.2**. Consequently, the SLS signal intensity decreases with increasing urea concentration, which results in a decrease of the S/N even without additional disturbing influences. At an S/N as low as for DDM micelles in the presence of 4–8 M urea, imperfect baseline correction described above has a measurable effect on data quality such that molar masses vary across the peak.

The presence of high urea concentrations during triple-detection SEC causes changes in the elution volume and disturbance of the baseline stability of the RI signal. Furthermore, the shrinkage of micelles with increasing urea concentration leads to a lower S/N. Elution volume changes can be assigned to changes in the (apparent) hydrodynamic volume of the particles and their hindered diffusion and does not adversely affect triple-detection SEC measurements as long as successful particle separation is assured. The disturbed baseline stability and very low S/N render the molar mass determination slightly less confident than in urea-free conditions. However, micelle and protein masses can still be estimated reasonably and sufficiently accurately for the sought investigations of PDCs.

6.2 Investigation of detergent micelles

When working with membrane proteins in vitro, the presence of any membrane mimetic is unavoidable. Detergent micelles are the simplest and probably most commonly used membrane-mimetic system. Also in this study, they are of high importance, and their behaviour in triple-detection SEC in dependence on concentration, detergent monomer size, and micelle shape is discussed on the basis of investigations on alkyl maltosides with tails comprising 9–12 carbon atoms (**Section 5.3** and **5.4.2**) and the fluorinated detergent F_6OM (**Section 5.6**).

6.2.1 Triple-detection SEC as method for micelle size determination

Detergent micelles have been studied by a variety of methods. Infrared spectroscopy [156] and neutron diffraction [157] were used to obtain low-resolution structural information. NMR relaxation experiments provided relaxation times and order parameters for the HC tail [158, 159]. Extensive physico-chemical studies yield average values for diffusion coefficients and aggregate size [160]. Some of the methods already mentioned, for example, neutron diffraction, but also AUC sedimentation measurements and fluorescence quenching [84] are used to determine detergent aggregation numbers. Although reliable, these methods are not well suited as a routine approach for fast determination of micelle sizes in terms of mass and aggregation number. The results of molecular dynamics (MD) studies, which are extensively used to determine the dynamics of micelle formation [161–163], can depend drastically on the assumed aggregation number [72, 75, 164]. Furthermore, it was suggested that, analogous to the hydrophobic mismatch reported for lipids [165–169], the hydrophobic thickness of micelles needs to match that of the membrane protein to maintain proper fold and function [14, 170–172]. Therefore, systematic investigations of factors influencing size and shape of detergent micelles as performed, for example, by Oliver et al. [173] might provide a basis for the understanding of protein–detergent interactions and the successful choice of detergent for membrane-protein solubilisation, stabilisation, and crystallisation. For both verification of MD results and choice of detergent for membrane-protein investigations, extremely long and costly measurements are undesirable.
Measurements of alkyl maltoside micelles with triple-detection SEC in a standard aqueous buffer (**Section 5.3.2**) yielded results close to literature values summarised by Broecker and Keller [81]. Additionally, the increase of the aggregation number by ∼20 monomers per additional methylene group in the HC chain faces 16±3 monomers found by Oliver et al. [173] by small-angle X-ray scattering (SAXS) measurements. Considering the dependence of aggregation numbers on, for example, buffer composition, these results can be regarded as being consistent. In comparison with other techniques such as fluorescence quenching, triple-detection SEC is additionally able to provide molar mass distributions and, thus, size-resolved data. This is especially useful for detergents that show a concentration-dependent micelle size like F_6OM (**Section 5.6.1**). There, the molar mass measured close at the CMC differs significantly from data measured far above the CMC. Hence, most techniques determine an average value for all aggregates present in the sample and cannot account for sample polydispersity. Only AUC also combines separation and analysis in a single measurement, allowing for determination of size distributions. However, Salvay et al. [96] have reported measurement durations of 8 h for the determination of the aggregation number of DDM. If the detergent under investigation has a density close to the solvent density, so-called floating detergents, measurement durations have to be extended to 24 h if possible at all. By contrast, a triple-detection SEC measurement requires 1 h if the setup is already equilibrated, otherwise 3 h of unattended system equilibration have to be added.

Independence of triple-detection SEC on particle shape

Unlike other LS techniques, SLS does not require any specific particle shape for successful data analysis. In DLS, for example, particles are assumed to be spherical, at least to a first approximation. Multi-angle light scattering (MALS) can account for non-spherical scattering objects by considering an intensity distribution function (**Equations 19** and **46**). If particles are too small to introduce a significant angle-dependency, the particle shape does not matter and the mass can be determined correctly with one detector at any observation angle. For larger or differently shaped particles such as F_6OM, at least three detection angles are required to account for anisotropic scattering and to allow for fitting of an adequate scattering function. This enables mass determination for arbitrarily shaped particles, as demonstrated for rod-like F_6OM micelles by theoretical considerations (**Section 5.6.2**). The accuracy of the analysis is increased with the number of detection angles, which increases the number of data points to which a theoretical scattering function can be fitted.

6.2.2 Detector response to detergent micelles

Sometimes, negative detector signals are observed when applying detergent-containing samples to triple-detection SEC. Those are caused by depletion of the detergent from the chromatography buffer, as demonstrated by injection of a detergent-free sample into a system equilibrated with detergent-containing chromatography buffer (**Figure 12**). The negative signals appear at the same position as the positive signals of micelles and are caused by a consumption of detergent micelles from the chromatography buffer [19]. Excess or depleted detergent micelles occur if the detergent concentration in the sample and the chromatography buffer differ from each other. Usually, this is the case for almost all measurements with detergents regardless of how carefully the solutions were prepared. The occurrence of depletion also illustrates the necessity of detergent in the chromatography buffer. Otherwise, the absence of detergent would lead to micelle disintegration and, in the case of PDCs, to protein precipitation. Hence, a first inspection of PDC chromatograms might give a hint if the detergent concentration fits the demands of the protein. If the detergent concentration in the sample is higher than the required amount, a positive detergent peak occurs because of excess micelles in the sample. By contrast, if it is less, a negative peak occurs because of the consumption of detergent from the running buffer.

6.2.3 Concentration dependence of elution profiles

The concentration series on four different alkyl maltoside detergents with tail lengths of 9–12 carbon atoms shows a concentration-dependent increase in the LS signal, as well as a concentration-dependent shift in the elution volumes for DM and NM detergent micelles

(**Section 5.3.2**). The elution profiles of the two short-chain length detergents additionally exhibit distinct tailing, which is more pronounced for NM.
At a first glance, changes in the elution volume might be interpreted as increase in micelle size with concentration. Analysis of molar masses of alkyl maltoside micelles, however, reveal no significant change in micelle mass with concentration within typical statistical uncertainties (**Table 3**). Moreover, the observed tailing cannot be attributed to micelle polydisperisty since the investigated micelles are homogeneous in mass across the entire peak, and a comparison of M_w and M_n reveals a polydisperisty index of $\sim$1.
Overloading of the column is another effect that might explain the observed concentration dependency accompanied by tailing. However, it occurs more likely in preparative than analytical SEC because of the higher sample volumes of several millilitres instead of 100–200 µL. This might also be excluded here because of the small injection volumes of at most 100 µL.
Typically, elution profiles are concentration-independent because the assumption that the distribution constant for the particle distribution between stationary and mobile phase is constant is valid in most SEC cases. Consequently, SEC elution peaks are symmetric with a width that only depends on the kinetic properties of the column [150]. If the assumption of a constant distribution is not valid because there are, for example, unspecific interactions between analyte and column material, this may result in concentration-dependent retention times and peak asymmetries [174, 175], as observed for DM and NM micelles. Despite its general chemical inertness, almost each column material exhibits a number of sorption sites, which might attract the detergents. At low concentrations, many of the sorption sites are unoccupied and can retain analytes. At higher concentrations, the number of unoccupied sorption sites is rapidly reduced because of saturation. Thus, the analyte moves faster through the column than at lower concentrations, as it is not retained by non-specific column interactions. Consequently, the elution peak develops a tail at its rear.

6.2.4 Urea-induced changes in micelle size

Co-solvents such as urea can drastically change the micellisation behaviour of detergents. For alkyl maltosides, for example, it has been shown by DLS that the micelle size decreases in the presence of denaturant [81]. However, size determination by DLS provides only the z-average R_H of scattering particles, which, additionally, is influenced by hydration of detergent head groups. Since hydration is also affected by denaturants, a decrease in hydrodynamic particle size could result from changes in head group hydration and/or intrinsic micelle size. By contrast, size information deduced from static light scattering is less sensitive to hydration effects; thus, changes in molar mass can almost unambiguously be ascribed to changes in micellisation behaviour. For verification of the DLS data from Broecker and Keller [81], alkyl maltosides carrying chains comprising 9–12 carbon atoms were investigated regarding their micelle molar mass (**Section 5.4.2**).

As described in **Section 6.1**, urea affects the performance of triple-detection SEC beyond its direct effect on, for example, detergent micelles. Nevertheless, the average molar mass values across the entire peaks are usually still reliable. Hence, the observed decrease in micelle size induced by 6 M urea can be clearly assigned to a reduction in aggregation number to roughly half of the aggregation number in the absence of urea. The only exception is NM, where the size reduction is even more pronounced (**Section 5.4.2**). The size reduction can be ascribed to a direct influence of urea on the micelle structure. Although urea does not penetrate into the hydrophobic core of detergent micelles [176], it accumulates at the polar–apolar interface and increases the effective size of the head group region by an enhanced solvation of the head groups. Thus, the intrinsic curvature is increased and the size of micelles is reduced [80, 81]. Moreover, the interfacial tension is decreased by the incorporation of urea in the micellar interface, rendering the exposure of apolar tails energetically less unfavourable and leading to the formation of smaller micelles. This effect is more pronounced for smaller micelles, which consist of detergents with shorter alkyl chains [177] and, thus, might be an explanation for the more pronounced size reduction in NM micelles compared with the other alkyl maltoside micelles of the series.

6.2.5 Determination of micelle shape

The shape of detergent micelles is often assumed as mainly spherical. However, Tanford showed already in 1972 [73] by simple geometrical considerations that for most detergent micelles an ellipsoidal shape might be more realistic. This was confirmed systematically for a series of detergents commonly used in membrane-protein studies with the aid of SAXS [173]. SAXS and the related small-angle neutron scattering (SANS) are techniques commonly used for shape determination [84]. Additionally, TEM realised as cryo-EM or negative-staining EM is used to determine structure and shape of macromolecular assemblies [130]. However, the two aforementioned scattering techniques, as well as EM, require experienced users and instruments not necessarily considerable as standard equipment. In polymer research, triple-detection SEC is an established method not only for the determination of molar masses but also R_{RMS} of polymers, which enables the identification of polymer branching ratios or polymer shapes by so-called conformation plots (**Section 2.4**) [100]. Here, the conformation-plot approach was applied to F_6OM micelles to demonstrate as proof-of-principle the suitability of triple-detection SEC for the determination of micelle shapes.

F_6OM micelles were used as model system because their self-assembly into elongated rod-like aggregates has been shown by negative-staining TEM [74]. Moreover, alkyl maltoside and LDAO micelles investigated within this thesis were too small to exhibit angle-dependent scattering intensities and, thus, allow for reliable R_{RMS} determination and conformation estimation. Analysis of the most intense part of the F_6OM peak yields a slope of one and, thus, indicates a rod-like structure of the micelles. An alternative

approach is to compare R_{RMS} and R_{H} of a particle for shape estimation. Similar to R_{RMS}–M_w pairs, different R_{RMS}–R_{H} ratios indicate different conformations [178]. This is based on the different definitions of R_{RMS} and R_{H}, which reflect different properties of the particle, namely the distribution of mass with respect to the centre of gravity and the hydrodynamic dimension [92, 178]. Erik Frotscher, M.Sc., determined the R_{H} of F_6OM in dependence on detergent concentration in his Master thesis [179]. The R_{H} at ∼2 mM, which roughly represents the detergent concentration at the most intense part of the chromatogram (**Figure 28**), is 20 nm. The corresponding R_{RMS} amounts to 30–35 nm. This yields an R_{RMS}–R_{H} ratio of 1.5–1.7 and, thus, values expected for rod-like structures [101]. However, as indicated by the conformation plot, shape analysis of small particles always has to be taken with caution. Signal intensities in the border areas of the peak are very low because of the small size of the particles. Therefore, especially determination of the R_{RMS} is very error-prone if possible at all. Additionally, particles with a $R_{\mathrm{RMS}} < \lambda/10$ show no significant angle-dependent deviation in scattering intensity, impeding R_{RMS} determination. However, this is not a sharp limit but depends on concentration and particle shape as well. Low concentrations, and with them low S/N, can impair R_{RMS} determination for even larger particles. By contrast, particles with shapes deviating significantly from spheres might exhibit anisotropic scattering at smaller sizes. Moreover, the presented measurements suffer from poorly resolved scattering functions because they were recorded at three different angles only. Three detection angles represent the minimum number of data points required for R_{RMS} determination. Aside from the indirect approaches presented above, shape estimation from the scattering function directly might be considered possible by comparing experimental and theoretical P_Θ. However, this approach requires a wide range of P_Θ usually not accessible by even large micelles [92].
Generally, it is possible to estimate micelle structures with medium resolution from triple-detection SEC measurements if the micelles are large enough or show a distinct deviation from a spherical shape like rod-like structures. They have per se a higher R_{RMS} because of their elongated shape. However, sufficiently high concentrations are necessary, in addition to the size of the particles, to achieve valuable scattering and concentration data for reliable R_{RMS} and mass values. Structural information derived from triple-detection SEC provides valuable hints for aggregates with R_{RMS} >10 nm, but these data should be confirmed with techniques providing higher resolution even at lower diameter size like EM or scattering techniques like SAXS and SANS. For quick screening of structural features without the need of higher resolution, triple-detection SEC can provide valuable information.

In general, triple-detection SEC provides a fast and reliable method for the determination of molar masses and aggregation numbers of arbitrarily shaped detergent micelles irrespective of the buffer composition. Additionally, information about the polydispersity of the preparation is provided. Hence, it is especially useful to facilitate information re-

quired to verify, for example, MD simulation data or to set the decision for a detergent for membrane-protein solubilisation or stabilisation onto a more qualified level. For particles big enough to exhibit anisotropic scattering, the estimation of the particles' shape is possible.

6.3 Investigation of PDCs

The amount of detergent bound to a membrane protein varies significantly among different proteins. The *E. coli* multidrug transporter EmrE, for example, has been shown to be associated with DDM with a mass ratio δ of 4 [180, 181], whereas for the Na^+-K^+-ATPase a binding ratio of 0.5 [182] has been reported. Additionally, the results for protein–detergent interactions yielded in MD simulations may also depend on the number of detergent molecules initially assigned to the complex [183], similar to pure detergent simulations discussed in **Section 6.2.1**. Because of these facts, the amount of detergent required to stabilise a certain protein in its functional state, by avoiding disintegration of detergent complexes by excess detergent, cannot be estimated ad hoc in most cases. Hence, a fast and easy-to-perform method is convenient. Triple-detection SEC has become particularly popular in the field of membrane-protein analysis [14, 16–20]. The suitability of triple-detection SEC for characterising the composition of PDCs was also demonstrated within this work by the analysis of OmpLA–LDAO complexes (**Section 5.5.2**). If the hydrodynamic volume of PDC and protein-free micelle are different, triple-detection SEC can separate both species with baseline resolution allowing for straightforward and independent determination of the molar mass and composition of both species. The obtained results represent a typical well-behaved membrane-protein–detergent mixture comprising two species that can be neatly separated by SEC. The Mistic–NM complex also represents such a typical result.

However, Mistic–DM, –UM, and –DDM complexes are prone to overestimation of the amount of detergent that is associated with the protein. This is due to poor separation by SEC of these PDCs from the corresponding protein-free micelles. If incomplete separation occurs, contributions from different species to the signal cannot be separated out neatly and data analysis requires more caution. In the case of DM, PDCs and protein-free micelles are only partially separated but can still be analysed separately, provided that the peak boundaries are set such that the overlap between the two peaks is minimised. By contrast, elution profiles in the presence of UM or DDM give rise to only one peak. There, the molar mass and the oligomeric state of the protein can still be estimated reasonably. However, the amount of bound detergent becomes difficult or impossible to quantify because triple-detection SEC averages masses across all species present in the analysis range. In particular, the detergent concentration derived from the RI signal is the sum of bound detergent and detergent co-eluting in the form of protein-free micelles. Since protein-free alkyl maltoside micelles contain more detergent than the PDCs, this results in overesti-

mation of the amount of detergent bound to Mistic. If the protein-free micelles contain less detergent than the PDC under investigation, the amount of protein-bound detergent is underestimated. The UV signal represents solely protein, which enables correct determination of the protein concentration. Thus, the contribution of the protein to the overall mass can be derived correctly. This is only possible because alkyl maltosides exhibit no absorbance at 280 nm, which could interfere with the protein absorbance. Otherwise, neither detergent nor protein masses can be determined accurately in the case of co-elution of PDCs and protein-free micelles.

6.3.1 Composition of PDCs in the presence of urea

In experiments relying on the chemical unfolding of a detergent-solubilised membrane protein, the unfolded polypeptide in the presence of high denaturant concentrations serves as a common reference state, enabling the comparison of protein conformational stability among different detergents, but this approach is applicable only if the unfolded state is not associated with detergent [15]. Triple-detection SEC of Mistic in the presence of 6 M urea allowed to demonstrate that the protein's unfolded state is detergent-free (**Section 5.5.4**) and may serve as a common reference state for protein-folding studies [14]. At high urea concentrations, baseline instabilities prevent reliable data analysis (**Section 6.1.2**) such that the highest urea concentration that was used was fixed to 6 M. However, for most alkyl maltosides, quantitative analysis based on light scattering theory was straightforward, yielding unfolded Mistic without any bound detergent as suggested by CD and DLS measurements [14]. In contrast with CD and DLS measurements, which show only indirectly by comparison of CD-spectra and aggregation studies that the unfolded state of Mistic is detergent-free, triple-detection SEC provides a direct measure. Additionally, analysis of the protein-free peaks resembled data obtained from the measurements of the corresponding detergents without protein, verifying that under unfolding conditions protein and detergent contributions can be analysed independently. Contrary to previous claims [104], these results demonstrate that triple-detection SEC is also compatible with the use of detergents and high concentrations of chemical denaturants in general.

6.4 Accuracy of triple-detection SEC

Folta-Stogniew and co-workers have studied the accuracy of triple-detection SEC for 14 water-soluble proteins over a broad range of molar masses (14–475 kDa), and have found it to be within ±5% for a single measurement [18]. This makes the method suitable for the determination of the oligomeric state of homo-oligomers of up to 20 subunits [19]. For the determination of protein masses in PDCs, the uncertainty is slightly increased compared with water-soluble proteins. The determined mass of OmpLA in a complex

with LDAO deviates by ±6–7% from the nominal value. This decrease in accuracy can be assigned to the necessity of three detectors in contrast with soluble proteins, which can be analysed by an LS and one additional concentration-sensitive detector. In addition to the uncertainty introduced by the detectors themselves, the absorbance coefficients for the protein and absorbing detergents and refractive index increments for both have to be known and are an additional source of error. Especially, because for some proteins, the extinction coefficient calculated from the primary structure differs significantly from experimental values [184] and the refractive index increment of any substance depends on a number of factors, including buffer composition, wavelength, and temperature. To ensure data quality, detergent refractive index increments should be determined newly for, at least, very different buffer compositions, such as urea-free and urea-containing buffer. Additionally, Schuck and co-workers have demonstrated that the $\mathrm{d}n/\mathrm{d}c$ value of proteins of 0.185–0.187 mL/g is not as universally applicable as generally assumed [185]. However, it can be estimated from the protein's amino acid sequence analogous to extinction coefficients [185]. This might provide a more accurate estimate than using standard values, and can help in increasing accuracy also for detergent mass determination. Despite all these hindering factors, membrane proteins with up to ten subunits have been studied successfully [186]. The presence of high urea concentrations slightly decreases both accuracy and precision in comparison with soluble proteins. This is mainly influenced by lower S/N due to reduced signal intensities and increased baseline instabilities.
In summary, even under non-optimal conditions, protein molar masses in PDCs can be determined with an uncertainty <7%. For well-behaved systems, accuracies within ±2% for a single measurement are possible.

6.5 Limitations of triple-detection SEC

Coupling of LS with SEC overcomes the two main obstacles that impede reliable mass determination with either one of the methods. The applicability of LS is widened by the separation power of SEC to samples containing polydisperse particles or multiple particles of different size. Additionally, an altered chromatography behaviour does not influence mass determination, as it does in analytical SEC measurements. However, triple-detection SEC also faces limitations.
The determination of the R_{RMS}, and with it conformation estimation, requires particles with $R_{\mathrm{RMS}} > \lambda/10$. Mainly globular water-soluble proteins exhibit such R_{RMS} at a molar mass of at least $\sim 10^6$ kg/mol [92]. Membrane proteins that can be associated with relatively high amounts of detergent might exhibit anisotropic scattering at slightly lower molar masses. Nevertheless, even DDM micelles, which are rather big in size, are too small for R_{RMS} determination by triple-detection SEC. This limits the technique as method for conformation analysis to elongated rod-like detergent micelles or big detergent–lipid assemblies like bicelles.

As demonstrated in analysing Mistic–detergent complexes, simultaneous passage of several co-eluting species through the detection volumes of UV, SLS, and RI detectors adversely affects data analysis. The (partially) overlapping elution of PDCs and protein-free micelles causes an average value for the amount of bound detergent and the amount of detergent in protein-free micelles. Both species cause signals in LS and RI detection simultaneously and do not allow for discrimination between protein-associated detergent and detergent assembled in micelles. The accurate determination of protein mass is only possible if the detergents do not absorb at 280 nm and PDCs and protein-free micelles are similar in mass. If the masses of two simultaneously eluting species are very different from each other, like Mistic and DDM micelles, even protein-mass determination must fail. All scattering particles in a given elution slice contribute to the LS signal, which is assumed to be caused by one species. If only PDCs are present, two concentration detectors allow for weighted deconvolution of the total complex mass into the contributions of protein and detergent. In the case of co-eluting species, this approach fails, because protein and detergent contribute completely independently to the LS signal. For similar-sized PDCs and protein-free micelles, also one scattering species is assumed, but because of the similar size only the detergent concentration is erroneous. If nominal or experimental data for (some of) the pure species are available, the contributions of protein and detergent to the three signals can be distinguished, so that determination of both masses is possible even under such challenging conditions.

6.6 Outlook

The extension of triple-detection SEC from standard applications such as PDCs analysis in mainly aqueous buffer to applications requiring high amounts of denaturant, for example, is the most significant achievement of this work. It can be used for direct characterisation of the unfolded state of membrane proteins in terms of detergent association in a fast and straightforward manner. This allows for routine application in membrane-protein folding for the confirmation of common reference states. To my knowledge, up to now, this verification has been possible only by indirect methods, such as comparison of CD spectra or aggregation tests by turbidity measurements or DLS. The procedure presented in this thesis can be applied to any detergent-suspended protein and, with minor changes to the setup, also to other membrane-mimetic systems such as lipid–polymer particles bound by styrene maleic acid (SMA) copolymers [187] and bicelles.

Dipl.-Biophys. Anne Grethen investigated the solubilisation efficiency of SMA on OmpLA-containing 1-palmitoyl-2-oleoyl-*sn*-glycero-3-phosphocholine (POPC) and 1,2-didodecanoyl-*sn*-glycero-3-phosphocholine (DLPC) vesicles in her diploma thesis [188]. There, she could verify successful solubilisation of proteoliposomes by SMA, and distinguished between protein-loaded and protein-free SMA–lipid particles (SMALPs) by comparing elution profiles recorded with absorbance at 280 nm and 260 nm and RI detection. The

addition of LS detection transfers triple-detection SEC into tetra-detection SEC and, thus, in principle allows for the determination of four quantities. Such quantities might be protein, SMA, and lipid concentrations and the molar mass of the complex. The exact SMALP composition regarding protein–SMA–lipid ratio, however, remains unclear in these investigations because of the additional presence of detergent. To account for this, the use of a fluoresence detector as fourth concentration-depended detector might be a solution. In the interplay with fluorescent lipids, independent OmpLA, SMA, and lipid concentration profiles can be provided, and the distribution of all components among aggregates, mixed micelles, and SMALPs can be determined.

In addition to the investigation of SMALPs, Abraham Olusegun Oluwole, M.Sc., is examining further polymers like, for example, poly(di-isobutylene-*alt*-maleic-acid)(DIBMA), which exhibits vesicle solubilisation properties but absorbs less at 260 nm than SMA and, thus, will not interfere with spectroscopic studies of proteins like SMA. However, the resulting polymer–lipid particles are even less characterised in terms of lipid–polymer stoichiometry than SMALPs. Here, triple-detection SEC can be a perfect method for fast initial investigation of various lipid–polymer ratios and the resulting polymer–lipid particles. In the case of protein-free particles, the setup presented in this work is perfectly suited if the absorbance at 260 nm is monitored instead of that at 280 nm. Protein-containing particles can be investigated by an enhanced setup, similar to the one sketched for SMALPs in the paragraph above.

In contrast with polymer–lipid particles, bicelles are not intended for directly solubilising membrane proteins but are of high interest as membrane-mimetic systems for structural [189] and protein-folding [190] studies. Bicelles are nanometre-sized, disk-shaped aggregates with a highly curved detergent-rich rim that surrounds a planar phospholipid-rich core. They are formed in certain mixtures of long-chain phospholipids and a short-chain lipid or detergent. However, their formation strongly depends on various factors, such as temperature, hydration, and the mole fraction of the two amphiphiles [191]. In mixtures of two bicelle-forming amphiphiles, phase transitions lead to different morphologies, including disk-shaped bicelles but also perforated vesicles, extended lamellae, and spherical or cylindrical mixed micelles [192]. Dipl.-Biophys. Johannes Klingler is aiming at the quantitative description of the thermodynamics underlying the observed phase transitions and the concomitant morphologies in his PhD thesis. Investigations of the different structures, so far, have been performed using a combination of SANS and NMR studies by Li et al. [191]. However, these methods are costly and time-consuming. Triple-detection SEC can overcome this problem by using the shape-dependent angle-dependency of scattering intensity to determine the structure of scattering particles, and additionally provides information about bicelle composition.

7 Conclusions

This thesis aimed at the expansion of the field of application of triple-detection SEC in membrane-protein research, especially for challenging membrane-protein samples, which so far eluded routine approaches. To this end, the standard experimental and data analysis procedure of triple-detection SEC was refined for the use of complex samples in difficult solvents such as concentrated denaturant solutions. The main conclusions from this work are:

- Triple-detection SEC is a straightforward and robust technique for analysing detergent-suspended membrane-protein samples in terms of PDC composition and oligomeric state.
- Chemically unfolded proteins can be characterised in terms of protein mass and amount of bound detergent at high denaturant concentrations despite the effects of high urea concentrations on baseline stability and elution volume.
- For co-eluting particles, the availability of nominal or experimental data for (some of) the pure species allows distinction of the contribution of protein and detergent to the three signals. Then, the determination of both masses is possible even under these conditions.
- For non-absorbing detergents, the protein mass can still be estimated reasonably in case of co-elution of PDCs and detergent micelles of similar size. However, detergent masses are determined as average between the amount that is protein-associated and the amount that is incorporated in protein-free micelles.
- For large, non-spherical particles, triple-detection SEC can provide an estimate of medium resolution on the particle shape within a single measurement.

Bibliography

[1] E. Pebay-Peyroula, Biophysical analysis of membrane proteins: Investigating structure and function. chap. 1, Wiley-VHC, Weinheim, Germany, **2007**, 3–30.

[2] N. Bordag and S. Keller, α-Helical transmembrane peptides: A "divide and conquer" approach to membrane proteins. *Chemistry and Physics of Lipids*, **2010**, *163*, 1–26.

[3] M. Le Maire, P. Champeil, and J. V. Møller, Interaction of membrane proteins and lipids with solubilizing detergents. *Biochimica et Biophysica Acta*, **2000**, *1508*, 86–111.

[4] Y. Wei, H. Li, and D. Fu, Oligomeric state of the *Escherichia coli* metal transporter YiiP. *Journal of Biological Chemistry*, **2004**, *279*, 39251–39259.

[5] L. Bamber, M. Harding, P. J. G. Butler, and E. R. S. Kunji, Yeast mitochondrial ADP/ATP carriers are monomeric in detergents. *Proceedings of the National Academy of Sciences of the United States of America*, **2006**, *103*, 16224–16229.

[6] M. Herrmann, B. Danielczak, M. Textor, J. Klement, and S. Keller, Modulating bilayer mechanical properties to promote the coupled folding and insertion of an integral membrane protein. *European Biophysics Journal*, **2015**, *44*, 503–512.

[7] K. Skaar, H. J. Korza, M. Tarry, P. Sekyrova, and M. Högbom, Expression and subcellular distribution of GFP-tagged human tetraspanin proteins in *Saccharomyces cerevisiae*. *PLoS ONE*, **2015**, *10*.

[8] C. Hitscherich, J. Kaplan, M. Allaman, J. Wiencek, and P. J. Loll, Static light scattering studies of OmpF porin: Implications for integral membrane protein crystallization. *Protein Science*, **2000**, *9*, 1559–1566.

[9] J. Khao, J. Arce-Lopera, J. N. Sturgis, and J.-P. Duneau, Structure of a protein–detergent complex: The balance between detergent cohesion and binding. *European Biophysics Journal*, **2011**, *40*, 1143–1155.

[10] C. Breyton, C. Tribet, J. Olive, J.-P. Dubacq, and J.-L. Popot, Dimer to monomer conversion of the Cytochrome b_6f complex. *Journal of Biological*, **1997**, *272*, 21892–21900.

[11] G. G. Privé, Detergents for the stabilization and crystallization of membrane proteins. *Methods*, **2007**, *41*, 388–397.

[12] C. C. Prince and Z. Jia, Detergent quantification in membrane protein samples and its application to crystallization experiments. *Amino Acids*, **2013**, *45*, 1293–1302.

[13] T. Jacso, B. Bardiaux, J. Broecker, S. Fiedler, T. Baerwinkel, A. Mainz, U. Fink, C. Vargas, H. Oschkinat, S. Keller, and B. Reif, The mechanism of denaturation and the unfolded state of the α-helical membrane-associated protein Mistic. *Journal of the American Chemical Society*, **2013**, *135*, 18884–18891.

[14] J. Broecker, S. Fiedler, K. Gimpl, and S. Keller, Polar interactions trump hydrophobicity in stabilizing of the self-inserting membrane protein Mistic. *Journal of the American Chemical Society*, **2014**, *136*, 13761–13768.

[15] S. Fiedler, J. Broecker, and S. Keller, Protein folding in membranes. *Cellular and Molecular Life Sciences*, **2010**, *67*, 1779–1798.

[16] S. Maezawa, Y. Hayashi, T. Nakae, J. Ishii, K. Kameyama, and T. Takagi, Determination of molecular weight of membrane proteins by the use of low-angle laser light scattering combined with high-performance gel chromatography in the presence of a non-ionic surfactant. *Biochimica et Biophysica Acta*, **1983**, *747*, 291–297.

[17] J. Wen, T. Arakawa, and J. S. Philo, Size-exclusion chromatography with on-line light-scattering, absorbance, and refractive index detectors for studying proteins and their interactions. *Analytical Biochemistry*, **1996**, *240*, 155–166.

[18] E. Folta-Stogniew and K. R. Williams, Determination of molecular masses of proteins in solution: Implementation of an HPLC size exclusion chromatography and laser light scattering service in a core laboratory. *Journal of Biomolecular Techniques*, **1999**, *10*, 51–63.

[19] D. J. Slotboom, R. H. Duurkens, K. Olieman, and G. B. Erkens, Static light scattering to characterize membrane proteins in detergent solution. *Methods*, **2008**, *46*, 73–82.

[20] A. Korepanova and E. D. Matayoshi, HPLC-SEC characterization of membrane protein–detergent complexes. *Current Protocols in Protein Science*, **2012**, *1*, 1–12.

[21] C. Tanford, The Hydrophobic Effect: Formation of Micelles and Biological Membranes. John Wiley & Sons, Hoboken, NJ, USA, **1973**.

[22] K. A. Dill, Dominant forces in protein folding. *Biochemistry*, **1990**, *29*, 7133–7155.

[23] D. M. Engelman and G. Zaccai, Bacteriorhodopsin is an inside-out protein. *Proceedings of the National Academy of Sciences of the United States of America*, **1980**, *77*, 5894–5898.

[24] J. Deisenhofer, O. Epp, K. Miki, R. Huber, and H. Michel, X-ray structure analysis of a membrane protein complex. *Journal of Molecular Biology*, **1984**, *180*, 385–398.

[25] D. Rees, L. DeAntonio, and D. Eisenberg, Hydrophobic organization of membrane proteins. *Science*, **1989**, *245*, 510–513.

[26] F. A. Samatey, C. Xu, and J. L. Popot, On the distribution of amino acid residues in transmembrane α-helix bundles. *Proceedings of the National Academy of Sciences of the United States of America*, **1995**, *92*, 4577–81.

[27] D. M. Engelman, T. A. Steitz, and A. Goldman, Identifying nonpolar transbilayer helices in amino acid sequences of membrane proteins. *Annual Review of Biophysics and Biophysical Chemistry*, **1986**, *15*, 321–353.

[28] S. H. White and W. C. Wimley, Membrane protein folding and stability: Physical principles. *Annual Review of Biophysics and Biomolecular Structure*, **1999**, *28*, 319–65.

[29] C. M. Bishop, W. F. Walkenhorst, and W. C. Wimley, Folding of β-sheets in membranes: specificity and promiscuity in peptide model systems. *Journal of Molecular Biology*, **2001**, *309*, 975–88.

[30] G. E. Schulz, β-Barrel membrane proteins. *Current Opinion in Structural Biology*, **2000**, *10*, 443–447.

[31] L. K. Tamm, A. Arora, and J. H. Kleinschmidt, Structure and assembly of β-barrel membrane proteins. *Journal of Biological Chemistry*, **2001**, *276*, 32399–32402.

[32] W. C. Wimley, The versatile β-barrel membrane protein. *Current Opinion in Structural Biology*, **2003**, *13*, 404–411.

[33] H. R. Bigelow, D. S. Petrey, J. Liu, D. Przybylski, and B. Rost, Predicting transmembrane β-barrels in proteomes. *Nucleic Acids Research*, **2004**, *32*, 2566–77.

[34] E. Wallin and G. von Heijne, Genome-wide analysis of integral membrane proteins from eubacterial, archaean, and eukaryotic organisms. *Protein Science*, **1998**, *7*, 1029–38.

[35] J. P. Overington, B. Al-Lazikani, and A. L. Hopkins, How many drug targets are there? *Nature Reviews Drug Discovery*, **2006**, *5*, 993–6.

[36] C. M. Dobson, Protein folding and misfolding. *Nature*, **2003**, *426*, 884–90.

[37] C. R. Sanders and J. K. Myers, Disease-related misassembly of membrane proteins. *Annual Review of Biophysics and Biomolecular Structure*, **2004**, *33*, 25–51.

[38] J. F. Hunt, T. N. Earnest, O. Bousché, K. Kalghatgi, K. Reilly, C. Horváth, K. J. Rothschild, and D. M. Engelman, A biophysical study of integral membrane protein folding. *Biochemistry*, **1997**, *36*, 15156–76.

[39] N. Dekker, J. Tommassen, A. Lustig, J. P. Rosenbusch, H. M. Verheij, and P. Rosenbusch, Dimerization regulates the enzymatic activity of *Escherichia coli* outer membrane phospholipase A. *The Journal of Biological Chemistry*, **1997**, *272*, 3179–3184.

[40] H. Homma, T. Kobayashi, N. Chiba, K. Karasawa, H. Mizushima, I. Kudo, K. Inoue, H. Ikeda, M. Sekiguchi, and S. Nojima, The DNA sequence encoding *pldA* gene, the structural gene for detergent-resistant phospholipase A of *E. coli*. *Journal of Biochemistry*, **1984**, *96*, 1655–64.

[41] C. J. Scandella and A. Kornberg, Membrane-bound phospholipase A1 purified from *Escherichia coli*. *Biochemistry*, **1971**, *10*, 4447–4456.

[42] H. J. Snijder, I. Ubarretxena-Belandia, M. Blaauw, K. H. Kalk, H. M. Verheij, M. R. Egmond, N. Dekker, and B. W. Dijkstra, Structural evidence for dimerization-regulated activation of an integral membrane phospholipase. *Nature*, **1999**, *401*, 717–721.

[43] J. Luirink, C. van der Sande, J. Tommassen, E. Veltkamp, F. K. De Graaf, and B. Oudega, Effects of divalent cations and of phospholipase A activity on excretion of cloacin DF13 and lysis of host cells. *Journal of General Microbiology*, **1986**, *132*, 825–34.

[44] P. de Geus, I. van Die, H. Bergmans, J. Tommassen, and G. de Haas, Molecular cloning of *pldA*, the structural gene for outer membrane phospholipase of *E. coli* K12. *Molecular and General Genetics*, **1983**, *190*, 150–155.

[45] H. Homma, N. Chiba, T. Kobayashi, I. Kudo, K. Inoue, H. Ikeda, M. Sekiguchi, and S. Nojima, Characteristics of detergent-resistant phospholipase A overproduced in *E. coli* cells bearing its cloned structural gene. *Journal of Biochemistry*, **1984**, *96*, 1645–53.

[46] N. Dekker, J. Tommassen, and H. M. Verheij, Bacteriocin release protein triggers dimerization of outer membrane phospholipase A in vivo. *Journal of Bacteriology*, **1999**, *181*, 3281–3283.

[47] J. E. J. Cronan and D. L. Wulff, A role for phospholipid hydrolysis in the lysis of *Escherichia coli* infected with bacteriophage T4. *Virology*, **1969**, *38*, 241 – 246.

[48] A. Audet, G. Nantel, and P. Proulx, Phospholipase A activity in growing *Escherichia coli* cells. *Biochimica et Biophysica Acta*, **1974**, *348*, 334–43.

[49] H. Snijder and B. Dijkstra, Bacterial phospholipase A: Structure and function of an integral membrane phospholipase. *Biochimica et Biophysica Acta*, **2000**, *1488*, 91–101.

[50] M. Nishijima, S. Nakaike, Y. Tamori, and S. Nojima, Detergent-resistant phospholipase a of *Escherichia coli* K-12. purification and properties. *European Journal of Biochemistry*, **1977**, 115–124.

[51] I. Ubarretxena-Belandia, J. W. P. Boots, H. M. Verheij, and N. Dekker, Role of the cofactor calcium in the activation of outer membrane phospholipase A. *Biochemistry*, **1998**, *37*, 16011–16018.

[52] K. A. Grant, I. U. Belandia, N. Dekker, P. T. Richardson, and S. F. Park, Molecular characterization of *pldA*, the structural gene for a phospholipase A from *Campylobacter coli*, and its contribution to cell-associated hemolysis. *Infection and immunity*, **1997**, *65*, 1172–80.

[53] G. Bukholm, T. Tannaes, P. Nedenskov, Y. Esbensen, H. J. Grav, T. Hovig, S. Ariansen, and I. Guldvog, Colony variation of *Helicobacter pylori*: Pathogenic potential is correlated to cell wall lipid composition. *Scandinavian Journal of Gastroenterology*, **1997**, *32*, 445–54.

[54] N. Dekker, Outer-membrane phospholipase A: Known structure, unknown biological function. *Molecular Microbiology*, **2000**, *35*, 711–717.

[55] Schrödinger, LLC, The PyMOL molecular graphics system, version 1.8, **2015**.

[56] T. P. Roosild, J. Greenwald, M. Vega, S. Castronovo, R. Riek, and S. Choe, NMR structure of Mistic, a membrane-integrating protein for membrane protein expression. *Science*, **2005**, *307*, 1317–1321.

[57] T. P. Roosild, M. Vega, S. Castronovo, and S. Choe, Characterization of the family of Mistic homologues. *Structural Biology*, **2006**, *6*, 10.

[58] T. Jacso, W. T. Franks, H. Rose, U. Fink, J. Broecker, S. Keller, H. Oschkinat, and B. Reif, Characterization of membrane proteins in isolated native cellular membranes by dynamic nuclear polarization solid-state NMR spectroscopy without purification and reconstitution. *Angewandte Chemie—International Edition*, **2012**, *51*, 432–435.

[59] D. K. Debnath, R. V. Basaiawmoit, K. L. Nielsen, and D. E. Otzen, The role of membrane properties in Mistic folding and dimerisation. *Protein Engineering, Design & Selection*, **2011**, *24*, 89–97.

[60] S. J. Singer, The molecular organization of membranes. *Annual Review of Biochemistry*, **1974**, *43*, 805–33.

[61] G. Kefala, W. Kwiatkowski, L. Esquivies, I. Maslennikov, and S. Choe, Application of Mistic to improving the expression and membrane integration of histidine kinase receptors from *Escherichia coli*. *Journal of Structural and Functional Genomics*, **2007**, *8*, 167–172.

[62] F. Bernaudat, A. Frelet-Barrand, N. Pochon, S. Dementin, P. Hivin, S. Boutigny, J.-B. Rioux, D. Salvi, D. Seigneurin-Berny, P. Richaud, J. Joyard, D. Pignol, M. Sabaty, T. Desnos, E. Pebay-Peyroula, E. Darrouzet, T. Vernet, and N. Rolland, Heterologous expression of membrane proteins: Choosing the appropriate host. *PloS ONE*, **2011**, *6*.

[63] M. E. Lundberg, E. C. Becker, and S. Choe, Mstx and a putative potassium channel facilitate biofilm formation in *Bacillus subtilis*. *PLoS ONE*, **2013**, *8*.

[64] R. Renthal, An unfolding story of helical transmembrane proteins. *Biochemistry*, **2006**, *45*, 14559–66.

[65] A. M. Stanley and K. G. Fleming, The process of folding proteins into membranes: Challenges and progress. *Archives of Biochemistry and Biophysics*, **2008**, *469*, 46–66.

[66] J. Broecker, New approaches to studying membrane-protein stability and high-affinity protein–inhibitor interactions. *PhD Thesis*, **2011**.

[67] R. M. Garavito and S. Ferguson-Miller, Detergents as tools in membrane biochemistry. *Journal of Biological Chemistry*, **2001**, *276*, 32403–32406.

[68] J.-L. Rigaud and D. Lévy, Liposomes: Part B. Methods in Enzymology, Elsevier, Amsterdam, Netherlands, **2003**.

[69] A. Helenius and K. Simons, Solubilization of membranes by detergents. *Biochimica et Biophysica Acta*, **1975**, *415*, 29–79.

[70] L. R. Fisher and D. G. Oakenfull, Micelles in aqueous solution. *Chemical Society Reviews*, **1977**, *6*, 25.

[71] J. N. Israelachvili, S. Marčelja, and R. G. Horn, Physical principles of membrane organization. *Quarterly Reviews of Biophysics*, **1980**, *13*, 121.

[72] S. Bogusz, R. M. Venable, and R. W. Pastor, Molecular Dynamics Simulations of Octyl Glucoside Micelles: Structural Properties. *The Journal of Physical Chemistry B*, **2000**, *104*, 5462–5470.

[73] C. Tanford, Micelle shape and size. *The Journal of Physical Chemistry*, **1972**, *76*, 3020–3024.

[74] E. Frotscher, B. Danielczak, C. Vargas, A. Meister, G. Durand, and S. Keller, A fluorinated detergent for membrane-protein applications. *Angewandte Chemie—International Edition*, **2015**, *54*, 5069–5073.

[75] D. P. Tieleman, D. van der Spoel, and H. J. C. Berendsen, Molecular dynamics simulations of dodecylphosphocholine micelles at three different aggregate sizes: Micellar structure and chain relaxation. *The Journal of Physical Chemistry B*, **2000**, *104*, 6380–6388.

[76] G. Gunnarsson, B. Joensson, and H. Wennerstroem, Surfactant association into micelles. An electrostatic approach. *The Journal of Physical Chemistry*, **1980**, *84*, 3114–3121.

[77] T. Arnold and D. Linke, The use of detergents to purify membrane proteins. *Current Protocols in Protein Science*, **2008**, 1–30.

[78] C. C. Ruiz and F. G. Sánchez, Effect of urea on aggregation behavior of Triton X-100 micellar solutions: A photophysical study. *Journal of Colloid and Interface Science*, **1994**, *165*, 110–115.

[79] A. Walter, G. Kuehl, K. Barnes, and G. VanderWaerdt, The vesicle-to-micelle transition of phosphatidylcholine vesicles induced by nonionic detergents: Effects of sodium chloride, sucrose and urea. *Biochimica et Biophysica Acta*, **2000**, *1508*, 20–33.

[80] H. Patel, G. Raval, M. Nazari, and H. Heerklotz, Effects of glycerol and urea on micellization, membrane partitioning and solubilization by a non-ionic surfactant. *Biophysical Chemistry*, **2010**, *150*, 119–128.

[81] J. Broecker and S. Keller, Impact of urea on detergent micelle properties. *Langmuir*, **2013**, *29*, 8502–8510.

[82] M. le Maire, B. Arnou, C. Olesen, D. Georgin, C. Ebel, and J. V. Møller, Gel chromatography and analytical ultracentrifugation to determine the extent of detergent binding and aggregation, and Stokes radius of membrane proteins using sarcoplasmic reticulum Ca^{2+}-ATPase as an example. *Nature Protocols*, **2008**, *3*, 1782–1795.

[83] N. Turro and A. Yekta, Luminescent probes for detergent solutions. a simple procedure for determination of the mean aggregation number of micelles. *Journal of the American Chemical Society*, **1978**, *100*, 5951–5952.

[84] P. Tummino and A. Gafni, Determination of the aggregation number of detergent micelles using steady-state fluorescence quenching. *Biophysical Journal*, **1993**, *64*, 1580–1587.

[85] U. K. Laemmli, Cleavage of structural proteins during the assembly of the head of bacteriophage T4. *Nature*, **1970**, *227*, 680–685.

[86] H. Schägger, H. Aquila, and G. Von Jagow, Coomassie blue-sodium dodecyl sulfate-polyacrylamide gel electrophoresis for direct visualization of polypeptides during electrophoresis. *Analytical Biochemistry*, **1988**, *173*, 201–205.

[87] A. Rath, M. Glibowicka, V. G. Nadeau, G. Chen, and C. M. Deber, Detergent binding explains anomalous SDS-PAGE migration of membrane proteins. *Proceedings of the National Academy of Sciences of the United States of America*, **2009**, *106*, 1760–5.

[88] E. R. S. Kunji, M. Harding, P. J. G. Butler, and P. Akamine, Determination of the molecular mass and dimensions of membrane proteins by size exclusion chromatography. *Methods*, **2008**, *46*, 62–72.

[89] R. Murphy, Static and dynamic light scattering of biological macromolecules: What can we learn? *Current Opinion in Biotechnology*, **1997**, *8*, 25–30.

[90] K. Gast and A. J. Modler, Studying protein folding and aggregation by laser light scattering. In Protein Folding Handbook, chap. 19, Wiley-VCH, Weinheim, Germany, **2008**, 673–709.

[91] M. J. Schurr and V. Bloomfield, Dynamic light scattering of biopolymers and biocolloid. *Critical Reviews in Biochemistry and Molecular Biology*, **1977**, *4*, 371–431.

[92] S. Podzimek, Light Scattering, Size Exclusion Chromatography and Asymmetric Flow Field Flow Fractionation: Powerful Tools for the Characterization of Polymers, Proteins and Nanoparticles. John Wiley & Sons, Hoboken, NJ, USA, **2011**.

[93] J. L. Cole, J. W. Lary, T. P. Moody, and T. M. Laue, Analytical ultracentrifugation: Sedimentation velocity and sedimentation equilibrium. *Methods in Cell Biology*, **2008**, *84*, 143–179.

[94] J. X. Lu, S. Sharpe, R. Ghirlando, W. M. Yau, and R. Tycko, Oligomerization state and supramolecular structure of the HIV-1 Vpu protein transmembrane segment in phospholipid bilayers. *Protein Science*, **2010**, *19*, 1877–1896.

[95] R. Ghirlando, The analysis of macromolecular interactions by sedimentation equilibrium. *Methods*, **2011**, *54*, 145–156.

[96] A. G. Salvay and C. Ebel, Analytical ultracentrifuge for the characterization of detergent in solution. *Progress in Colloid and Polymer Science*, **2006**, *131*, 74–82.

[97] C. Ebel, Sedimentation velocity to characterize surfactants and solubilized membrane proteins. *Methods*, **2011**, *54*, 56–66.

[98] A. Le Roy, C. Breyton, and C. Ebel, Analytical ultracentrifugation and size-exclusion chromatography coupled with light scattering for characterization of membrane proteins in solution. In I. Mus-Veteau, editor, Membrane Proteins Production for Structural Analysis, chap. 10, Springer, New York, **2014**, 267–288.

[99] D. J. Winzor, Analytical exclusion chromatography. *Journal of Biochemical and Biophysical Methods*, **2003**, *56*, 15–52.

[100] S. Podzimek, The use of GPC coupled with a multiangle laser light scattering photometer for the characterization of polymers. On the determination of molecular weight, size and branching. *Journal of Applied Polymer Science*, **1994**, *54*, 91–103.

[101] A. Striegel, W. W. Yau, J. J. Kirkland, and D. D. Bly, Modern size-exclusion liquid chromatography: Practice of gel permeation and gel filtration chromatography. chap. 11, John Wiley & Sons, Hoboken, NJ, USA, **2009**.

[102] J. C. Giddings, F. J. Yang, and M. N. Myers, Flow-field-flow fractionation: a versatile new separation method. *Science*, **1976**, *193*, 1244–1245.

[103] J. C. Giddings, F. J. F. Yang, and M. N. Myers, Sedimentation field-flow fractionation. *Analytical Chemistry*, **1974**, *46*, 1917–1924.

[104] M. Tanase, V. Zolla, C. C. Clement, F. Borghi, A. M. Urbanska, J. A. Rodriguez-Navarro, B. Roda, A. Zattoni, P. Reschiglian, A. M. Cuervo, and L. Santambrogio, Hydrodynamic size-based separation and characterization of protein aggregates from total cell lysates. *Nature Protocols*, **2014**, *10*, 134–148.

[105] J. C. Giddings, A new separation concept based on a coupling of concentration and flow nonuniformities. *Separation Science*, **1966**, *1*, 123–125.

[106] M. Plevin, Multiangle light scattering. In Encyclopedia of Biophysics, Springer, Heidelberg, **2013**, 2767.

[107] B. H. Zimm, The scattering of light and the radial distribution function of high polymer solutions. *The Journal of Chemical Physics*, **1948**, *16*, 1093.

[108] K. Gimpl, J. Klement, and S. Keller, Characterising protein/detergent complexes by triple-detection size-exclusion chromatography. *Biological Procedures Online*, **2016**, *18*, 1–18.

[109] H. Friedrich, Scattering Theory. Lecture Notes in Physics, Springer Berlin Heidelberg, **2013**.

[110] P. Debye, Light scattering in solutions. *Journal of Applied Physics*, **1944**, *15*, 338–342.

[111] B. H. Zimm, Molecular theory of the scattering of light in fluids. *The Journal of Chemical Physics*, **1945**, *13*, 141.

[112] B. H. Zimm, The dependence of the scattering of light on angle and concetration in linear polymer solutions. *The Journal of Chemical Physics*, **1947**, *16*, 1048.

[113] B. H. Zimm, Apparatus and methods for measurement and interpretation of the angular variation of light scattering; preliminary results on polystyrene solutions. *The Journal of Chemical Physics*, **1948**, *16*, 1099.

[114] P. J. Wyatt, Light scattering and the absolute characterization of macromolecules. *Analytica Chimica Acta*, **1993**, *272*, 1–40.

[115] D. F. Swinehart, The Beer-Lambert Law. *Journal of Chemical Education*, **1962**, *39*, 333.

[116] N. J. Anthis and G. M. Clore, Sequence-specific determination of protein and peptide concentrations by absorbance at 205 nm. *Protein Science*, **2013**, *22*, 851–858.

[117] B. Tieke, Makromolekulare Chemie: Eine Einführung. 3rd edn., Wiley-VHC, Weinheim, Germany, **1997**.

[118] R. F. T. Stepto, Dispersity in polymer science (IUPAC Recommendations 2009). *Pure and Applied Chemistry*, **2009**, *81*, 351–353.

[119] M. J. R. Cantow, editor, Polymer Fractionation. Academic Press, New York, **1967**.

[120] D. Linke, Detergents. In Methods in Enzymology, chap. 34, Elsevier, Amsterdam, Netherlands, **2009**, 603–617.

[121] C. N. Pace, Determination and analysis of urea and guanidine hydrochloride denaturation curves. *Methods in Enzymology*, **1986**, *131*, 266–280.

[122] J. R. Warren and J. A. Gordon, On the refractive indices of aqueous solutions of urea. *The Journal of Physical Chemistry*, **1966**, *70*, 297–300.

[123] L. R. Eriks, J. a. Mayor, and R. S. Kaplan, A strategy for identification and quantification of detergents frequently used in the purification of membrane proteins. *Analytical Biochemistry*, **2003**, *323*, 234–241.

[124] C. A. Schneider, W. S. Rasband, and K. W. Eliceiri, NIH Image to ImageJ: 25 years of image analysis. *Nature Methods*, **2012**, *9*, 671–675.

[125] V. Ball and J. J. Ramsden, Buffer dependence of refractive index increments of protein solutions. *Biopolymers*, **1998**, *46*, 489–492.

[126] K. Hirayama, S. Akashi, M. Furuya, and K.-i. Fukuhara, Rapid confirmation and revision of the primary structure of bovine serum albumin by ESIMS and frit-FAB LC/MS. *Biochemical and Biophysical Research Communications*, **1990**, *173*, 639–646.

[127] R. Feng, Y. Konishi, and A. W. Bell, High accuracy molecular weight determination and variation characterization of proteins up to 80 ku by ionspray mass spectrometry. *Journal of the American Society for Mass Spectrometry*, **1991**, *2*, 387–401.

[128] S. Fiedler, Thermodynamic stability of the α-helical membrane-interacting protein Mistic in detergent micelles. *PhD Thesis*, **2013**.

[129] V. Srinivasan and D. Blankschtein, Prediction of conformational characteristics and micellar solution properties of fluorocarbon surfactants. *Langmuir*, **2005**, *21*, 1647–1660.

[130] K. Köhler, G. Förster, A. Hauser, B. Dobner, U. F. Heiser, F. Ziethe, W. Richter, F. Steiniger, M. Drechsler, H. Stettin, and A. Blume, Temperature-dependent behavior of a symmetric long-chain bolaamphiphile with phosphocholine headgroups in water: From hydrogel to nanoparticles. *Journal of the American Chemical Society*, **2004**, *126*, 16804–16813.

[131] S. Kawaguchi, G. Imai, J. Suzuki, A. Miyahara, T. Kitano, and K. Ito, Aqueous solution properties of oligo- and poly(ethylene oxide) by static light scattering and intrinsic viscosity. *Polymer*, **1997**, *38*, 2885–2891.

[132] F. Ferri, M. Greco, and M. Rocco, On the determination of the average molecular weight, radius of gyration, and mass/length ratio of polydisperse solutions of polymerizing rod-like macromolecular monomers by multi-angle static light scattering. *Macromolecular Symposia*, **2000**, *162*, 23–43.

[133] D. Wolff, S. Czapla, A. Heyer, S. Radosta, P. Mischnick, and J. Springer, Globular shape of high molar mass inulin revealed by static light scattering and viscometry. *Polymer*, **2000**, *41*, 8009–8016.

[134] Y. Liu, S. Bo, Y. Zhu, and W. Zhang, Determination of molecular weight and molecular sizes of polymers by high temperature gel permeation chromatography with a static and dynamic laser light scattering detector. *Polymer*, **2003**, *44*, 7209–7220.

[135] K. Kameyama, T. Nakae, and T. Takagi, Estimation of molecular weights of membrane proteins in the presence of SDS by low-angle laser light scattering combined with high-performance porous silica gel chromatography. Confirmation of the trimer structure of porin of the *E. coli* outer membrane. *Biochimica et Biophysica Acta*, **1982**, *706*, 19–26.

[136] K. Kawahara and C. Tanford, Viscosity and density of aqueous solutions of urea and guanidine hydrochloride. *The Journal of Biological Chemistry*, **1966**, *241*, 3228–32.

[137] R. Itri, W. Caetano, L. R. S. Barbosa, and M. S. Baptista, Effect of urea on bovine serum albumin in aqueous and reverse micelle environments investigated by small angle X-ray scattering, fluorescence, and circular dichroism. *Brazilian Journal of Physics*, **2004**, *34*, 58–63.

[138] R. J. Corbett and R. S. Roche, Use of high-speed size-exclusion chromatography for the study of protein folding and stability. *Biochemistry*, **1984**, *23*, 1888–94.

[139] V. N. Uversky, Use of fast protein size-exclusion liquid chromatography to study the unfolding of proteins which denature through the molten globule. *Biochemistry*, **1993**, *32*, 13288–13298.

[140] B. Batas, H. R. Jones, and J. B. Chaudhuri, Studies of the hydrodynamic volume changes that occur during refolding of lysozyme using size-exclusion chromatography. *Journal of Chromatography A*, **1997**, *766*, 109–119.

[141] M. E. Himmel and P. G. Squire, High pressure gel permeation chromatography of native proteins on TSK-SW columns. *International Journal of Peptide and Protein Research*, **1981**, *17*, 365–73.

[142] K. Unger, The application of size exclusion chromatography to the analysis of biopolymers. *Trends in Analytical Chemistry*, **1983**, *2*, 271–274.

[143] H. Yuan, I. Souvignet, and S. V. Olesik, High-performace size exclusion chromatography using enhanced-fluidity liquid mobile phases. *Journal of Chromatographic Science*, **1997**, *35*, 409–416.

[144] A. L. Kholodenko and J. F. Douglas, Generalized Stokes–Einstein equation for spherical particle suspensions. *Physical Review E*, **1995**, *51*, 1081–1090.

[145] A. Lomakin, D. B. Teplow, and G. B. Benedek, Quasielastic light scattering for protein assembly studies. *Methods in Molecular Biology*, **2005**, *299*, 153–74.

[146] A. S. Parmar and M. Muschol, Lysozyme as diffusion tracer for measuring aqueous solution viscosity. *Journal of Colloid and Interface Science*, **2009**, *339*, 243–248.

[147] F. He, G. W. Becker, J. R. Litowski, L. O. Narhi, D. N. Brems, and V. I. Razinkov, High-throughput dynamic light scattering method for measuring viscosity of concentrated protein solutions. *Analytical Biochemistry*, **2010**, *399*, 141–143.

[148] A. M. Striegel, Longitudinal diffusion in size-exclusion chromatography: A stop-flow size-exclusion chromatography study. *Journal of Chromatography A*, **2001**, *932*, 21–31.

[149] W. W. Yau, C. P. Malone, and H. L. Suchan, Separation Mechanisms in Gel Permeation Chromatography. *Separation Science*, **1970**, 259–271.

[150] C. Poole, The essence of chromatography. chap. 1, Elsevier, Amsterdam, Netherlands, **2003**.

[151] J. Cazes, Encyclopedia of Chromatography. Dekker Encyclopedias Series, Taylor & Francis, **2005**.

[152] I. Thormählen, J. Straub, and U. Grigull, Refractive index of water and its dependence on wavelength, temperature, and density. *Journal of Physical and Chemical Reference Data*, **1985**, *14*, 933.

[153] P. K. D. Gupta and S. P. Moulik, Interaction of urea with weak acids and water. *The Journal of Physical Chemistry*, **1987**, *91*, 5826–5832.

[154] L. Ramesh, S. S. Dhondge, and M. N. Ray, Volumetric and compressibility properties of aqueous solutions of urea and ethylene glycol. *Indian Journal of Chemistry*, **1999**, *38A*, 70–72.

[155] D. Parriott, A Practical Guide to HPLC Detection. Elsevier, Amsterdam, Netherlands, **2012**.

[156] F. Holler and J. B. Callis, Conformation of the hydrocarbon chains of sodium dodecyl sulfate molecules in micelles: an FTIR study. *The Journal of Physical Chemistry*, **1989**, *93*, 2053–2058.

[157] D. Bendedouch, S. H. Chen, and W. C. Koehler, Structure of ionic micelles from small angle neutron scattering. *The Journal of Physical Chemistry*, **1983**, *87*, 153–159.

[158] H. Wennerstroem, B. Lindman, O. Soederman, T. Drakenberg, and J. B. Rosenholm, Carbon-13 magnetic relaxation in micellar solutions. influence of aggregate motion on T_1. *Journal of the American Chemical Society*, **1979**, *101*, 6860–6864.

[159] O. Soederman, H. Walderhaug, U. Henriksson, and P. Stilbs, NMR relaxation in isotropic surfactant systems. a deuterium, carbon-13, and nitrogen-14 NMR study of

the micellar (L_1) and cubic (I_1) phases in the dodecyltrimethylammonium chloride water system. *The Journal of Physical Chemistry*, **1985**, *89*, 3693–3701.

[160] J. Lauterwein, C. Bösch, L. R. Brown, and K. Wüthrich, Physicochemical studies of the protein–lipid interactions in melittin-containing micelles. *Biochimica et Biophysica Acta*, **1979**, *556*, 244–264.

[161] J. C. Shelley, M. Sprik, and M. L. Klein, Molecular dynamics simulation of an aqueous sodium octanoate micelle using polarizable surfactant molecules. *Langmuir*, **1993**, *9*, 916–926.

[162] J. Boecker, J. Brickmann, and P. Bopp, Molecular dynamics simulation study of an *n*-decyltrimethylammonium chloride micelle in water. *The Journal of Physical Chemistry*, **1994**, *98*, 712–717.

[163] B. Aoun, V. K. Sharma, E. Pellegrini, S. Mitra, M. Johnson, and R. Mukhopadhyay, Structure and dynamics of ionic micelles: MD simulation and neutron scattering study. *The Journal of Physical Chemistry B*, **2015**, *119*, 5079–86.

[164] S. J. Marrink, D. P. Tieleman, and A. E. Mark, Molecular dynamics simulation of the kinetics of spontaneous micelle formation. *The Journal of Physical Chemistry B*, **2000**, *104*, 12165–12173.

[165] P. A. Baldwin and W. L. Hubbell, Effects of lipid environment on the light-induced conformational changes of rhodopsin. 2. Roles of lipid chain length, unsaturation, and phase state. *Biochemistry*, **1985**, *24*, 2633–2639.

[166] J. D. Pilot, J. M. East, and A. G. Lee, Effects of bilayer thickness on the activity of diacylglycerol kinase of *Escherichia coli*. *Biochemistry*, **2001**, *40*, 8188–8195.

[167] M. R. R. de Planque and J. A. Killian, Protein-lipid interactions studied with designed transmembrane peptides: role of hydrophobic matching and interfacial anchoring. *Molecular Membrane Biology*, **2003**, *20*, 271–284.

[168] A. G. Lee, How lipids affect the activities of integral membrane proteins. *Biochimica et Biophysica Acta*, **2004**, *1666*, 62–87.

[169] J. U. Bowie, Solving the membrane protein folding problem. *Nature*, **2005**, *438*, 581–9.

[170] C. Fernández, C. Hilty, G. Wider, and K. Wüthrich, Lipid-protein interactions in DHPC micelles containing the integral membrane protein OmpX investigated by NMR spectroscopy. *Proceedings of the National Academy of Sciences of the United States of America*, **2002**, *99*, 13533–7.

[171] M. G. Santonicola, A. M. Lenhoff, and E. W. Kaler, Binding of alkyl polyglucoside surfactants to bacteriorhodopsin and its relation to protein stability. *Biophysical Journal*, **2008**, *94*, 3647–58.

[172] L. Columbus, J. Lipfert, K. Jambunathan, D. A. Fox, A. Y. L. Sim, S. Doniach, and S. A. Lesley, Mixing and matching detergents for membrane protein NMR structure determination. *Journal of the American Chemical Society*, **2009**, *131*, 7320–6.

[173] R. C. Oliver, J. Lipfert, D. a. Fox, R. H. Lo, S. Doniach, and L. Columbus, Dependence of micelle size and shape on detergent alkyl chain length and head group. *PLoS ONE*, **2013**, *8*.

[174] H. Poppe, Distribution isotherms in reversed-phase systems. *Journal of Chromatography A*, **1993**, *656*, 19–36.

[175] N. Katsanos and F. Roubani-Kalantzopoulou, Advances in physico-chemical measurements using inverse gas chromatography. *Advances in Chromatography*, **2000**, *40*, 231–73.

[176] H. Raghuraman, S. K. Pradhan, and A. Chattopadhyay, Effect of urea on the organization and dynamics of Triton X-100 micelles: A fluorescence approach. *The Journal of Physical Chemistry B*, **2004**, *108*, 2489–2496.

[177] M. Nazari, H. Y. Fan, and H. Heerklotz, Effect of hydrophobic interactions on volume and thermal expansivity as derived from micelle formation. *Langmuir*, **2012**, *28*, 14129–36.

[178] W. Burchard, M. Schmidt, and W. H. Stockmayer, Information on polydispersity and branching from combined quasi-elastic and integrated scattering. *Macromolecules*, **1980**, *13*, 1265–1272.

[179] E. Frotscher, Interactions of fluorinated surfactants with classical membrane-mimetic systems. *Master Thesis*, **2014**.

[180] P. J. G. Butler, I. Ubarretxena-Belandia, T. Warne, and C. G. Tate, The *Escherichia coli* multidrug transporter EmrE is a dimer in the detergent-solubilised state. *Journal of Molecular Biology*, **2004**, *340*, 797–808.

[181] T. L. Winstone, M. Jidenko, M. le Maire, C. Ebel, K. A. Duncalf, and R. J. Turner, Organic solvent extracted EmrE solubilized in dodecyl maltoside is monomeric and binds drug ligand. *Biochemical and Biophysical Research Communications*, **2005**, *327*, 437–45.

[182] E. Cohen, R. Goldshleger, A. Shainskaya, D. M. Tal, C. Ebel, M. le Maire, and S. J. D. Karlish, Purification of Na^+,K^+-ATPase expressed in *Pichia pastoris* reveals an essential role of phospholipid–protein interactions. *Journal of Biological Chemistry*, **2005**, *280*, 16610–16618.

[183] E. Psachoulia, P. J. Bond, and M. S. P. Sansom, MD simulations of Mistic: conformational stability in detergent micelles and water. *Biochemistry*, **2006**, *45*, 9053–8.

[184] H. Mach, C. Middaugh, and R. V. Lewis, Statistical determination of the average values of the extinction coefficients of tryptophan and tyrosine in native proteins. *Analytical Biochemistry*, **1992**, *200*, 74–80.

[185] H. Zhao, P. H. Brown, and P. Schuck, On the distribution of protein refractive index increments. *Biophysical Journal*, **2011**, *100*, 2309–2317.

[186] R. A. Albright, J.-L. V. Ibar, C. U. Kim, S. M. Gruner, and J. H. Morais-Cabral, The RCK domain of the KtrAB K^+ transporter: Multiple conformations of an octameric ring. *Cell*, **2006**, *126*, 1147–59.

[187] D. J. K. Swainsbury, S. Scheidelaar, R. van Grondelle, J. A. Killian, M. R. Jones, R. van Grondelle, J. A. Killian, and M. R. Jones, Bacterial reaction centers purified with styrene maleic acid copolymer retain native membrane functional properties and display enhanced stability. *Angewandte Chemie—International Edition*, **2014**, *53*, 11803–11807.

[188] A. Grethen, Solubilisation of OmpLA proteoliposomes with styrene-maleic acid copolymer. *Diploma Thesis*, **2015**.

[189] J. A. Whiles, R. Deems, R. R. Vold, and E. A. Dennis, Bicelles in structure-function studies of membrane-associated proteins. *Bioorganic Chemistry*, **2002**, *30*, 431–442.

[190] C. McKibbin, N. A. Farmer, P. C. Edwards, C. Villa, and P. J. Booth, Urea unfolding of opsin in phospholipid bicelles. *Photochemistry and Photobiology*, **2009**, *85*, 494–500.

[191] M. Li, H. H. Morales, J. Katsaras, N. Kučerka, Y. Yang, P. M. Macdonald, and M. P. Nieh, Morphological characterization of DMPC/CHAPSO bicellar mixtures: A combined SANS and NMR study. *Langmuir*, **2013**, *29*, 15943–15957.

[192] U. H. Dürr, R. Soong, and A. Ramamoorthy, When detergent meets bilayer: Birth and coming of age of lipid bicelles. *Progress in Nuclear Magnetic Resonance Spectroscopy*, **2013**, *69*, 1–22.

Acknowledgments

This thesis could not have been accomplished without the continued support and involvement of many people. In particular, I thank:

- Prof. Sandro Keller (University of Kaiserslautern) for his outstanding commitment in supervising this work, for many stimulating discussions and helpful advice, and for both scientific and personal guidance;

- Prof. Rolf Diller (University of Kaiserslautern) for agreeing to act as second adviser for this thesis;

- Prof. Nicole Frankenberg-Dinkel (University of Kaiserslautern) for agreeing to act as chairperson during my oral thesis defence;

- Prof. Hans Hasse (University of Kaiserslautern) for the opportunity to perform all the light scattering experiments in his laboratory;

- Dr. Albert Werner (BASF SE, Ludwigshafen), Eva Hackemann, and Agnes Fröscher (both University of Kaiserslautern) for all their technical help with the triple-detection SEC setup and their support in organising measurement times even with short-term notice;

- Bartholomäus Danielczak (University of Kaiserslautern) for the painful but very helpful determination of various refractive index increments and for preparative work on Mistic;

- Michaela Herrmann and Jessica Klement (both University of Kaiserslautern) for preparative work on OmpLA;

- Dr. Jana Bröcker and Dr. Sebastian Fiedler (both University of Toronto) for sharing their extensive knowledge, not only but particularly, about membrane-protein production, protein folding, and all the other laboratory issues and for their scientific and personal guidance. You have embossed my scientific work;

- all current and former colleagues at the University of Kaiserslautern—in particular, Dr. Jana Bröcker, Rodrigo Cuevas Arenas, Bartholomäus Danielczak, Christian Dautermann, Tim Diederichs, Jonas Dörr, Markus Fleisch, Dr. Sebastian Fiedler,

Erik Frotscher, Anindya Ghosh Roy, Anne Grethen, Ina Heimann, Michaela Herrmann, Jonas Höring, Dr. Nadin Jahnke, Jennifer Jung, Benjamin Klement, Jessica Klement, Johannes Klingler, Georg Krainer, Dr. Bert Lägel, Dr. Thomas Löber, Abraham Olusegun Oluwole, Henryke Rath, Johannes Schnur, Martin Textor, Sebastian Unger, Dr. Carolyn Vargas, Andreas Werle-Rutter, Dr. Sandra Wolf, and Sally Wu—for their help and the enjoyable time we spent together throughout the years;

- Christian Dautermann for support with virtually any technical problem;
- the neighbours from the Human Biology department (University of Kaiserslautern) for uncomplicated access to their equipment at all times;
- the groups of Cell Biology and Cellular Biochemistry (both University of Kaiserslautern) for access to their equipment and their help with all molecular-biology-related questions;
- the Carl-Zeiss-Stiftung for the generous funding of this thesis;
- Jonas and Ryke for the great time we spent in the "girls' lab";
- Judith, Michael, Thomas[2], Pia, Tassilo, Balthasar, Carina, and Johannes for their friendship and the great time we spent throughout the years. Thank you for all your support, not only during our student time but also in every part of our lives;
- Laura Kreiner for her friendship and brutal honesty since schooldays;
- meinen Geschwistern Alexander, Verena und Isabell, für die schonungslose Ehrlichkeit, den Spaß, die Albernheiten, und die Gewissheit, dass wir immer aufeinander vertrauen können;
- meinen Eltern, für die immerwährende Unterstützung, Hilfe und Rat wann immer ich darum gebeten habe und ihr Vertrauen in mich und meine Entscheidungen;
- Tom, my fiancé for almost ten years of friendship and unconditional support. I am deeply grateful that I can share my life with you, and I am very much looking forward to the years that are still to come.

List of Publications

- Gimpl K., Textor M., Keller S., Polarisationsspektroskopie zur biophysikalischen Charakterisierung von Proteinen. *Analytik News* **2013**.

Peer-Reviewed

- Broecker J., Fiedler S., Gimpl K., and Keller S., Polar interactions trump hydrophobicity in stabilizing the self-inserting membrane protein Mistic. *Journal of the American Chemical Society* **2014**, *136*, 13761–13768.

- Gimpl K., Klement J., and Keller S., Characterising protein/detergent complexes by triple-detection size-exclusion chromatography. *Biological Procedures Online* **2016**, *18*, 1–18.

- Panigrahi R., Arutyunova E., Panwar P., Gimpl K., Keller S., and Lemieux M. J., Reversible unfolding of rhomboid intramembrane proteases. *Biophysical Journal* **2016**, *110*, 1379–1390.

Curriculum Vitae

Personal data

Name:	Katharina Gimpl

Education

since 01.2012	**PhD Thesis**, Molecular Biophysics, University of Kaiserslautern Prof. Sandro Keller
10.2006–08.2011	**University of Kaiserslautern** Dipl.-Biophys. Specialisation in Biology
12.2010–08.2011	**Diploma Thesis** Molecular Biophysics, University of Kaiserslautern Prof. Sandro Keller *Heterologous expression of the transmembrane protein CopA from Archaeoglobus fulgidus and Bacillus subtilis*
01.2010–06.2010	**Uppsala University (Uppsala Universitet)** Physics department
09.1997–06.2006	**Willibald-Gluck-Gymnasium, Neumarkt i. d. OPf.** Abitur

Organised conferences

05.2013	**1st Retreat of the Molecular Biophysics group** Diez, Germany
05.2014	**564. WE-Heraeus-Seminar: Physical Approaches to Membrane Proteins** Bad Honnef, Germany
10.2014	**2nd Retreat of the Molecular Biophysics group** Feldberg, Germany

Stipends

07.2012–06.2015	**Carl Zeiss Foundation** PhD Fellowship
01.2010–06.2010	**ERASMUS Fellowship**

Katharina Gimpl Kaiserslautern, 09.04.2016

Eidesstattliche Erklärung

Ich erkläre an Eides statt, dass mir die Promotionsordnung des Fachbereiches Biologie der Technischen Universität Kaiserslautern in der derzeit gültigen Fassung bekannt ist. Desweiteren versichere ich, dass ich die vorliegende Arbeit selbstständig verfasst, keine anderen als die angegebenen Quellen und Hilfsmittel verwendet, sowie die Ergebnisse anderer Mitarbeiter sowie anderer Autoren klar gekennzeichnet habe. Ich habe diese Dissertation oder Teile daraus keinem anderen Fachbereich vorgelegt und mich zu keinem früheren Zeitpunkt um den Doktorgrad beworben.

Katharina Gimpl Kaiserslautern, 09.04.2016